Characterization and Modeling of a Methanol Reforming Fuel Cell System

Karakterisering og Modellering af en Methanol Reformering Fuel Cell System

Sahlin, Simon Lennart

DOI (link to publication from Publisher):
10.5278/vbn.phd.engsci.00059

Publication date:
2016

Document Version
Publisher's PDF, also known as Version of record

CHARACTERIZATION AND MODELING OF A METHANOL REFORMING FUEL CELL SYSTEM

BY
SIMON LENNART SAHLIN

DISSERTATION SUBMITTED 2016

AALBORG UNIVERSITY
DENMARK

Characterization and Modeling of a Methanol Reforming Fuel Cell System

Ph.D. Dissertation
Simon Lennart Sahlin

Dissertation submitted January, 2016

Thesis submitted:	January 2016
PhD supervisor:	Associate Prof. Søren Juhl Andreasen Aalborg University, Department of Energy Technology
PhD committee:	Associate Professor Mads Pagh Nielsen (chairman) Aalborg University
	Professor and Canada Research Chair in Fuel Cells Brant Peppley Queen's University
	Associate Professor Masoud Roki DTU, Department of Mechanical Engineering
PhD Series:	Faculty of Engineering and Science, Aalborg University

ISSN (online): 2246-1248
ISBN (online): 978-87-7112-466-8

Published by:
Aalborg University Press
Skjernvej 4A, 2nd floor
DK – 9220 Aalborg Ø
Phone: +45 99407140
aauf@forlag.aau.dk
forlag.aau.dk

Printed in Denmark by Rosendahls, 2016

Thesis Details

Thesis Title:	Characterization and Modeling of a Methanol Reforming Fuel Cell System
Ph.D. Student:	Simon Lennart Sahlin
Supervisors:	Assoc. Prof. Søren Juhl Andreasen, Aalborg University

The main body of this thesis consist of the following papers.

[A] Simon Lennart Sahlin, Søren Juhl Andreasen, Søren Knudsen Kær, "System Model Development for a Methanol Reformed 5kW High Temperature PEM Fuel Cell System," *Journal paper*, accepted in International Journal of Hydrogen Energy, Volume 40, Issue 38, 15 October 2015, Pages 13080-13089

[B] Simon Lennart Sahlin, Samuel Simon Araya, Søren Juhl Andreasen, Søren Knudsen Kær, "Parametric Characterization of Reformate-operated and PBI-based High Temperature PEM Fuel Cell Stack," *Journal paper*, Submitted to International Journal of Energy.

[C] Gia Nguyen, Simon Sahlin, Søren Juhl Andreasen, Jack Brouwer, "Dynamic modeling and experimental investigation of a high temperature PEM fuel cell stack," *Journal paper*, under review in International Journal of Hydrogen Energy, 2015

[D] Søren Juhl Andreasen, Leanne Ashworth, Simon Sahlin, Hans-Christian Becker Jensen, Søren Knudsen Kær, "Test of hybrid power system for electrical vehicles using a lithium-ion battery pack and a reformed methanol fuel cell range extender," *Journal paper*, International Journal of Hydrogen Energy, Volume 39, Issue 4, 22 January 2014, Pages 1856-1863

In addition to the main papers, the following publications have also been made.

[1] Simon Lennart Sahlin, Søren Juhl Andreasen, “System model development for evaluation of control strategies for a 5kW high temperature PEM fuel fell system,” *Conference paper*, Presented at FDFC 2013, Karlsruhe

[2] Søren Juhl Andreasen, Søren Knudsen Kær, Simon Sahlin, “Control and experimental characterization of a methanol reformer for a 350 W high temperature polymer electrolyte membrane fuel cell system,” *Journal paper* International Journal of Hydrogen Energy, Volume 38, Issue 3, 6 February 2013, Pages 1676-1684

Additionally, the PhD Student has been a co-author of chapter 21 in the following book.

- Qingfeng Li, David Aili, Hans Aage Hjuler, Jens Oluf Jensen, "High Temperature Polymer Electrolyte Membrane Fuel Cells, Approaches, Status, and Perspectives", published by: Springer International Publishing on the 14th of September 2015, Li et al. [2015]

This thesis has been submitted for assessment in partial fulfillment of the PhD degree. The thesis is based on the submitted or published scientific papers which are listed above. Parts of the papers are used directly or indirectly in the extended summary of the thesis. As part of the assessment, co-author statements have been made available to the assessment committee and are also available at the Faculty.

Abstract

Fuel cells are today being widely accepted as the technology to replace the internal combustion engines. Fuel cells have a series of advantages which include higher efficiency, wide power output range, and silent operation. Additionally, is the fuel cell locally low polluting as only by-product is water. Also, fuel cells have a low greenhouse gas impact if the source of hydrogen is from a renewable source. A potential economic independence is available if the hydrogen is produced locally, thereby reducing the dependency on oil producing countries.

Many fuel cells systems today are operated with compressed hydrogen which has great benefits because of the purity of the hydrogen and the relatively simple storage of the fuel. However, compressed hydrogen is stored in the range of 800 bar, which can be cumbersome and expensive to compress. Alternative system designs are therefore of great interest and liquid fuel can be a solution to this problem. One of those topologies is the Reformed Methanol Fuel Cell (RMFC) system which is operated on a mix of methanol and water. The fuel is reformed with a steam reforming to a hydrogen rich gas, however with additional formation of Carbon Monoxide (CO) and Carbon Dioxide (CO_2). The CO is regarded as poison for the low temperature fuel cells, however, High Temperature Polymer Electrolyte Membrane Fuel Cell (HT-PEMFC) has the benefit of being resistant to CO poisoning. The HT-PEM fuel cell operates at elevated temperatures (above 100 °C) and therefore uses phosphoric acid as a proton conductor. HT-PEM can, because of the elevated temperatures, tolerable higher amounts of CO (up to 3 %) without permanent damage, whereas the Low Temperature PEM fuel cell (LT-PEMFC) only show tolerable amounts in the range of 1 ppm.

Using a HT-PEMFC in a RMFC system enables the use of exhaust gas from the fuel cell in a catalytic burner which is able to heat up the steam reforming process. However, utilizing the excess hydrogen in the system complicates the RMFC system as the amount of hydrogen can vary depending on the fuel methanol supply, fuel cell load and the reformer gas composition. This PhD

study has therefore been involved in investigating the gas composition of the reformer and the affects to the HT-PEM fuel cell. Additional, a focus on the dynamics and system control of the RMFC have been studied, which have also been a big part of the motivation for this work.

A 17-cell HT-PEM fuel cell stack was tested with various operating temperatures on both pure hydrogen and reformate gas. The test on the HT-PEM fuel cell stack confirmed the resistance to CO poisoning. Furthermore, decreased performance was detected under low stoichiometry on both the hydrogen and air side. The fuel cell was analyzed using polarization and Electrochemical Impedance Spectroscopy (EIS) techniques. The EIS tests showed how the fuel cell stack was influenced by isolating the different losses in the fuel cell stack. A dynamic model of the fuel cell stack was made based on the polarization curves and load step tests.

A dynamic model of the RMFC system was made and include the dynamics of reformer, fuel cell, burner, and evaporator. The dynamic model is based on a 5kW electric RMFC system with a 120 cell HT-PEM fuel cell stack. The dynamic model was made with focus on analyzing the temperature distribution in the system and to create a model can be used to evaluate control techniques. A cascade control system is proposed and tested using the RMFC model, where the controller uses the reformate temperature to control the setpoint for the burner temperature. A cascade controller is possible because the burner feedback loop is significantly faster compared to the reformer feedback. The time constant for the burner is found to be 10 seconds and the reformer is 97 seconds.

The burner is temperature controlled using the burner air fan, however the implemented controller enables the system to decrease the stoichiometry to a lower level, thereby increasing the efficiency of the system and lowering temperature of the burner. A minimum allowable stoichiometry set for the controller which is determined by the HT-PEMFC. The lowest possible stoichiometry used for the model is 1.3 and corresponds to an electric system efficiency of 29 %, which corresponds to a levelized cost of electricity of €0.22/kWh without distribution cost and taxes.

Resumé

Brændselsceller i dag er generelt tænkt som den teknologi som skal erstatte de interne forbrændingsmotore(IFM). Brændselsceller har en serie af fordele i forhold til IFM's, så som højere effektivitet og lydsvag drift. Derudover er der en lav lokal udledning af forurening fordi den eneste udledning er vand. Brændselsceller har også en lav udledning af drivhusgas hvis hydrogenen er baseret på vedvarende energikilder. En potentiel økonomisk uafhængighed er tilgængelig hvis hydrogen er produceret lokalt, derved reducere afhængigheden til olieproducerende lande.

Mange brændselscellesystemer i dag er forsynet fra komprimeret hydrogen som har fordele på grund af renheden af gassen og den relative simple opbevaring af brændslet. Ulemperne er dog at komprimeret hydrogen er i området af 800 bar kan være svær at håndtere og dyrt at komprimere. Alternative systemer er derfor meget interessante og et flydende brændstof kan være en løsning på problemet. En af de muligheder er et Reformeret Methanol Fuel Cell (RMFC) system som kan blive drevet af en blanding af methanol og vand. Brændslet bliver her reformeret til en hydrogen-rig gas, dog med en ekstra formation af Kulmonoxid CO og CO_2. CO er kendt som en forgiftning af lav temperatur brændselsceller, dog har Høj Temperatur "Polymer Electrolyte Membrane" (HT-PEM) brændselsceller den fordel at de kan håndtere højere mængder af CO uden af blive forgiftet. HT-PEM brændselsceller har mulighed for at operere ved forhøjede temperature (over 100 °C) og bruger phosphorsyre som proton leder. Dette gør at HT-PEM brændselsceller kan tolerere højere mængder af CO (op til 3 %) uden at tage varig skade, hvor en lav temperature PEM (LT-PEM) brændselscelle kun kan håndtere CO op til 1 ppm.

Ved at bruge HT-PEM brændselsceller i et RMFC system gør at man kan udnytte udstødningsgassen fra brændselscellen til at opvarme en katalytisk brænder. Udnyttelsen af den overskydende hydrogen gør dog RMFC systemet mere kompliceret fordi mængden af hydrogen kan variere afhængig af methanol tilførslen, brændselscellens forbrug og gassens sammensætning ud af reformeren.

Denne PhD afhandling har derfor fokuseret i at undersøge gas sammensætningen ud af reformeren og dens påvirkning af HT-PEM brændselscellen. Derudover er dynamikken og kontrol af RMFC systemet blevet studeret og har desuden være en primær motivation for dette projekt.

En 17-celle HT-PEM brændselscellestak er blevet testet ved forskellige temperature ved både tør hydrogen og reformat gas. Testen på HT-PEM brændselscellestakken bekræftede modstanden overfor CO forgiftningen. Derudover, blev en lavere ydeevne fundet under lavere støkiometri på både hydrogen og luft siden. Brændselscellen var analyseret ved hjælp af polariseringskurver og "Elektrochemical Impedance Spectroscopy" (EIS) teknikker. EIS teknikken viste hvordan brændselscellen var påvirket ved at isolere de forskellige tab i brændselscellestakken. En dynamisk model blev lavet på baggrund af polariseringskurverne og ved et stigningsskift på den elektronisk belastning.

En dynamisk model af RMFC system blev lavet og inkluderede dynamikken af reformeren, brændselscellen, brænderen og fordamperen. Den dynamiske model blev baseret på en 5kW elektrisk RMFC system med en 120 celle HT-PEM brændselscellestak. Den dynamiske model var lavet med fokus på at analysere temperaturfordelingen i systemet og for at lave en model der kan bruges til at teste kontrol teknikker. Et kaskade kontrol system er blevet testet med RMFC modellen, hvor kontrollen bruger reformer temperaturen til at kontrollere brænderens temperature sætpunkt. En kaskade kontroller er mulig fordi at brænderens kontrol loop er meget hurtigere end reformerens. Tidskonstanten for brænderen er fundet til 10 sekunder og er for reformeren 97 sekunder. Brænderens temperatur er kontrolleret ved hjælp af brænderens blæser, men den implementere kontroller gør det muligt at sænke støkiometrien til et lavere niveau, derved forhøjer effektiviteten på systemet og sænker brænderens temperatur. Et minimum tilladt stoichiometri på 1.3 var brugt og dette gav en elektrisk system effektivitet på 29 %, som svare til en operationel pris på €0.22/kWh(1.64 kr/kWh) uden distributions omkostninger og skatter.

Baseret på temperaturen af reformeren er det muligt at tilpasse gas kompositionen under operation. Dette gøres ved at udnytte viden omkring gassen konposition under forskellige reformer temperature og methanol flowet. Et eksempel på et stabilt slip på 2 % er præsenteret og bekræfter en on-line gas komposition fastsættelse.

Acknowledgments

The time have come where the end of this scientific journey has come to an end and I will try here to express my gratitude to the people who have helped me. First, I would like to thank my supervisor, Søren Juhl Andreasen, who has been letting me explore the topics that I found exiting, giving me good feedback, and putting up with me when things get a bit too creative. I would also like to thank Samuel Simon Araya for the great discussions and help with writing this thesis.

My colleagues at the Department of Energy Technology also deserves thanks, for all the good times we had together and especially the technical staff in the lab for their help and feedback in the process of creating this project. I would also like to thank my office mates Kristian Kjær Justesen and Christian Jeppesen for the many great discussions, both scientific and otherwise.

A big thanks to the good people at the University of California, Irvine for the great time I had under my study abroad. I would like to especially thank Professor Jack Brouwer for the supervision during my stay and for giving me the opportunity to visit their department.

A special gratitude to the EUDP programme for providing funding for this project through the COmmercial Breakthrough of Advanced Fuel Cells II (COBRA II) project. A thanks also goes to the Serenergy A/S for supplying me with the components used in this work.

Finally a big thanks to all the friends and family for the support during my studies and a special gratitude to my girlfriend who has been a invaluable companion and support.

Contents

List of Figures

Nomenclature

CH_3OH Methanol

CO_2 Carbon Dioxide

CO Carbon Monooxide

H_2 Hydrogen

H_3PO_4 Phosphoric Acid

AFC Alkaline Fuel Cell

ATR Auto-thermal Reforming

CHP Combined Heat and Power

CL Catalyst layer

CPE Constant Phase element

CVM Cell voltage monitor

DMFC Direct Methanol Fuel Cell

EIS Electrochemical Impedance Spectrum

GDL Gas difusion layer

HF High Frequency

HT-PEMFC High Temperature Polymer Electrolyte Membrane Fuel Cell

I-V Current-Voltage

IF Intermediate Frequency

LF Low Frequency

MCFC Molten carbonate Fuel Cell

MEA Membrane Electrode Assembly

OCV Open circuit voltage

PA Phosphoric Acid

PAFC Phosphoric Acid Fuel Cell

PBI Polybenzimidazole

PEM Proton Exchange Membrane

pp percentage points

ppm parts per million

PV Photovoltaics

SOFC Solid Oxide Fuel Cell

SR Steam Reforming

UPS uninterruptible power systems

WGS Water-Gas-Shift

Part I

Introduction

Chapter 1

Introduction

1 Renewable Energy Technology

Increasing investments in renewable energy in the last decade have shown a significant focus in decreasing the use of fossil fuels. Based on a report from IEA [2014a] more than $1600 billion was, in 2013, invested in providing energy for the world's consumers, which is more than twice the amount of what was spend in 2000. The biggest part of the current investment, more than $1100 billion, is destined to the extraction and transportation of fossil fuels, oil refining, and the construction of fossil fueled power plants. The current annual investment in renewable resources is $250 billion, which is a step down from the high point of $300 billion in 2011. The investment to improve energy efficiency was $130 billion in 2013 [IEA, 2014a].

The increasing annual investment in renewable resources also increases the research in power conversion, smart distribution power networks, and energy storage. Despite the increasing global energy consumption, particularly in developing countries, the global carbon emissions associated with energy consumption remained stable in 2014 [Sawin et al., 2015]. In fig. 1.1 the progress of CO_2 emissions can be seen from 1990 to 2014 by region and it illustrates how China has expanded its fossil-powered stations. The largest emitting countries are shown in fig. 1.2 where the most significant is china with 30%, United states 15%, European Union 9.6%. The top three countries/regions account for 54% of the total global emissions. The emissions from 2013 to 2014 increased with 0.9% in China and the United States, where the European Union saw a decrease of 5.4% in 2014. A significant decrease in global emissions can be seen

in 2008 and can be explained by the economic crisis [Olivier et al., 2015]. CO_2 is by far the dominating part of the greenhouse gas emissions and represents about 70% of the global human caused emissions in the energy sector [IEA, 2014b]. Approximately 17% of CO_2 is estimated to be from the burning fuel in an internal combustion engine (ICE) [Park et al., 2015].

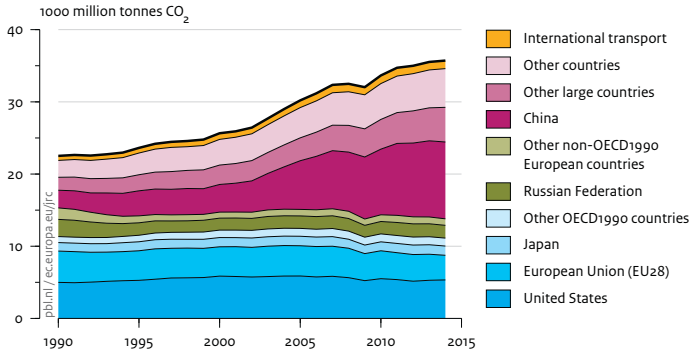

Source: EDGAR 4.3 (JRC/PBL, 2015) (1970-2012; notably IEA 2014 and NBS 2015); EDGAR 4.3FT2014 (2013-2014): BP 2015; GGFR 2015; USGS 2015; WSA 2015

Fig. 1.1: Global CO_2 emissions per region from fossil-fuel use and cement production 1990 -2014. *Reproduced from Olivier et al. [2015]*

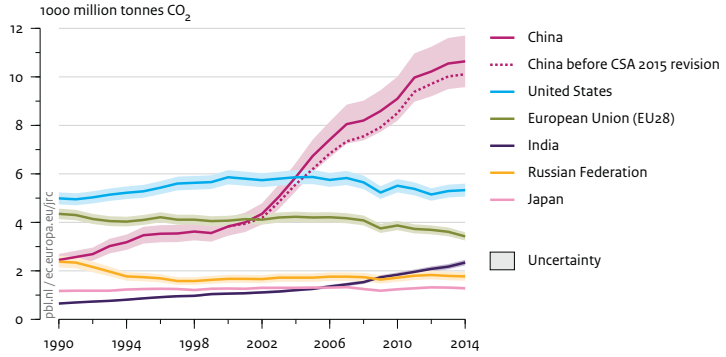

Source: EDGAR 4.3 (JRC/PBL, 2015) (1970-2012; notably IEA 2014 and NBS 2015); EDGAR 4.3FT2014 (2013-2014): BP 2015; GGFR 2015; USGS 2015; WSA 2015

Fig. 1.2: CO_2 emissions from fossil-fuel use and cement production in the top 5 emitting countries and the EU. *Reproduced from Olivier et al. [2015]*

Even though the greenhouse gas emissions have stabilized the need for a continued transition from the current energy system, which is based mainly on fossil fuels, more renewable energy sources is needed. The awareness of using renewable resources and energy efficiency is rising, both because of the benefits on the climate and the new economic opportunities. Global renewable

energy consumption in 2013 is estimated at 19.1% and growth in generation and capacity is continued in 2014. 58.5% of the investments in global power capacity in 2014 was based on renewable energy and was mainly focused on solar Photovoltaics(PV), wind and hydro power. By the end of 2014, estimates show global power generation capacity was 27.7% renewable sources, which supplies estimated 22.8% electricity. [Sawin et al., 2015].

By March 2012 the Danish Energy Agency [Danish Ministry of Climate, 2012] proposed a new energy agreement for reaching the danish goal of 100% renewable energy in Denmark by 2050. This goal is focused on providing a wide range of large investments into energy efficiency, renewable energy, and the energy system. The current goal is, by 202,0 to supply 50% of the electricity consumption by wind power and more than 35% renewable resources in final energy consumption. Further, a decrease of 7.6% in gross energy consumption compared to 2010 and 34% reduction in greenhouse gas emissions [Danish Ministry of Climate, 2012].

To reach these goals a mix of renewable sources can be introduced and implemented in the energy sector. A fuel cell is a versatile renewable energy conversion device and is expected to be one of the technologies that will be used to achieve the danish 2050 energy goals. If fuel cells are supplied with hydrogen derived from renewable energy sources (wind, biomass, solar etc.), they can be 100% CO_2 neutral and can positively influence the climate [Ehteshami and Chan, 2014; Barbir, 2005].

Increased share of renewable energy sources, such as wind and solar, increases the intermittency of power generation, and therefore, energy storage and conversion solutions are necessary to balance the grid. If a 100% supply of energy from renewable is to be reached, it will require the use of alternative storage solutions, both on a daily and seasonal term [Andresen et al., 2014]. These storage solutions could be batteries or a production of hydrogen through electrolysis, which also shows to be one of the most CO_2 friendly production methods, if it is supplied from a variety of sources (solar, wind, nuclear, geothermal) [Mueller-Langer et al., 2007].

Therefore, in combination with other renewable technologies, fuel cells can help reduce the problems with fossil fuel energy production, which includes air and noise pollution, greenhouse gas emissions (GHG) and the economical dependency on oil. Fuel cells have other significant advantages, compared to many other technologies, in that they can utilize a wide range of fuels, such as methane, methanol, biogas, etc. Flexibility in fuel source and clean energy is why the fuel cell technology is a suitable candidate for a sustainable energy future.

2 Fuel cell fundamentals

A fuel cell is a technology where chemical energy is converted from a fuel into electricity with chemical and electrochemical reactions of hydrogen and oxygen. Compared to batteries, a fuel cell requires a continuous supply of fuel and oxygen to be able to sustain the chemical reaction, whereas the chemicals present in the battery react to generate an electromotive force.

The fuel cell was first discovered in 1802 during the experiments by Humphry Davy, who was studying the chemical effects and their relation to electricity, which later would become known as electrolysis. Later in 1839 a Welsh lawyer, Sir William R. Grove, demonstrated the process that chemical decomposition could be reversed, and hydrogen and oxygen could be combined to form water [Fuel Cell Today, 2015]. The alkaline fuel cell was one of the first viable systems created by F. T. Bacon at Cambridge in 1950s and later demonstrated the use in agricultural tractors, power cars, offshore navigation equipment, boats, fork lifts and so on [Larminie and Dicks, 2003].

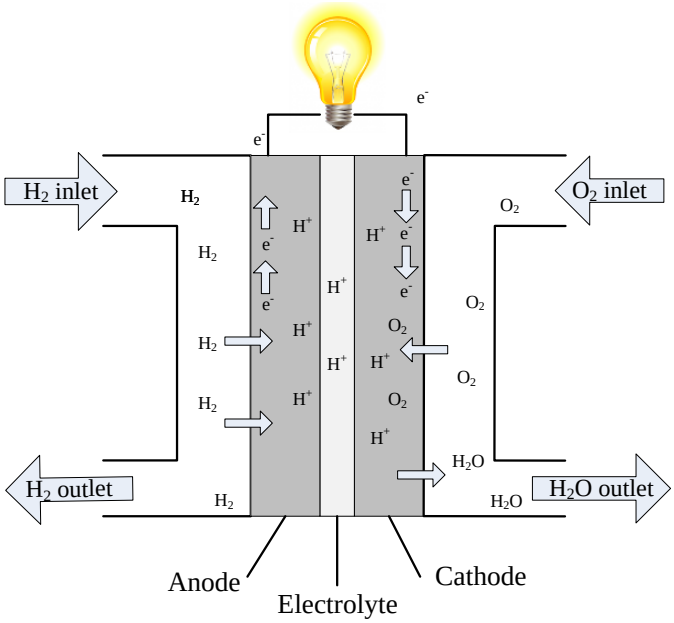

Fig. 1.3: Schematic of a proton conducting fuel cell.

The fuel cell technology was appealing for many scientists and engineers during the United States' space endeavors as it solved many of the problems with power in orbit. It was much lighter than any type of battery, less dangerous

than nuclear power, and a much simpler than any solar PV technology available at that time. NASA used the first PEM fuel cell in the 'Project Gemini' space missions. The PEM fuel cell only ran about 500 hours, but was sufficient for the early missions. Because of problems with water, management choose to use the alkaline fuel cell in later missions. Development of PEM fuel cells over recent years have brought current densities up to $1\,\mathrm{A/cm^2}$ and NASA have again chosen PEM fuel cells as the preferred option for space travel [Larminie and Dicks, 2003]. At the early age of PEM fuel cells the amount of catalyst was about $28\,\mathrm{mg/cm^2}$ platinum and has since been reduced to today's levels of $0.2\,\mathrm{mg/cm^2}$ or less [Martin et al., 2015].

Fuel cells are composed with an anode, a cathode, and an electrolyte that allow charged ions to pass between the sides of the fuel cell. A schematic of a hydrogen fuel cell can be seen from fig. 1.3. The anode and cathode are coated with a catalyst which causes the fuel to perform an oxidation reaction, where the hydrogen generates two hydrogen ions(protons) and two electrons. This reaction is seen from eq. 1.1. The electrons are passed through an external circuit and thereby producing a current of electricity. At the cathode side the hydrogen ions, electrons, and air are combined and react to form water as seen in eq. 1.2.

$$Anode : \mathrm{H_2} \leftrightarrow 2\mathrm{H^+} + 2\mathrm{e^-} \tag{1.1}$$

$$Cathode : \frac{1}{2}\mathrm{O_2} + 2\mathrm{H^+} + 2\mathrm{e^-} \leftrightarrow \mathrm{H_2O} \tag{1.2}$$

The temperature of a fuel cell can vary significantly depending on the material and type of fuel cell. The single cell fuel cell outputs an operational voltage of 0.6-0.8 V and to achieve a higher voltage the fuel cells can be put in series, also known as a fuel cell stack. The voltage can be determined based on the number of cells connected, stack temperature, and the type of electrode used. A simplified schematic of a fuel cell stack can be seen in fig. 1.4.

All the different types of fuel cells are able to be stacked together, however, the chemistry in the fuel cells are different. This is explained in the next section.

Types of fuel cells

Other than the practical issues such as material and manufacturing costs, it is still a problem that hydrogen is not a readily available fuel. To solve this

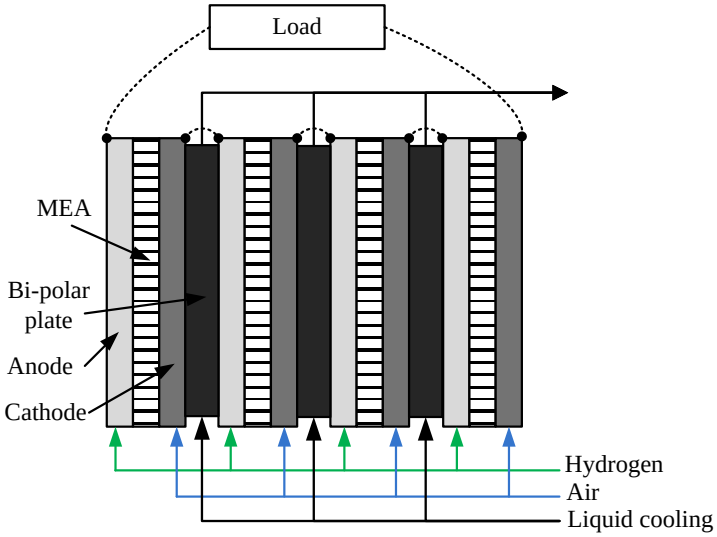

Fig. 1.4: Fuel cell stack with 4 cells in series. Bipolar plates separate the anode and cathode with a membrane sandwiched in between

problem many fuel cell types have been tested and the different types can be distinguished by the electrolyte they use. A list of common type of fuel cells can be found in table 1.1. The table shows the mobile ion, the operating temperature, and a typical use for the fuel cell.

A common way to operate a fuel cell is shown in fig. 1.5. The system consists of a hydrogen tank and an air compressor as input for the fuel cell. The hydrogen output is either a closed- or open-ended output. For a closed-ended system the hydrogen output is closed with a purge valve and is opened in short bursts at given interval corresponding to the power output from the fuel cell stack. This purge valve opening is to avoid an inert atmosphere inside the fuel cell stack. The duration of the purge depends on the size and pressure of the stack as long as enough gas is replaced.

An open-ended fuel cell is designed with an open purge valve, as shown in fig. 1.5, and has a constant flow of hydrogen through the fuel cell. The flow required in the fuel cell is shown in eq. 1.3

$$FC_{\mathrm{H}_2}[kmol/s] = \frac{i \cdot n_{cell} \cdot A_{cell}}{2 \cdot F} \cdot \lambda_{\mathrm{H}_2} \tag{1.3}$$

where i is the current, n_{cell} is the number of cells, A_{cell} is the cell area, F is

Table 1.1: Different types of fuel cells [Larminie and Dicks, 2003].

Fuel cell type	Mobile ion	Operating temperature	Typical use
Alkaline (AFC)	OH^-	50 - 200 °C	Used in early space vehicles
High Temperature Proton Exchange Membrane Fuel Cell (HT-PEMFC)	H^+	120-200°C	Used for stationary, vehicle and mobile applications
Proton Exchange Membrane Fuel Cell (PEMFC)	H^+	30-100°C	Most widely used FC. Used for stationary, vehicle and mobile applications
Direct methanol (DMFC)	H^+	20-90 °C	Suitable for small portable electronic systems
Phosphoric acid (PAFC)	H^+	150-210 °C	Used for stationary power applications. Large number of 200-kW CHP systems in use
Molten carbonate Fuel Cell (MCFC)	CO_3^{2-}	650 °C	Used for stationary power applications
Solid oxide Fuel Cell (SOFC)	O^{2-}	1000 °C	Used for all size stationary power applications, 2kW to multi-MW

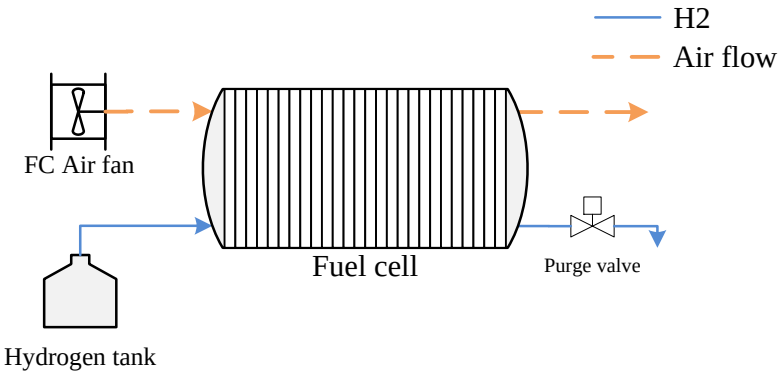

Fig. 1.5: Typical hydrogen fuel cell system design

the Faraday constant and λ_{H_2} is the stoichiometry used for the fuel cell. The stoichiometry is a ratio between the input fuel and the fuel used in the fuel cell. A stoichiometry of $1 - 1.25$ is commonly seen for PEM fuel cells with pure hydrogen. [Liang et al., 2009].

Some of the applications where fuel cell power can be used is for backup power or uninterruptible power systems (UPS), Combined heat and power system(CHP) for domestic houses, or for transport applications like boats, cars and buses. Using the fuel cell as an range extender can have some advantages which are described below.

2.1 HTPEMFC as range extender

The use of a fuel cell system as a range extender have been studied in paper [D] where a $\sim$11 kWh battery pack and a 5kW HTPEM fuel cell stack are tested and evaluated. The New European Drive Cycles(NEDC) was run twice on the battery pack with and without the fuel cell as a range extender. The fuel cell stack operated at a voltage of 79.5 V and a current of 21.5 A which is approximately 1.6 kW. The DC-DC converter was set to a constant output voltage that matched the desired charging voltage of the battery pack.

In fig. 1.6, it can be seen that running with the range extender superpositions the power output. This means that when the power is positive the battery is charged and when the power is negative the battery pack is discharged.

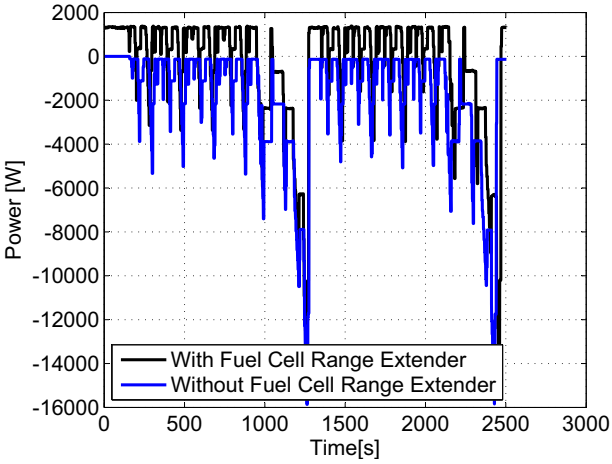

Fig. 1.6: Comparison of the power using two NEDC's. Two experiments was conducted, one with a range extender ,and on without. *Reproduced from [Andreasen et al., 2014]*

By integrating the two power profiles in fig. 1.6 the total energy cosumed can be compared and the effect of the range extender can be evaluated. The comparison can be seen in fig. 1.7 and it can be seen how the fuel cell stack drastically increases the potential range of the car. The figure shows that initially the fuel cell delivers more total energy to the battery.

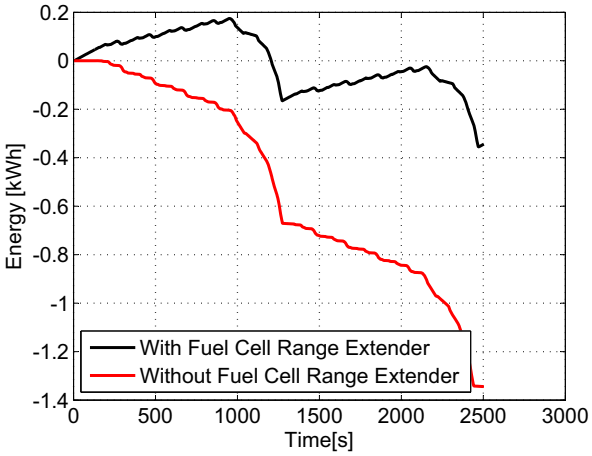

Fig. 1.7: Battery range with and without range extender. *Reproduced from [Andreasen et al., 2014]*

The figure shows that even though the power output, from the fuel cell, relatively low(1.6 kW) there is still a significant gain in using fuel cells as a range extender. This work show that the combination of a battery pack and a fuel cell can either extend the range of the vehicle or make it possible to decrease the size of the battery pack.

This work uses dry hydrogen as the source for the HTPEM, however, alternative methods for powering the fuel cell is available and described below.

3 Hydrogen carriers

Several fuel cell types are available and all of them have advantages and disadvantages when it comes to the input fuel. A flowchart of common production routes from fuel to fuel cell can be seen in fig. 1.8. The figure starts out with the resources; petroleum, natural gas, coal, nuclear, and solar/wind. The resource can be followed from raw material, through the different processes and sorted into a range of fuel cells. Intermediate products are listed which can illustrate mediums, which are able to be transported and converted on-site or possibly

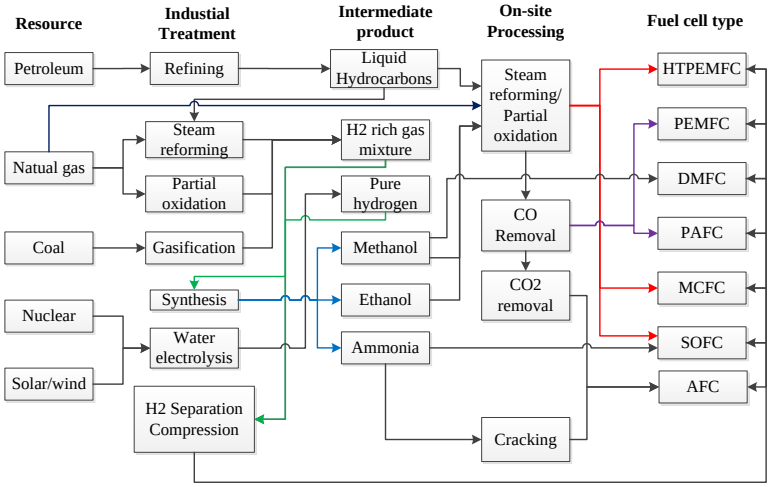

Fig. 1.8: Resource processing and production for the different fuel cells. *Reproduced from Prigent [1997]*

cleaned, compressed, or liquefied.

Each full cell, illustrated in fig. 1.8, has a selected available fuel, however common for them all is pure hydrogen(Except DMFC which only runs on pure methanol and water). It can also be seen that it is possible to produce hydrogen from all listed resources via reforming, gassification, or electrolysis [Mueller-Langer et al., 2007]. The SOFC fuel cell has the possibility of utilizing several gas compositions, including using CO, CO_2 and ammonia as fuel. It operates at a temperature of 650 °C to 1000 °C which means high energy loss and relatively long start-up time [Fuerte et al., 2009]. Using ethanol in steam reforming have been studied extensively and shown good results, however, the temperature is around 700 °C which also is high compared to methanol. Methanol can be steam reformed at temperatures at 180 °C to 250 °C, which makes it a good candidate when operating with fuel cells [Lee et al., 2004; Yong et al., 2013; Justesen et al., 2013].

The production of hydrogen through steam reforming is not a new idea. The Danish chemist J. A. Christiansen discovered, during his study at Copenhagen University in 1921, that a CH_3OH and H_2O mixture sent over reduced copper at 250 °C would convert to a gas mixture containing three parts hydrogen and one part carbon dioxide. The gas was also discovered to contain traces of carbon monoxide [Christiansen, 1921; Christiansen and Huffman, 1930; Christiansen, 1931].

To ease the introduction of fuel cells in transportation a liquid hydrogen carrier could be a solution as the distribution network is readily available. Several studies have investigated the use of alternative liquid carriers and have compared them to a system with compressed hydrogen [Niaz et al., 2015] [Durbin and Malardier-Jugroot, 2013]. Solutions with metal hydrides and liquid storage (−253 °C) have been studied and they are all heavy and take a significant amount of space and are not suitable for a mobile application. Compressed hydrogen is currently used for many applications, however, the cost of production, storage, and distribution is high. The current development in using hydrogen in automotive applications is using compressed hydrogen at about 70 MPa (700 Bar) because of the reliability and to simplify the system [Jorgensen, 2011]. However, the high hydrogen pressure introduces several challenges with storage as the tank needs to be reliable and safe. Furthermore, because hydrogen is the smallest molecule it is expensive to compress relative to other gases, it is highly diffusive, buoyant, and can cause material embrittlement [Cotterill, 1961].

Using a fuel cell system with a liquid fuel would solve many problems with distribution and storage. A fuel cell driven on methanol can be achieved with the Direct Methanol Fuel Cell (DMFC), which uses the methanol directly in the fuel cell. The advantage of a DMFC is the simplicity in the design, however, it is not commonly used because of a lower efficiency(up to 40%). The DMFC could be suitable to replace the batteries in portable devices, however, the technology still needs to mature before implementation [Mekhilef et al., 2012].

Using methanol in a steam reforming system have shown promise as a technology with both HTPEM and LTPEM fuel cells. However, the use of LTPEM fuel cells requires a CO cleaning unit, which complicates the system [Ercolino et al., 2015]. The use of HTPEM fuel cells avoid this problem because the HTPEM fuel cell can tolerate a small amount of CO.

3.1 Reformed methanol fuel cell system

Steam reforming is a method for producing hydrogen using a device called a reformer which reacts steam at high temperatures with a fossil fuel, such as methane, methanol, gasoline, diesel or ethanol. The steam reforming process of methanol can be seen from eq. 1.4.

$$CH_3OH + H_2O \rightarrow 3H_2 + CO_2 \qquad \Delta H^0 = 49.2 \frac{kJ}{mol} \tag{1.4}$$

Partial oxidation is also a possibility if oxygen is available and this reaction can be seen from 1.5.

$$CH_3OH + \frac{1}{2}O_2 \rightarrow 2H_2 + CO_2 \qquad \Delta H^0 = -192.2\frac{kJ}{mol} \tag{1.5}$$

The endothermic steam reforming reaction reforms methanol and water into hydrogen and carbon dioxide (CO_2) at about 180 to 300℃. At these temperatures a decomposition of methanol is occurring and introduces carbon monooxide (CO) into the gas. This reaction is shown as eq. 1.6.

$$CH_3OH \rightarrow 2H_2 + CO \qquad \Delta H^0 = 128\frac{kJ}{mol} \tag{1.6}$$

Some of this CO is removed by the water gas shift reaction shown in

$$CO + H_2O \rightarrow H_2 + CO_2 \qquad \Delta H^0 = -41.1\frac{kJ}{mol} \tag{1.7}$$

The CO content is not removed completely with this process and is documented in this PhD study, which shows a CO content from 0to 2 % CO based on operating temperature and methanol flow.

The steam reforming reaction, shown in eq. 1.4, is an endothermic reaction which means $49\,4\frac{kJ}{mol}$ of heat needs to be added to the reaction. With partial reforming $192,2\frac{kJ}{mol}$ is released from the reaction, however, the result is a lower hydrogen output. The advantage with partial reforming is the possibility to run the process without external heating.

The use of reformate gas in a PEM fuel cell requires an open ended fuel cell system, as shown in fig. 1.5, as the CO_2 and CO is accumulating in the fuel cell and will significantly decrease performance. The amount of hydrogen in the output stream from the fuel cell depends on the fuel cell current and the hydrogen stoichiometry. This means that the amount of hydrogen is higher, compared to the hydrogen used in the fuel cell. The excess hydrogen from the fuel cell can be used as a fuel for a burner in the reforming system. A reforming system utilizing the excess fuel in a burner can be configured as shown in fig. 1.9.

A steam reforming system introduces a CO amount up to 1 % into the gas stream, which would be a significant degrading issue in a low temperature PEM (LTPEM) fuel cell. To use a LTPEM fuel cell in a system with a steam reformer, an extra Water-Gas-Shift (WGS) cleaning unit is normally used [Wiese

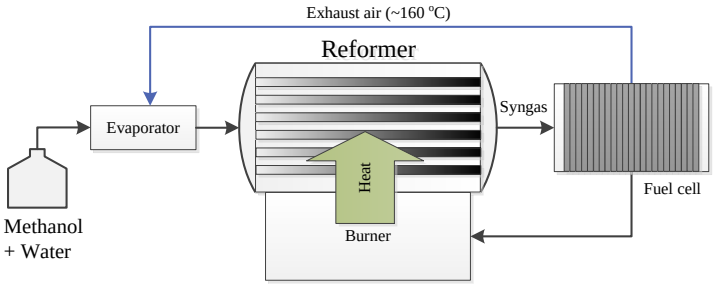

Fig. 1.9: Schematic of a methanol reforming fuel cell system.

et al., 1999]. High temperature PEM (HTPEM) fuel cells have shown good performance towards CO up to 1%, which would be ideal to be used with a reformer [Korsgaard et al., 2006] [Andreasen et al., 2011a]. This means that with careful temperature control the cleaning unit can be avoided. The temperature of a HTPEM fuel cell (160-200 °C) is close to that of the reformer, which means a closely integrated system solution is possible.

To use methanol reforming and a fuel cell in a system, a careful control of the output gas is needed to avoid hydrogen starvation in the fuel cell. Previous work on HTPEM fuel cell degradation was done by Zhou et al. [2015a] and showed accelerated degradation based on hydrogen starvation. This starvation can occur in operating conditions during a rapid load increase or during startup/shutdown procedures. To avoid this, a constant load and fuel flow are needed and are used by many commercial systems. If this strategy is used in a mobile application it will require an additional amount of energy storage, like a battery, to be used in case of a rapid change in load. If the change of operating conditions can be carried out without losing significant stability or performance, the battery size needed would be smaller. For this reason, a control system would significantly increase the usability of the technology.

3.2 Control of RMFC system

Using the exhaust gas as heating for the reforming process requires the system to be controlled. Several factors in a RMFC system can cause an emergency shutdown or in worst case damaging components in the system. One of the components which is subjected to degradation is the HTPEM fuel cell. As the gas output from the reformer is a mix of H_2, CO_2, CO, CH_3OH and water, a careful observation of the fuel cell needs to be done during the operation. Because exhaust hydrogen from the fuel cell is used as a fuel for the burner, as shown in fig. 1.9, the operation of the fuel cell needs to be supplied with

the correct amount of fuel. If the fuel cell is not supplied with enough fuel it would be subjected to significant degradation, this issue is discussed further in chapter 2 of this thesis.

If the fuel cell is supplied with too much fuel, the excess fuel will be led directly to the burner. A consequence of this oversupply of fuel can be damaging to the burner itself or the components connected. An oil circuit is used in this work for the purpose of increasing the control of the burner and reformer temperature. The temperature of the reformer is critical to get a well suited gas composition for the HTPEM fuel cell and the temperature of the burner may be easier to control. The temperature of the different components in the system is investigated in Chapter 3 where a model in Matlab Simulink is created.

A model of the system is suitable to investigate the dynamics and temperature of the components. Additionally, a model can be used as a simulation tool to investigate control system designs. A design of a control system for the fuel cell system is described in Chapter 5. There is currently, to the authors knowledge, no suitable way to measure the hydrogen flow or the CO content *in-situ* of the reformate gas. This lack of knowledge requires a careful study of the reformer in the system and thereby a knowledge of the other components. An investigation into the reformate gas output from the reformer used in this work is presented in Chapter 3. If the reformate gas composition and flow rate are known it is possible to control the input methanol flow to match the required fuel for the fuel cell and the burner. This also means that more dynamic operation is possible during changes in load or ambient changes.

Chapter 2

High Temperature PEMFC

1 Background

A polymer electrolyte membrane fuel cell (PEMFC) is a type of fuel cell that uses a solid polymer as an electrolyte and is normally classified as a low temperature fuel cell. A PEM fuel cell is one of the most widely used fuel cells available and is increasing its dominance in many sectors. Molten carbonate fuel cells rival the PEM fuel cell by the amount of Megawatts used, as these fuel cells are mainly used in power stations. 88% of the total fuel cell shipments in 2012 were PEMFC, and as the fuel cell type is the preferred type for mobile applications the trend is likely to continue [Fuel Cell Today, 2013].

The fuel cell investigated in this research is an offspring to PEM fuel cells which operates at a higher temperature. The fuel cell uses an acid-based polymer, instead of a water-based in the PEMFC, because the temperature is higher than 100℃. This type of fuel cell is called a High Temperature Proton Exchange Membrane Fuel cell (HT-PEMFC) and excels in having a higher tolerance to impurities such as CO, higher heat rejection, and simpler water management with respect to LT-PEMFC, which operates under 100℃[Wang et al., 2011; Li et al., 2009].

The higher tolerance towards impurities and higher temperatures open HT-PEMFCs up for additional uses and applications. The fuel can be made from a variety of sources and the excess heat from the fuel cell can be utilized for a larger range of applications. HT-PEM fuel cells can be a solution to many of the distribution and storage problems as the fuel cell can be operated on hydrogen

reformed from hydrocarbons and liquid carriers, such as ethanol, gasoline, and methanol. The convenience in utilizing the already present infrastructure can impact the introduction of fuel cells positively as the cost of changing the infrastructure can be delayed or eliminated. The advantages of simpler design and integration with reformers will in time reduce cost enough to make HT-PEMs an attractive power source for automotive and stationary applications, like a micro-Combined Heat and Power (μ-CHP) system [Zhang et al., 2006; Andreasen et al., 2011b; Romero-Pascual and Soler, 2014].

This chapter investigates the limits and effects of stoichiometry and temperature on degradation and durability issues in fuel cells, especially the presence of CO, CO2 and water. The fuel cell tested is used for creating a model for further use in system integration and control.

2 HT-PEMFC Fundamentals

The difference between a PEM and a HT-PEM fuel cell is almost exclusively the temperature where it operates. The HT-PEM fuel cell operates at 160 °C to 180 °C whereas a PEM fuel cell operates at about 60 °C. The half-cell reactions are identical and illustrated in fig. 1.3. Hydrogen is fed into the anode side and oxygen on the cathode side. The hydrogen oxidation reaction and the oxygen reduction reaction will take place at the respective sides to produce electricity, heat, and water. Water is used as the proton conductor in a PEM fuel cell, using a Nafion membrane, which means the humidification of the fuel cell is essential for the operation. Because of the elevated temperature, a HT-PEM fuel cell is not able to use liquid water and instead uses a PBI membrane doped with phosphoric acid. In the absence of water, phosphoric acid can conduct protons and will ensure a high efficiency at high temperatures.

The PBI membrane is sandwiched in between an anode and cathode Gas Diffusion Layer (GDL) and then a bipolar plate. A schematic of a single fuel cell with bipolar plates is shown in fig. 2.1. The bipolar plate is made from an electric conductive material, such as graphite or polymer composites [Planes et al., 2012], for each side and the air and hydrogen are distributed around the cell. Some fuel cells are equipped with flow channels for better heat distribution and cooling.

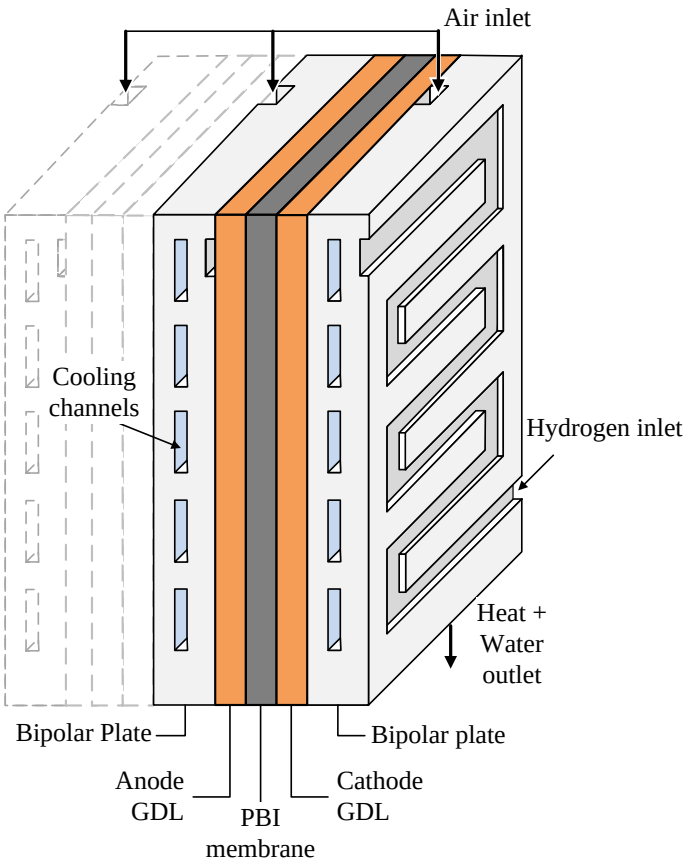

Fig. 2.1: Schematic diagram of a PEM fuel cell. The single cell consists of a PBI membrane sandwiched between GDL and bipolar plates.

2.1 Membrane Electrode Assembly, MEA

For the majority of PEMFCs the proton exchange membrane is based on perfluorosulphonic acid (PFSA) polymers, like Nafion®. The membrane has a high conductivity, excellent chemical stability, mechanical strength, and flexibility. However, for it to function, it will need to be in a highly hydrated state and is therefore limited in temperature up to 80℃in order to retain a high water content in the membrane. If operated above 100℃, at ambient pressure, the water evaporates and a pressure of 15 atm is required if saturated water vapour, if liquid water is required [Li et al., 2009]. This pressure will increase the complexity of the fuel cell significantly if saturated water is used during operation. To avoid water as the proton conductor, an acid-doped membrane is an effective

approach to use in a fuel cell. Phosphoric acid shows good proton conductivity, thermal stability, and low vapour pressure at elevated pressures. The breakthrough for HT-PEM was the introduction of polybenzimidazole (PBI) for acid-doped membranes. The first patent on fuel cells and PBI membranes was issued to Savinell's group [Savinell and Litt, 1996] on the use of H_3PO_4-doped PBI membranes. The HT-PEM excels at having good protonic conductivity at high temperatures, close to zero electroosmotic drag, low gas permeability, and low methanol crossover [Bouchet, 1999; Martin et al., 2015].

The MEA consists of electrodes on both sides of the membrane. The electrodes are based on a combination of a porous Gas Diffusion Layer (GDL) and a catalyst layer (CL). The GDL consists of a carbon fiber layer and is there to disperse the fuel over the Catalyst Layer. The GDL also acts as an electric connection to the flow plates.

2.2 Fuel cell degradation

Durability and degradation issues are currently one of the last challenges to overcome in the introduction of HT-PEM fuel cells. If combustion engines are to be replaced, an inexpensive, durable, and efficient technology needs to be tested for durability. Durability is stated as the ability to resist permanent change over time. This means that durability does not lead to catastrophic failure but indicates the decrease in performance over time. Reliability is an indication of the ability to keep performance at normal conditions for a period of time. It also includes catastrophic failures and performance over an acceptable level. [Wu et al., 2008]

Even though numerous advantages of using HT-PEM fuel cells exist, some issues still need to be addressed before a wide commercialization is possible. Durability and degradation are still being studied and a lot of research is done in this area. Cost is a significant challenge that is being addressed, mainly by reducing the platinum (Pt) catalyst [Martin et al., 2015].

Degradation is still being researched and is still not fully understood. For PBI fuel cells the most likely degradation mechanism is acid loss, degradation of the polymer, and loss of catalyst activities due to catalyst dissolution, catalyst sintering or carbon support corrosion [Li et al., 2009].

Simon Araya et al. [2014] studied the influence of methanol on a HT-PEM cell, ranging temperatures from 140 to 180°C, and shows an overall negligible effect of methanol-water vapor up to 3 vol-% in the anode gas stream. This study does not consider CO and CO_2 and covers only the methanol-water

effects on the fuel cell. Further studies show that increased methanol feed, up to 8 vol-% for around 1250h, will recover the initial performance if methanol is lowered to 3 vol-% feed. [Simon Araya et al., 2014, 2012a]

Phosphoric acid (H_3PO_4) loss

The phosphoric acid (H_3PO_4) is a crucial element for the HT-PEM fuel cell to operate and therefore a lot of research has been done to reduce the acid loss and strengthen the membranes capability to retain the acid [Li et al., 2009; Park et al., 2015; Wu et al., 2008].

A popular doping method is where the PBI membrane is immersed in an aqueous phosphoric acid solution and an equilibrium is reached after about 50 h at room temperature. During experiments, by Oono et al. [2009], he showed that with a certain temperature and immersion time it is possible to get a specific doping level. Tests with 20, 40 and 60 °C were performed and at 60 °C a doping level of 78% was achieved in 10 min with an 85 % phosphoric acid solution. The same doping level was achieved with 20 and 40 °C though with a doping time of approximately 30 min and 300 min, respectively. All temperatures ended at the same equilibrium at 78 %. The doping level is defined as the percentage ratio of the membrane weight before and after doping [Oono et al., 2009]. The acid doping level is also sometimes defined as the mole ratio between the phosphoric acid(Calculated based on weight measured before and after doping) and the repeating unit of PBI(dry weight) [Martin et al., 2015].

The loss of acid in the fuel cell may occur through different mechanisms like diffusion, capilary transport, membrane compression, evaporator, or leaching. Especially during startup and shutdown leaching is increased by the condensed water as the temperature is lower than 100 °C [Park et al., 2015]. Previous studies have shown promising techniques by using heated cathode air to decrease startup time [Andreasen and Kær, 2008].

Li et al. [2009] shows that a 5kW system running at 160 °C with 2100 g of acid will have an estimated acid loss at 0.6 µg /(m^2 s), which corresponds to about 40.000 h of operation. Acid content can be identified by observing the resistance change in the membrane. Yu et al. [2008] demonstrated a PA loss rate in the order of ng/(cm^2 h) corresponding to a very low percentage loss during a life of 40.000 h.

Catalyst degradation

The common use of catalyst in a HT-PEM fuel cell is carbon-supported platinum(Pt) and is considered one of the most important degradation issues in the HT-PEM fuel cells. The amount of platinum and the surface area is highly significant to the performance of the fuel cell. Zhou et al. [2015a] investigated the decreased cell performance on a HT-PEM and observed a drop in electrochemical catalyst surface area, which was caused by degradation in the catalyst layer and growth of platinum particles. Rapid growth of Pt particles was shown by Liu et al. [2006], where the presence of H_3PO_4 and high temperature suggest a speed up in Pt dissolution and re-deposition. Growth in particles reduces the electrochemical surface area (ECSA) of the catalyst, thereby reducing the performance of the fuel cell [Martin et al., 2015].

Adsorption of impurities on the surface is another factor that can decrease the performance of the platinum-based fuel cells. This performance loss is decreased with higher temperatures and explains the relatively high resistance to impurities as CO at elevated temperatures. Related to methanol-reforming, the CO content is still the most significant negative influence for fuel cells and is an important topic [Li et al., 2003; Zhou et al., 2015b; Andreasen et al., 2011b].

Methanol-based reformate systems show a methanol electrooxidation on the platinum surface and can cause performance loss and lifetime issues. Degradation issues and performance were studied by Simon Araya et al. [2014] and showed a negligible effect with up to 3 vol % of methanol feed in a pure hydrogen fuel cell test with temperatures from 140 °C to 180 °C.

Carbon support degradation

Carbon corrosion is one of the main issues in the HT-PEM fuel cells and is the cause of many critical failures during operation. During the lifetime of a fuel cell, it will sometimes experience carbon corrosion because of a local hydrogen starvation. During startup and shutdown a localized hydrogen starvation can occur as air can be present on the cathode and anode side. Carbon corrosion can lead to a higher fuel cross-over and pinhole formation because of the thinning of the membrane.

Work by Zhou et al. [2015a] have shown that carbon corrosion is occurring during fuel starvation. Previous work by Kang et al. [2010] with starvation on LT-PEM fuel cells show similar results with degradation issues. The process, kinetics, increase with temperature and is thereby more significant with HT-

PEMFC than with LT-PEMFC.

The degradation of the GDL, loss of acid, and membrane damage are some of the main issues in HT-PEM fuel cells. The issues with operating the fuel cell at elevated temperatures show a higher need for more research into the degrading issues and especially in methanol reformate systems, the starvation of oxygen or hydrogen is a potential issue during operation. The following section describes the electrochemical techniques used in this work to characterize the HT-PEM during operation.

3 Characterization techniques

This work utilizes two techniques to characterize the HT-PEM fuel cell stack. The first on the I-V curve and the second is the Electrochemical Impedance Spectroscopy (EIS) technique, which are both presented below.

3.1 I-V curve

The most common way to test and characterize a fuel cell or stack is to do a current sweep, commonly known as an I-V curve. The voltage is measured while the current density is increased over the fuel cell stack or cell. The polarization curve, which is created by this experimental method, shows the losses that can be identified in the I-V curve as activation, ohmic, and mass transport losses. The polarization curve is shown in fig. 2.2,

Polarization curves are a great tool to give a general idea of the performance of the fuel cell, though it is not as detailed and advanced as the Electrochemical Impedance spectroscopy(EIS) method can be. The different losses can be noticed at various parts of the current sweep. It can be seen that the activation losses are being introduced in the lower part of the load sweep. The ohmic resistance is constant at the whole range, as long as the temperature is not changed, and the mass transport loss is introduced at high load.

To generate the polarization curve a semi-steady-state current sweep should be followed, where the current density is changed stepwise and kept for a period of time until a steady state is reached. The current sweep should be measured for both increasing and decreasing load steps, going from open circuit voltage(OCV) to maximum current and reverse. This is to avoid hysteresis, which could be because of the temperature or losses from impurities.

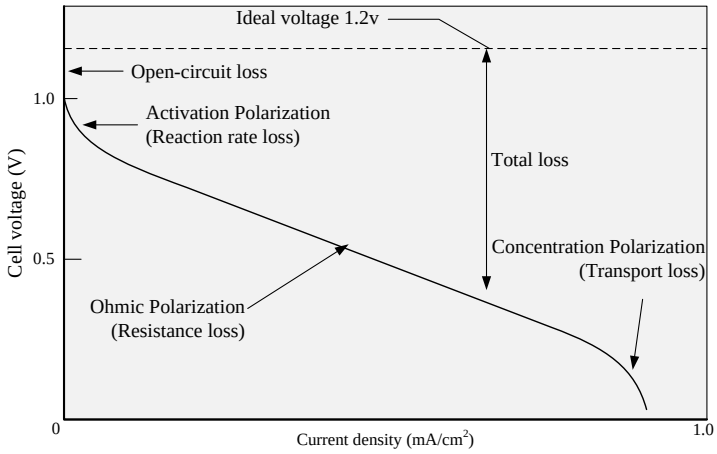

Fig. 2.2: Typical polarization curve with ohmic, activation, and mass transport losses

3.2 Electrochemical Impedance Spectroscopy

A powerful diagnostic tool to characterize a fuel cell during operation is using electrochemical impedance spectroscopy (EIS). EIS is a tool to better understand the voltage losses that occur in the fuel cell which can be identified as; the charge transfer activation or also called the kinetic losses, the mass transfer or concentration losses, and the ion and electron transport or ohmic losses. EIS is an experimental technique that can be used to separate and quantify the losses in the fuel cell under various conditions.

Impedance can be described as the ratio of the voltage to the current in the frequency domain. It is, like resistance, measured in ohm's [Ω] though with the difference that it is operating in alternating current (AC). The symbol for impedance is usually Z and can be represented by a magnitude and a phase. When operating in the DC realm there is no difference between resistance and impedance as the phase angel is always zero. The complex impedance function can be calculated by eq. 2.1.

$$Z = \frac{V_0\ e^{j(\omega t-\phi)}}{I_0 e^{j\omega t}} = \frac{V_0}{I_0} e^{-j\phi} = Z_0(\cos\phi - j\sin\phi) \tag{2.1}$$

Z in eq. 2.1 is the complex impedance response, V_0 [V] and I_0[A] is the ampitude of the voltage and current respectively, ω [rad/s] is the signal frequency, ϕ [rad] is the voltage phase shift and j is the imaginary part. The real ($Z_0(\cos\phi)$) and imaginary part ($Z_0 j(\sin\phi)$) are normally presented on a

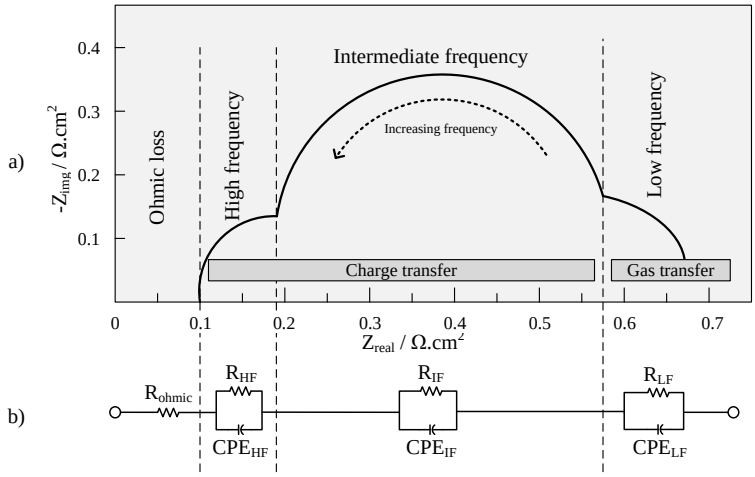

Fig. 2.3: Illustration of (a) Nyquist plot with EIS data and (b) the equivalent circuit model

Nyquist curve with the real part on the x-axis and the imaginary part on y-axis. The imaginary part is typically inverted to represent the data in a more readable condition. Both plots of the real and imaginary parts of the data can also be used. An illustration of a Nyquist plot with EIS data can be seen from fig. 2.3a. The impedance plot shows the high frequencies closest to the origin, with the frequency decreasing to the right.

The ohmic part can be seen as the offset between the origin of the real axis and the intersection between the real axis and the impedance spectrum. This ohmic part is related to the resistive losses in the fuel cell. The different processes that happen in the fuel cell will respond differently depending on the frequency. The low frequencies show the effects of the slower processes like gas transfer, where the higher frequencies show the faster processes like the charge transfer.

By applying equivalent circuit models to the EIS spectrum, it is possible to extract qualitative and quantitative information regarding the sources of losses within the fuel cell. By using a network of ideal circuit elements such as resistors, capacitors, and inductors, it is possible to create an equivalent circuit wherein the internal fuel cell information is located. In fig. 2.3b a typical Equivalent Circuit (EC) model of a HT-PEMFC is represented. The analysis with the equivalent circuit is done by fitting the EC model to the EIS data. However, the interpretation by EC model fitting can be highly ambiguous. Several EC models can be fitted to the same impedance data, which requires a good knowledge of the behavior of the tested device.

The EIS data is collected by perturbing an AC current signal to the fuel cell, which is possible without being intrusive to the operating condition. The AC signal is very small compared to the DC voltage that changes to the fuel cell are minimized. An amplitude of 5% compared to the DC voltage and a signal frequency from 20 kHz to 0.1 Hz are both common ranges [Yuan et al., 2006]. Since EIS is non-intrusive and can be performed *in-situ* a lot of current research uses the tool for optimization, characterization, and diagnostics [Vang et al., 2012; Andreasen et al., 2011b; Cruz-Manzo et al., 2015; Oono et al., 2009; Simon Araya et al., 2012b; Zhou et al., 2015a; Jespersen et al., 2009].

However, the data analysis has mainly been studied off-line and implementing this method as an online diagnostics tool is currently being researched [Hong et al., 2015; Hinaje et al., 2009]. The model fitted to the EIS data is an iterative training process, which requires knowledge and experience with the fuel cell to be valid. An easier way to get a diagnostic insight from a fuel cell is the I-V polarization curve, which is explained below.

4 Short HT-PEM stack experiments

This section will describe the test of a 17 cell HT-PEM fuel cell stack from Serenergy A/S [2013] and is also presented in paper [B]. The test was conducted to investigate the effects of reformate gas on a HT-PEM fuel cell stack under methanol reformed system conditions. The parameters that need to be controlled are stack temperature, current density, anode and cathode stoichiometry. The cell voltage needs to be monitored for each cell in the stack to ensure the stacks working condition. The voltage of the different cells during a polarization sweep will show performance loss and operational limits of the fuel cell. The HT-PEM stack will be tested with a variety of species to test the poisonous and degrading effects. Furthermore, stoichiometry on both anode and cathode is tested to evaluate the effects of fuel starvation.

The test was conducted on a Greenlight G200 with an external cooling cart. The Greenlight test station is equipped with an electronic 12kW load, temperature and humidity controlled cathode and anode gas, selectable gas composition, flow and stoiciometry control, and with a scriptable management system [Greenlight Innovation, 2014].

The test station is able to mix gas on both the anode and cathode side separately, where the anode side is capable of mixing several species(H_2, CO_2, CO, N_2, H_2O). The cathode is similarly able to mix species, though only with hydrogen, nitrogen, and water. The test station with the external cooling cart

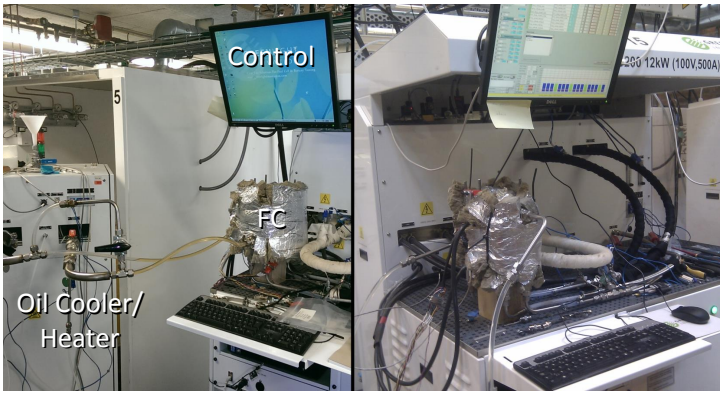

Fig. 2.4: 17 cell short stack HT-PEM fuel cell setup tested on a Greenlight G200 test station.

can be seen from fig. 2.4. Oil input temperature is controlled by a cooler or heater depending on the setpoint from the greenlight system. The stack is a liquid cooled stack and the cooling oil used is the mineral-oil Paratherm NF [Paratherm, 2014]. Each cell is monitored with a cell voltage monitor (CVM) system.

A picture of the fuel cell stack tested can be seen from fig. 2.5. The membranes in the stack are of the type BASF Celtec P H_3PO_4-doped PBI with an active cell area of 165.5 cm^2. The system is equipped with a Reference 3000 from Gamry instruments A/S for EIS experiments. A schematic of the fuel cell system, with EIS, Load, gas mixer, and oil heater/cooler systems, can be seen in fig. 2.6.

4.1 Test procedures

The fuel cell short stack is investigated against parametric changes and different fuel compositions, and the test procedures can be seen from table 2.1. The fuel cell stack was first run at break-in conditions at 160 °C, 0.2 A/cm^2 for 18 hours. After the break-in procedure the fuel cell was tested with three different fuel composition modes. The fuel compositions were chosen to simulate pure hydrogen operation, steam reforming(SR), and auto-thermal reforming(ATR) of methane. Steam reforming was simulated with 60 % H_2,15 % H_2O and CO levels from 0 % to 1 % and auto-thermal reforming with 41 % H_2, 8.5 % H_2O and 1 % CO. ATR is also included in this test because it have been seen in some commercial Combined heat and power (CHP) systems. Systems using ATR have been seen with an additional Water-Gas-Shift(WGS) reactor to clean the

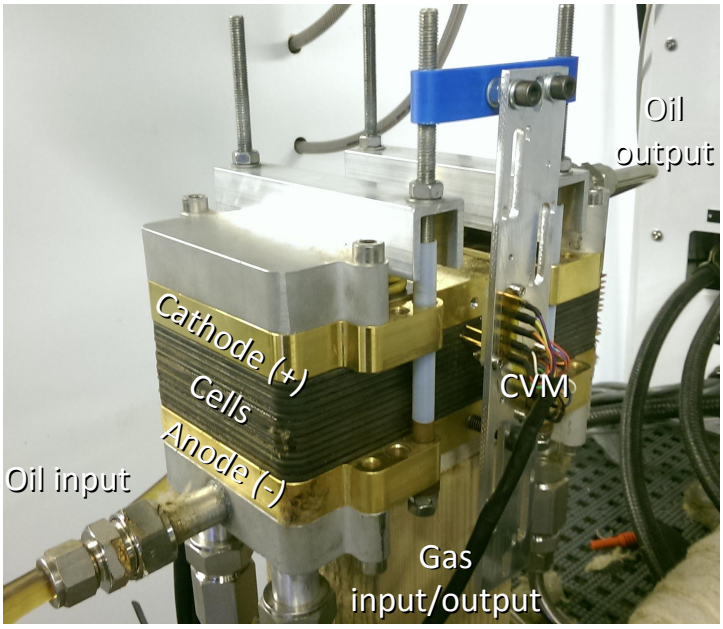

Fig. 2.5: Liquid cooled 17 cell HT-PEM fuel cell stack with CVM module

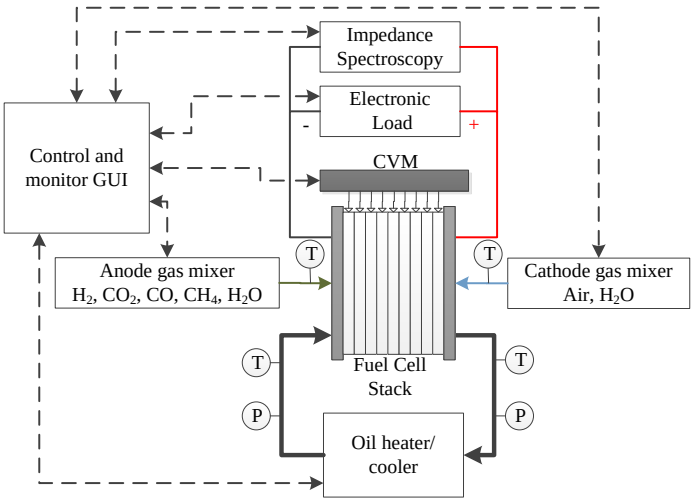

Fig. 2.6: HT-PEM test setup schematic

CO [Authayanun et al., 2015]. The efficiency with SR and ATR is investigated by Salemme et al. [2013], where they showed system efficiency with SR and ATR with methanol of 46.9 % and 38.1 %, respectively.

Polarization curve, EIS, and load step test were used as tools to investigate the influences of each of the tests. A polarization curve was conducted with an increasing step and a decreasing step, and an average of the two was made. The increasing polarization curve was stepped with 2 A and each step was held for about 10 seconds. The polarization test increased the current until a limit of $1\,A/cm^2$ for pure hydrogen or $0.6\,A/cm^2$ for reformate gas. However, if one cell reached a minimum of 0.2 V the polarization curve would also stop increasing. Depending on which limit is reached first, the polarization curve is reversed and a decreasing step of 4 A is conducted with the same 8 second wait period. The wait period was used to ensure a stable voltage under the given conditions though longer periods could be used to avoid increasing temperature.

After each polarization curve a test of three EIS tests were performed between 10 kHz and 0.1 Hz. The measurements were done in galvanostacic mode at a DC load of 33 A and with an sinusoidal amplitude of 1.5 A. Between each index test in table 2.1 the fuel cell is reset at 160 °C at pure hydrogen for 600 seconds. Additionally, every cell is monitored and the next test is not performed until at least 0.5 V is measured on each cell. If any of the cells did not recover the system would be stopped and the cell would be removed, causing the experiments to start from index 1.

The test session ended with a step in the anode and cathode stoichiometry during operation. Furthermore, a step in the electronic load was made where the current density was increased from $0.09\,A/cm^2$ to $0.18\,A/cm^2$, keeping the current at this level for 30 seconds until the voltage settles, then decreases current density back to $0.09\,A/cm^2$, as shown later in fig. 3.7.

Fuel cell stack fault

During the test, a few cells under-performed because of the nature of the tests in table 2.1. The fuel cell started out as a 17 cell stack, however, during the first test two of the cells needed to be removed because of a negative cell voltage under low stoichiometry tests. The cells were removed and the test session would be restarted, unfortunately the reversal of the cell voltage was not studied further before it was removed. It was concluded that the significant degradation tests was due to the low anode stoichiometry tests, (index 25-27). Previous studies by Zhou et al. [2015a] on accelerated fuel cell degradation, show similar fuel cell degradation as seen in the failed cells. Two

Table 2.1: Test matrix. N_2 is used for make-up gas

Anode:Pure-dry hydrogen				
Index	**Temp. (^{o}C)**	**Air stoic.**	**Anode Stoic.**	**CO (%)**
1	**150**	3.5	1.35	
2	**155**	3.5	1.35	
3	**160**	3.5	1.35	
4	**165**	3.5	1.35	
5	**170**	3.5	1.35	
6	**175**	3.5	1.35	
7	160	**2**	1.35	
8	160	**2.5**	1.35	
9	160	**3**	1.35	
10	160	**3.5**	1.35	
11	160	**4**	1.35	
12	160	3.5	**1.25**	
13	160	3.5	**1.3**	
14	160	3.5	**1.35**	
15	160	3.5	**1.4**	
Anode: Reformate gas simulation (60% H_2, 15% H_2O)				
16	**155**	3.5	1.35	0.8
17	**160**	3.5	1.35	0.8
18	**165**	3.5	1.35	0.8
19	**170**	3.5	1.35	0.8
20	**175**	3.5	1.35	0.8
21	160	3.5	1.35	**0.25**
22	160	3.5	1.35	**0.5**
23	160	3.5	1.35	**1**
24	160	3.5	**1.6**	0.8
25	160	3.5	**1.3**	0.8
26	160	3.5	**1.35**	0.8
27	160	3.5	**1.5**	0.8
28	160	**2**	1.35	0.8
29	160	**2.5**	1.35	0.8
30	160	**3**	1.35	0.8
31	160	**3.5**	1.35	0.8
Anode: auto-reformate gas simulation (41%H_2, 8.5% H_2O)				
32	**160**	3.5	1.35	1
33	**165**	3.5	1.35	1
34	**170**	3.5	1.35	1
35	**175**	3.5	1.35	1

discarded cells were removed because of low performance, which could suggest carbon corrosion and platinum agglomeration as the OCV only showed a minor decrease. One cell was removed because of a leak was detected, which could be explained by a local crack in the membrane.

The fuel cell stack showed a large difference in cell voltages during operation, however, for the bases of the dynamic fuel cell model, it was evaluated as sufficient as individual cells were monitored. A fuel cell in a methanol fuel cell system could, under poor operation conditions, be subjected to similar cell degradation which is worth investigating.

4.2 Development of an equivalent circuit model

The EIS spectrum of the fuel cell stack tested in this work show three distinct arcs, which can be seen in fig. 2.8. The arcs imply there are three time constants that correspond to three frequency intervals. The equivalent circuit, shown in fig. 2.7, is made up of three resistances, R_{HF}, R_{IF}, R_{LF}, an ohmic resistance R_{ohmic} and a line resistance R_L. The constant phase element (CPE) loops are used for impedance data interpretations, also done by Zhu et al. [2014] and Simon Araya et al. [2012b]. The intersection between the real axis and the impedance plot represents the ideal resistance, R_{ohmic}, and the data below the axis is usually represented by an ideal inductor for the wiring inductance contributions [Zhu et al., 2014; Boaventura and Mendes, 2010]. A variation of Randles' circuit (An active electrolyte resistance in series with the parallel combination with the charge transfer coefficient and a double-layer capacitance) have been proposed in combination with HT-PEM fuel cells [Boaventura and Mendes, 2010; Vang et al., 2014; Kondratenko et al., 2012; Siegel et al., 2013].

In this work it can be seen that the lines under the real axis bend toward the right, which would indicate wiring artifacts. The right bend is represented by the L-R arc in the EC model.

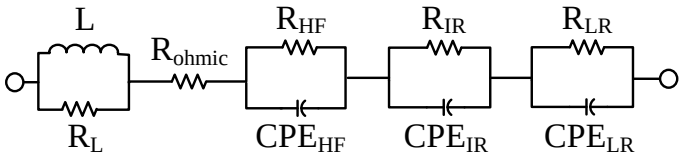

Fig. 2.7: EC model representation of HT-PEMFC stack used in this work

The circuit elements impedances used in the model are given here as a function of frequency [Yuan et al., 2010].

$$Z_R(\omega) = R \tag{2.2}$$

$$Z_L(\omega) = i\omega L \tag{2.3}$$

$$Z_{CPE}(\omega) = Q^{-1}(i\omega)^{-n} \tag{2.4}$$

where, $Z_R(\omega)$ is the impedance of a Resistor [Ω], R is the resistance [Ω], $Z_L(\omega)$ is the impedance of an inductor [Ω], $Z_{CPE}(\omega)$ is the impedance of a CPE [Ω],Q is the pseudo-capacitance [$\Omega^{-1}\mathrm{s}^{\mathrm{n}}\mathrm{cm}^{-2}$], and ω is the frequency [rad/s]. n is the CPE exponent to characterize the phase shift. This coefficient determines the nature of the CPE and when it is equal to 1 it represents a pure capacitor [Yuan et al., 2010]. This work uses n values of 0.95, 0.7 and 1 for high, intermediate and low frequency arcs, respectively.

The constant phase element (CPE) is a pseudo-capacitor used instead of ideal capacitors to fit the EC models to a real system impedance response. This is used to depress the center of the Nyquist plot semicircle arcs below the real axis, which is observed in real systems [Yuan et al., 2010].

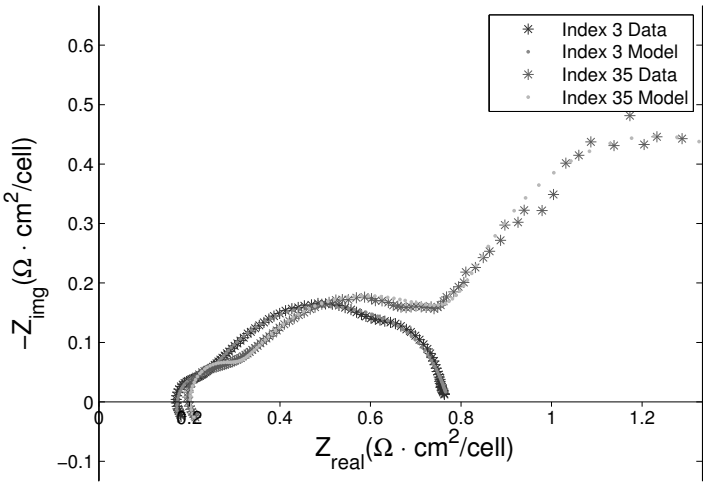

Fig. 2.8: Examples of curve fitting using the EC model in Fig. 2.7 . Indices 3 and 35 represent the respective test points in Tab. 2.1

The third arc is commonly seen as the mass transport effects, which also can be seen in fig. 2.8. The high frequency is widely agreed to represent the sum of ohmic resistance of the cell components such as membrane, catalyst, gas diffusion layer, flow plates, and contact resistance of the component connections [Zhu et al., 2014; YUAN et al., 2007; Yuan et al., 2010].

It can be difficult to distinguish the different contributions to the ohmic resistance, however, the proton conductivity can be attributed to changes during operation [Yuan et al., 2010; Kondratenko et al., 2012]. The proton conduction takes place in both the membrane electrolyte and in the electrolyte in the catalyst layer by means of proton hopping with anion chains, which is formed from self-ionization and self-hydration of H_3PO_4 [YUAN et al., 2007; Vayenas, 2011]

When isolating the three arcs of the impedance plots, the first arc corresponds to the high frequency and the EC model gives the high frequency resistance (R_{HF}). This resistance is assumed potential independentYUAN et al. [2007]; Freire and Gonzalez [2001]; Romero-Castañón et al. [2003]. Romero-Castañón et al. [2003] associated this independence to the construction of the structural features in the MEA. YUAN et al. [2007] argue that the fulle impedance of the fuel cell almost equals the cathode impedance due to the fast hydrogen oxidation reaction in H_2/air operation. Other authors make the separation between the anode and cathode, where the anode is the high frequency and the cathode is the intermediate resistance [Boaventura and Mendes, 2010; Mench et al., 2012]. According to Mench et al. [2012], the intermediate and low frequency resistance provide insight into degradation mechanisms in the cathode catalyst layer, with the intermediate frequency linked to the charge transfer and the lower frequency indicate mass transport issues. This work does not use these links directly and will keep the frequency spectrum separate from the anode and cathode, which means the frequency range is divided into high frequency resistance (R_{HF}), intermediate frequency resistance (R_{IF}) and low frequency resistance (R_{LF}).

EIS representation standardization

In the study for this work there was not found a standardized way of representing EIS data or fitted data. The literature presents several representations of impedance data, including, no units, Ohms (Ω) or $\Omega\ cm^2$, which is normalized with respect to unit cell area [Romero-Castañón et al., 2003; Lee et al., 2010; HU et al., 2006; Pérez-Page and Pérez-Herranz, 2014]. By multiplying the impedance and fitted EC model data with the active cell area, it makes it easier to compare EIS data based on research with single cells. However, this does not allow for comparability between single cell and fuel cell stacks, or comparability between fuel cell stacks of different cell numbers. To ease the comparability, this work encourages future research to show the EIS and EC model data multiplied with the cell area and divided with the number of cells in the fuel cell stack. The data in this thesis will be represented with the unit $\Omega\ cm^2/cell$.

5 Characterization based on EIS measurements

While the polarization curves provide a general view of the fuel cell performance, a more detailed test is required to differentiate between the main sources of losses in the fuel cell. Electrochemical impedance spectroscopy is a widely used technique for isolating the losses. Each polarization curve and EIS data legend show the test index which corresponds to the test in table 2.1.

5.1 Temperature characterization

The following section investigates the performance of the fuel cell stack with different temperatures under dry gas and reformate gas operation.

Dry hydrogen operation

The overall effect of temperature on performance of a PBI based HT-PEM FC is often seen as negligible with a slight tendency to increase with increasing temperatures. The polarization curves in fig. 2.9 show this slight increase in performance in the range of 150 °C to 175 °C. Literature show consistent results where the performance and temperature is observed [Su et al., 2012; Liu et al., 2015]. The increase in performance shown in this work is less marked, because smaller temperature steps of 5 °C are used in contrast to 20 °C in the cited papers. The EIS measurements show more details which are not visible in the polarization curves. In fig. 2.9 it can be seen that the impedance move towards the right in the range of 1 kHz to 10 kHz. The rightward movement of the intercept between the impedance spectra and the real axis is represented by the change in ohmic resistance (R_{ohmic}) in fig. 2.10. It increases slightly with temperature and can be attributed to the overall increase in contact resistance, including the membrane conductivity of the fuel cell stack. It appears, in contrast to most literature [Su et al., 2012; Li et al., 2009], that the membrane conductivity increases with temperature. Simon Araya et al. [2014] and Jespersen et al. [2009] independently found that the resistance decreases with increasing temperatures until 160 °C, and then increases with increasing temperatures. The majority of literature on this topic focuses on ex-situ membrane conductivity or single cell EIS, where the contact resistances are not found significant. However, the membrane is not the only contributor to the ohmic resistance. It is the sum of electrical resistances, like conductors and isolators in the fuel cell stack. The membrane can be considered an electric insulator and its resistance can theoretically be described as decreasing with increasing

temperatures. It can be seen by the current work that the total ohmic resistance increases with temperature and it may be caused by the conductive components, like the flow plates and the current collectors, which in a fuel cell stack are more significant compared to a single cell.

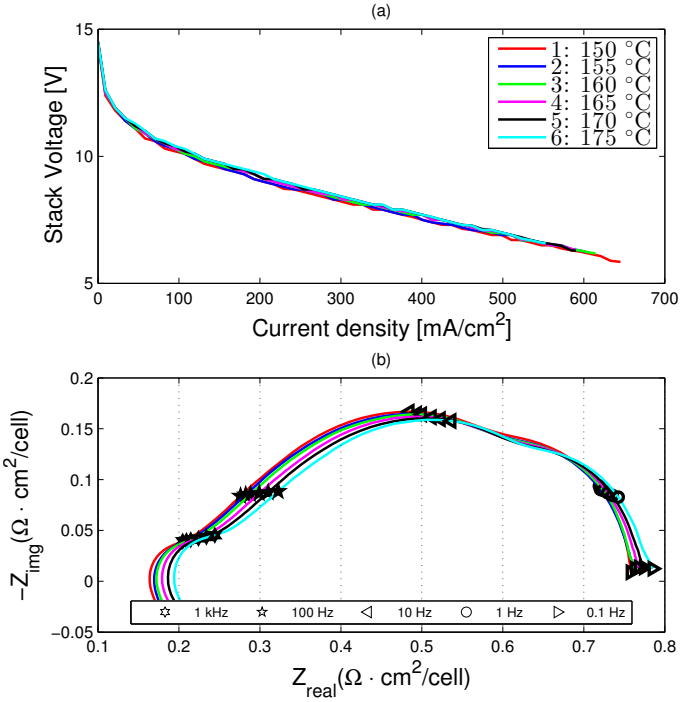

Fig. 2.9: Pure H2 temperature test

The low frequency resistance (R_{LF}) seems to decrease slightly with increasing temperatures while the intermediate frequency resistance (R_{IF}) is estimated to the same at all temperatures. The high frequency resistance (R_{HF}) shows a slight decrease from 155 °C to 160 °C with a small increase thereafter. This indicates that the charge transfer is not enhanced above 160 °C. Su et al. [2012] shows that the increase in performance with temperature is because of higher reaction rates and higher mass transfer, which is partly confirmed by this work by the slightly decreasing R_{LF}. Therefore, improvements in mass transport with increasing temperatures and the high frequency charge transfer up to 160 °C may be the main causes of the small performance enhancement achieve with increasing temperatures.

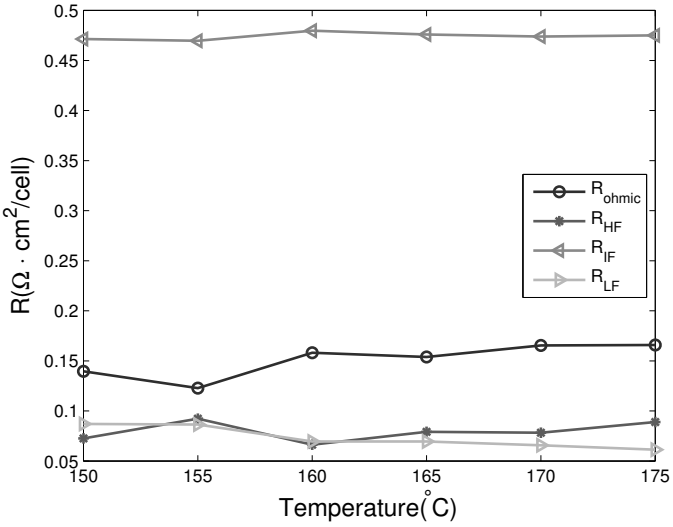

Fig. 2.10: Effects of temperature under dry H_2 operation

Reformate gas operation

fig. 2.11 shows the effects of reformate gas with temperatures from 160 °C to 175 °C. The increase in temperature, as with the dry hydrogen test, causes an increase in ohmic resistance, perhaps because of the increased electrical resistance of other conductive components in the fuel cell stack. This can be seen as a weakness of the EIS method as a characterization technique on stack level as the ohmic resistance does not correspond to a decrease in the ionic conductivity of the membrane nor to the decrease in stack performance. However, the polarization curves in fig. 2.11(a) show a slight increase in performance with temperature under reformate gas operation. The increase in ohmic resistance could also be related to the swelling of the membrane caused by water uptake [Li et al., 2009; Aili et al., 2014].

fig. 2.12 shows the model resistance under wet reformate gas conditions. It can be seen that R_{IF} and R_{LF} are slightly decreasing with temperature in accordance with the corresponding polarization curves in fig. 2.11(a). Unlike the dry hydrogen operation, a slight performance increase beyond 160 °C under reformate conditions is seen. This could be because the presence of water reduces the PA poisoning effects on the Pt reaction sites by hydrating the PA molecules [Orfanidi et al., 2013].

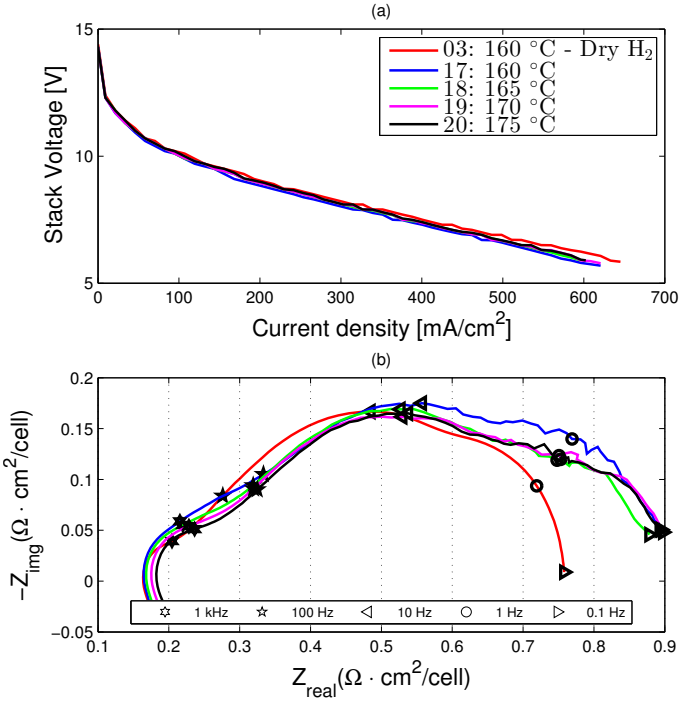

Fig. 2.11: Temperature test under reformate gas operation

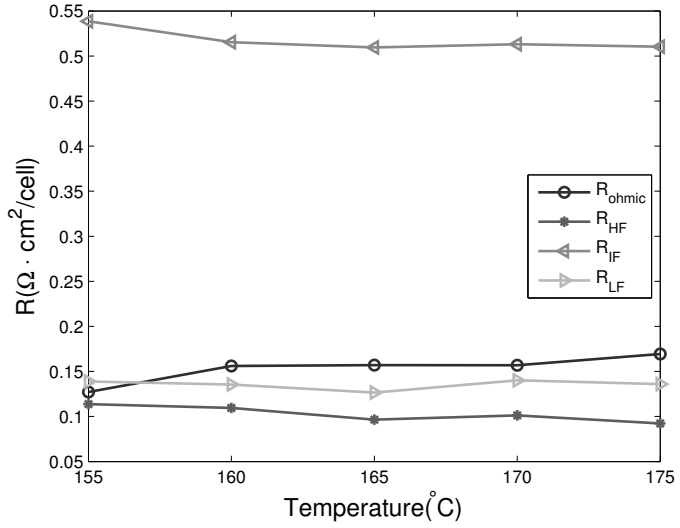

Fig. 2.12: Effects of temperature under reformate gas operation

5.2 Stoichiometry

The next section investigates the anode and cathode stoichiometric effects on both dry hydrogen and reformate gas operation mode. Below are the polarization and EIS data of the fuel cell stacks response to varying fuel composition and stoichiometric ratios.

Anode stoichiometry

fig. 2.13 shows the hydrogen stoichiometry and the influence on the performance on dry hydrogen. The stack is tested from anode stoichiometry 1.25 to 1.4. The polarization curves show a decreased performance with lower stoichiometry and the impedance spectra show significant changes in the lower frequencies which corresponds with mass transport issues.

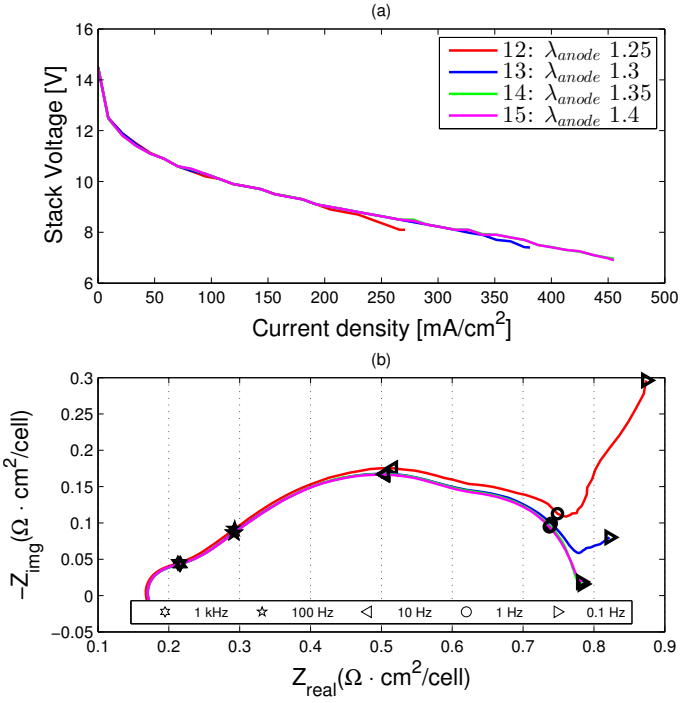

Fig. 2.13: Impedance plot with different anode stoichiometry levels with dry H_2

The model results, seen in fig. 2.14, show a significant decrease in the low frequency resistance, R_{LF} up to a stoichiometry of 1.3. After the stoichiometry of 1.3 is reached, the resistance R_{LF} levels out, which indicates that once

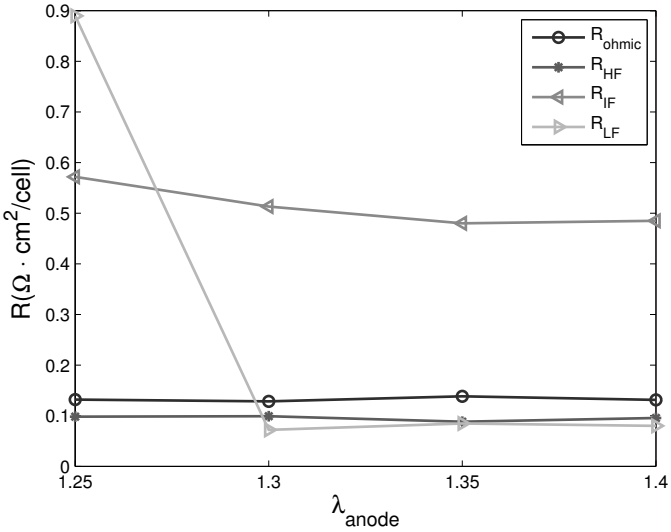

Fig. 2.14: Effects of anode stoichiometry under dry H_2 operation

hydrogen starvation is avoided, the increase in anode stoichiometry does not improve performance. Galbiati et al. [2012] shows that high anode stoichiometry reduces the water content in the anode. There was not found any clear correlation or diminishing performance, however, it needs to be investigated further.

The reformate gas operation can be seen in fig. 2.15 and a larger spread is noticed in the polarization curves. The anode stoichiometry was changed from 1.3 to 1.6. Similar to the dry hydrogen operation, impedance plots show similarities in all resistances, which implies that the effects are mass transport related. Similar improvements were found by Najafi et al. [2015] under reformate gas operation when increasing anode stoichiometry from 1.2 to 1.6.

Both the dry hydrogen(fig. 2.13) and reformate gas(fig. 2.15) show a 45° line in the low frequency range 1 Hz. Siegel et al. [2013] notices a similar 45° line during fuel starvation. This is typical of mass transfer frequency dependence, which is sometimes called the Warburg impedance [Yuan et al., 2010]. The impedance show how severe hydrogen starvation can be at low stoichiometry and how it can be avoided by operating slightly above the critical limit point of 1.3 on dry hydrogen and 1.35 on reformate gas. The Warburg diffusion is not used in this work for the mass transport to avoid more fitting parameters compared to a simple R-C loop. Also, some of the impedance spectra does not show the 45° slope, hence this model can fit all the operating conditions used.

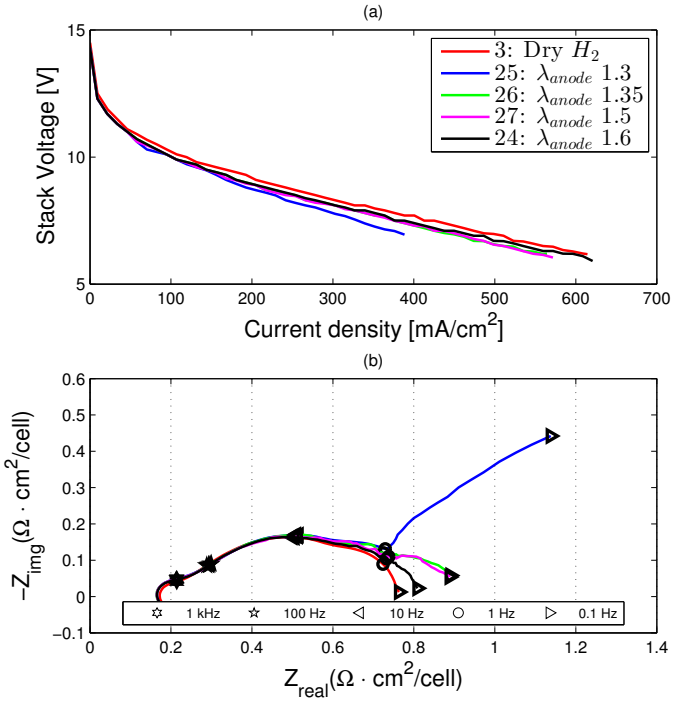

Fig. 2.15: Impedance plot with different anode stochiometry levels with reformate gas

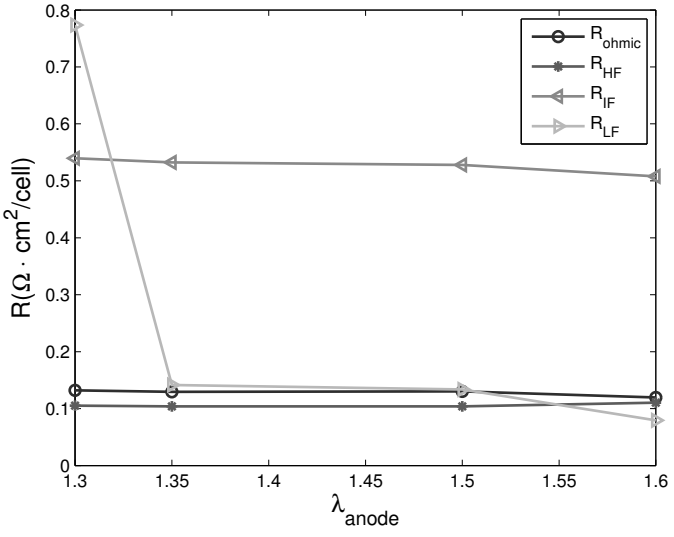

Fig. 2.16: Effects of anode stoichiometry under reformate gas operation

The results from the model are shown in fig. 2.16 and display a significant decrease in low frequency resistance and no significant changes in intermediate and higher frequency ranges. R_{LF} decreases significantly in the range of 1.3 to 1.35 and then slowly from 1.35 to 1.6. The results can be used as a tool to evaluate a suitable stoichiometry for both dry hydrogen and reformate operation. The low stoichiometry of 1.35 is in line with the manufacture's specifications for dry hydrogen operation [Serenergy A/S, 2013].

Cathode stoichiometry

The effects of cathode stoichiometry on the fuel cell stack are similar to the ones seen on the anode side, where the mass transport region is where the influence is seen. Cathode stoichiometry on reformate gas is shown in fig. 2.17(a), which indicates an increasing performance with increasing cathode stoichiometry.

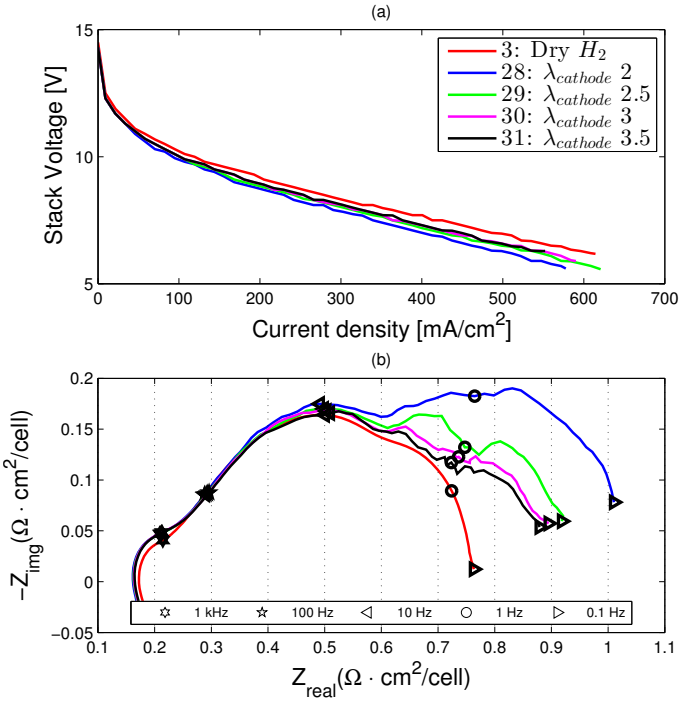

Fig. 2.17: Impedance plot at different air stoichiometry levels under SR gas operation

The resistances in fig. 2.18 show the most changes in the low frequency region, where there is a significant decrease in stoichiometry until 3 and then it slowly levels out. The experiment show that also in the case of air stoichiometry

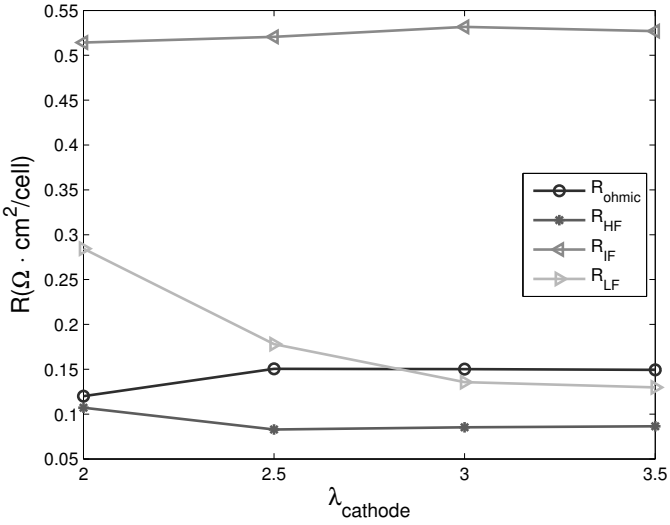

Fig. 2.18: Effects of air stoichiometry under SR gas operation

once reach a sufficient mass transport, no significant increase in performance is achieved. Jespersen et al. [2009] has reached similar conclusions, where fuel cell performance increase dramatically until a stoichiometry of 3 is reached and above 4 has only little effect. They tested this on a single cell assembly, however, the resistances are comparable as the current work normalizes the impedances for the stack. The other resistances does not show any significant changes besides stoichiometry below 2.5. The water vapor can show an influence in the water transport at low stoichiometry, which can be linked to the water transport in the cell [Galbiati et al., 2012]. However, these changes are too small to draw more detailed conclusions on the effect of stoichiometry on membrane and charge transfer resistances, besides the fact that they are not affected above 2.5.

5.3 CO Poisoning

The results from the reformate gas composition with varying CO content are presented in fig. 2.19. The CO content varied between 0.25 vol % to 1 vol % in the reformate gas feed, and it can be seen from the polarization curves in fig. 2.19(a) that the tests show very similar results. Similarly, the impedance plot in fig. 2.19(b) does not show any significant CO poisoning effects. It is widely accepted that the presence of CO in the hydrogen stream decreases performance, compared to pure hydrogen, because of surface adsorption of CO

on the Pt reaction sites [Bose et al., 2011; Li et al., 2003; Kaserer et al., 2013]

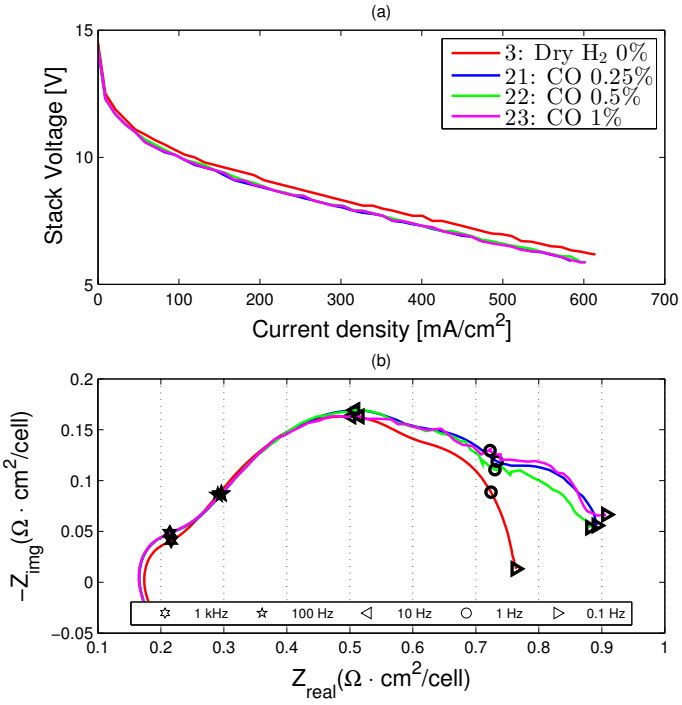

Fig. 2.19: Polarization plot and impedance spectrum for varying CO content in reformate gas.

It can be seen from fig. 2.20 that from 0.25 % to 0.5 % there is a decrease in R_{LF}, which show that the mass transport is slightly improved. This is contrary to expectations and the reason could be the relatively short duration of the experiment. The reaction rate was investigated by Vidaković [2005] using a CO stripping voltammetry on unsupported Pt surfaces and showed that the adsorption occurs even after 1 minute and increases rapidly until a saturation coverage is observed after 15 minutes. The experiment in this work used only 10 minutes before the first polarization curve was used. Therefore, prolonging the experiment to over 15 minutes may have increased the surface adsorption and resulted in a lower performance. However, the surface adsorption of CO on the Pt surface is a relatively fast process compared to H_2 adsorption, and since the effects are negligible it shows the advantage of HT-PEM over LT-PEM fuel cells.

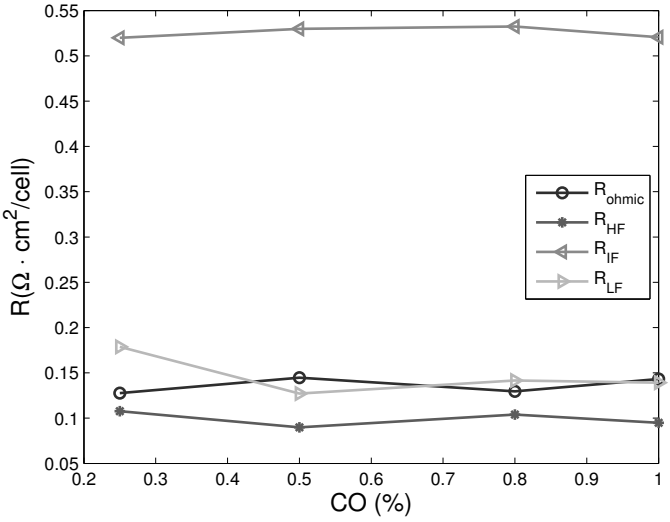

Fig. 2.20: Effects of co concentration under reformate gas operation

5.4 Comparison of H_2, SR and ATR gas operation

A comparison of the pure hydrogen, steam reforming gas, and auto-thermal gas is shown in fig. 2.21 and 2.22. It can be seen that the best performance is with dry H_2 and the worst is the ATR gas both for 160 °C and 170 °C. The explanation may lie in the vol. % of the gas in both SR gas and ATR gas, which are 60 % and 41 %, respectively.

The most significant change is seen below 10 Hz, which indicates that mass transport is the main issue. Similar results can be seen from the anode stoichiometry test, fig. 2.13, where moving from dry hydrogen, SR, and ATR show the same low frequency resistance. This indicates that operating the ATR with a higher stoichiometry will improve performance significantly.

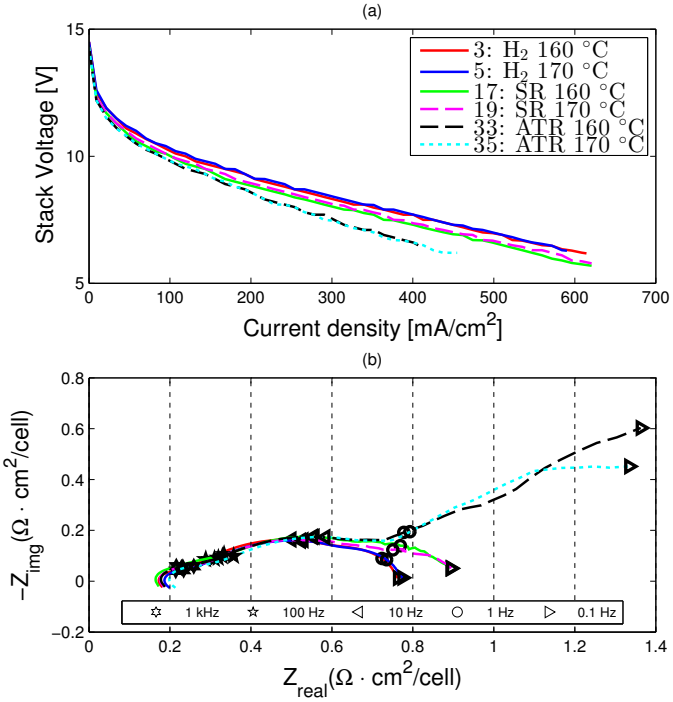

Fig. 2.21: Impedance plots comparing for dry H_2, SR gas and ATR gas operation modes at 160 °C and 170 °C

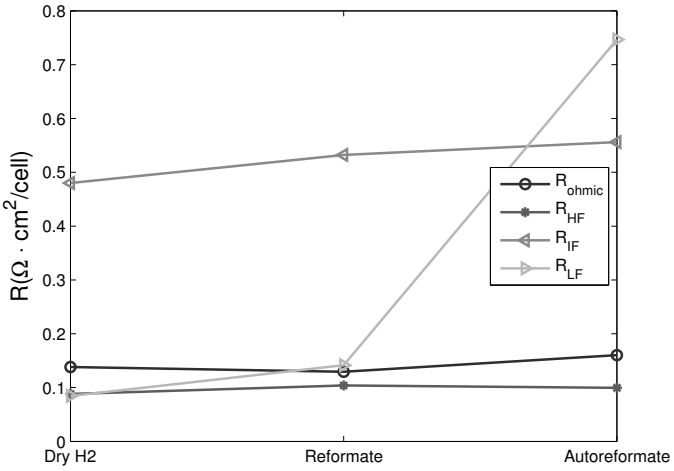

Fig. 2.22: Comparison of dry H_2, SR gas and ATR gas operation modes at 160 °C

Summary

All the tests were created using an automated test system that was able to test a significant amount of test points without downtime. Polarization curves and EIS data were collected for various temperatures, anode and cathode stoichiometry, dry hydrogen, reformate gas, and auto-thermal reformation. A dynamic model of the fuel cell was created which could simulate the fuel cell under steady state and under dynamic changes, both in stoichiometry and load changes. The model was fitted against good and bad performing cells, which can be used in combination with larger system models. The experiments confirmed the tolerance towards CO under normal operating conditions up to 1% with no significant poisoning. The lower stoichiometry limit for this fuel cell stack for both anode and cathode gas supply was estimated and found to be 1.35 and 3.5, respectively. The limit was found using an equivalent model based on the EIS data, which confirmed mass transport resistance as the significant factor.

The use of EIS measurements as an online diagnostic tool can also be a big improvement to implementation and use of a fuel cell stack. Research into break-in conditions, degradation, gas composition, fault detection shows how EIS can significantly improve fuel cells and can help expand their use. The use of EIS techniques in academic research can also help into better understanding the chemical and electrochemical reactions in fuel cells.

Chapter 3

Reformed methanol fuel cell system design

Fuel cell systems are suitable for electric power generation in situations where clean, silent, and efficient energy is demanded. Furthermore, the continuous operation of the fuel cell can be advantageous in many situations. This could be in applications as an emergency backup power or off-grid generation in remote rural areas. Using HTPEM fuel cell systems in these applications come both with advantages and disadvantages as studied in Chapter 2. This chapter presents a series of models at system level, aimed to analyze operation parameters and investigate various control schemes. The models used in this work are described in detail in paper [A]. The system model and control were implemented in Matlab Simulink™.

1 System description

The system is designed with four components; Reformer, burner, evaporator, and fuel cell, which can be seen from fig. 3.1. The system is connected with two oil circuits, one circuit between the reformer and the burner and one connecting the fuel cell and the evaporator. During operation, the methanol fuel is fed from the methanol/water tank to the evaporator. The fuel is evaporated and led into the reformer, which reforms it into a hydrogen rich gas. The hydrogen rich gas is led into the anode side of the HT-PEM fuel cell stack converts the hydrogen, and oxygen from the cathode side, to electricity. The fuel cell operates with an

open anode mode, which the exhaust gas is directed to the burner, where the hydrogen is used to heat the burner. The two oil pumps in the system are held at a constant flow rate around 10 l/min at the operating temperature, however, due to the high viscosity of the oil causes the actual flow to be lower at lower temperatures. Caution must be taken when operating liquid cooled fuel cells below normal operating temperatures, as the pressure can be higher than fuel cell stack can handle. The high pressure in the fuel cell stack oil circuit can cause cracks in the sealing between the oil and the MEA.

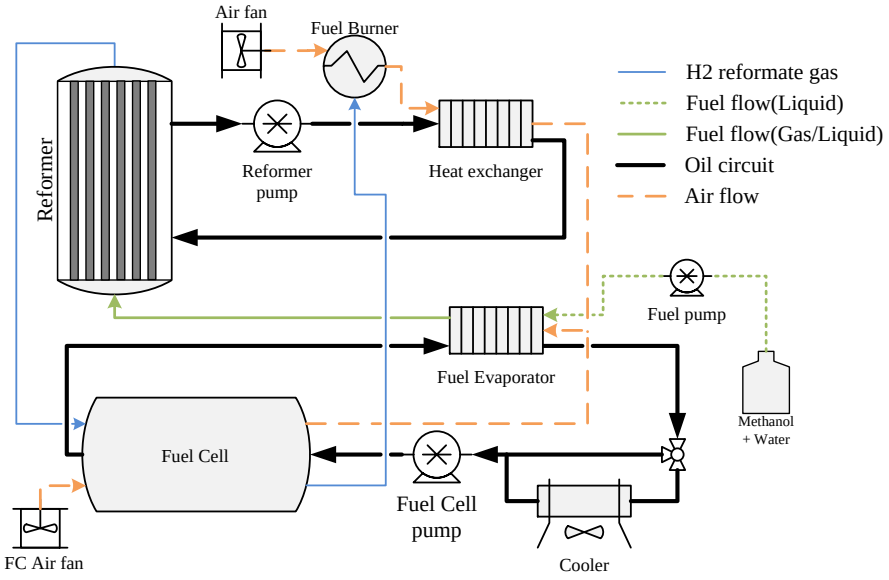

Fig. 3.1: Schematic of reformed methanol fuel cell system in operation mode.

The model simulates temperatures of the different components as lumped masses in order to simplify the dynamics in the system. Each component is measured with a temperature sensor placed inside the component and the temperature of the oil is monitored at the inlet and outlet of each component. The system contains in two separate oil circuits because of the temperature difference between the fuel cell and reformer. The reformer is connected to a catalytic burner, which is the main source of heat for the reforming process. The oil used in this system is Paratherm [2014], which is able to withstand the temperatures in the burner and reformer. The system is operated with a steam-to-carbon ratio of 1.5, which corresponds to approximately a 60/40 methanol/water ratio [Agrell et al., 2002; Iulianelli et al., 2014]. Research by Iulianelli et al. [2014] found that a H_2O/CH_3OH ratio of 1.5 gave the best results in preventing catalyst deactivation and coke formation.

The use of an oil heated reformer was chosen in an attempt to increase the overall efficiency and to ease the implementation of alternative heating methods. An initial design of the system was with a single oil circuit, however, the temperature difference between the fuel cell stack and the reformer was too large. Separating the two modules required the use of two liquid pumps instead of one, which decreases the system efficiency and increases the overall number of components. A similar 2.5/5 kW commercial methanol reforming fuel cell system was released by Serenergy A/S [2015] during the course of this PhD study. The systems uses the same type of fuel cell stack as the one studied in this work, however, the system has a combined burner/reformer system, which eliminates the use of several liquid pumps. Yet, using two oil circuits makes it possible to utilize an external heating source, if available, and with a liquid reformer it can be easier to manipulate the temperature along the flow channel.

The oil circuit for the fuel cell stack operates at about 160 °C and has an additional cooler in case the evaporator is not sufficient to cool the oil. The cooler used in this work is an electric air cooled radiator, which is connected to the oil circuit by a three way valve. To ensure that the fuel cell stack operates at a sufficiently low temperature, the cooler can be enabled depending on the temperature of the oil and the fuel cell stack. A PI-controller for the fuel cell stack temperature is implemented in the model and the experimental setup and operates independently of the main system.

The system is equipped with two separate air fans, one for the burner and one for the fuel cell system. The air fan in the burner is critical for the safety and operation of the system, being that, the catalytic reaction can flame back if the fan is turned too low. The catalytic burner operates at a temperature of about 500 °C with a low NOx output, and if operated at the right oxygen level there is a very low risk of fire [HARUTA and SANO, 1981].

For lower fuel cell stack sizes (<2kW), air is sufficient for cooling the stack, however at larger stack sizes a liquid cooling is often required [O'Hayre et al., 2005]. The liquid cooled HT-PEM fuel cell used in this work only requires the air fan for the internal reaction and not for cooling. In a previous study by Andreasen and Kær [2009] models the cooling of a 30 cell HTPEM fuel cell stack with the use of forced convection. Using convection as a heating strategy have been studied by Andreasen and Kær [2008] on a HTPEM fuel cell stack and shows a startup time of 6 minutes, however this work utilizes the liquid cooling system and burner for warm-up of the fuel cell stack and reformer.

1.1 Startup operation

The two oil loops for the reformer and fuel cell stack circuit make it possible to easily exchange heat between the burner and the fuel cell circuit. An alternative configuration is used as shown in fig. 3.2, where a heat exchanger is connected between the two loops. When the system is in this configuration, the burner is utilized to heat up the reformer, fuel cell, and evaporator. During startup, the reformer is not at an operating temperature, which means the burner is fed directly by methanol/water and air. When the reformer reaches the minimum reforming temperature the methanol/water is directed through the reformer, which changes the system to an operating state.

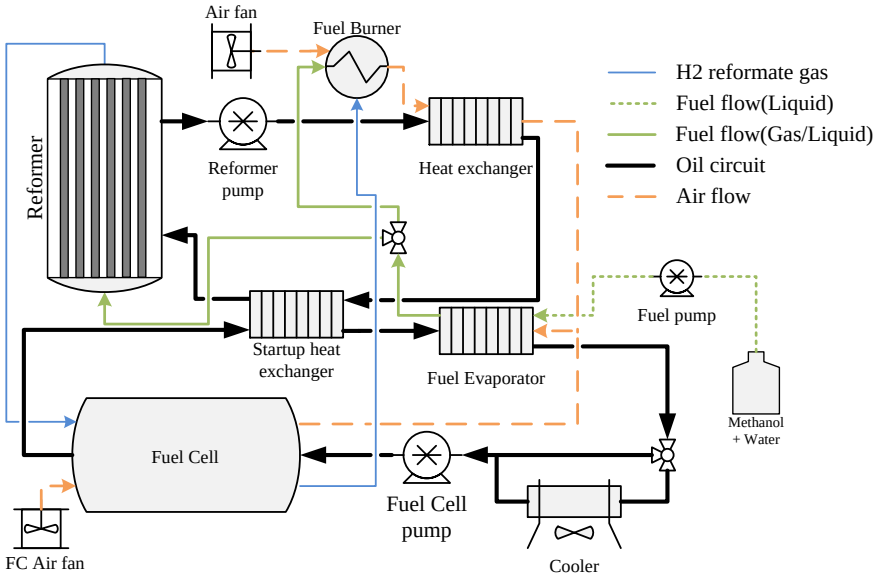

Fig. 3.2: Schematic of reformed methanol fuel cell system in startup mode.

This configuration has the advantage that the methanol/water mixture can be used as a backup heating source if the burner or reformer is operating too low. The startup procedure in this project was about 45 minutes, which is common for a systems similar to this.

2 HT-PEM fuel cell dynamic model

The dynamic model in this work is developed to identify the thermal, electrical, chemical and electrochemical response of the HT-PEM fuel cell stack. The model used in this work is presented in paper [C] The model is based on a simplified geometric representation of the stack which could be used in the development of a control systems. The model only resolves the unit cell control volumes (Bipolar plates, cathode and anode gas channels and MEA) to maintain a short simulation time. The model considers seven individual gases, which are CH_4, CO, CO_2, H_2, H_2O, N_2,and O_2. A set of variables is passed among the model parts, which are, temperature, gas concentration, and flow rate. The model simulates the fuel cell by dividing the fuel cell into nine control volumes in the perpendicular direction to the gas flow. In fig. 3.3 the five types of control volumes can be seen are the Solid plate, gas channel, GDL, MEA, and coolant channel. The model calculates the heat transfer and mass transport to evaluate the temperature and gas concentration.

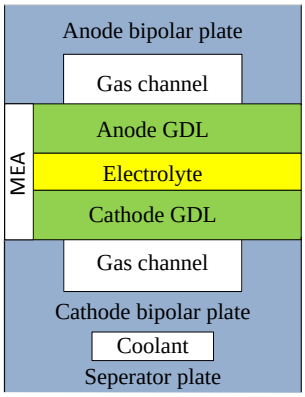

Fig. 3.3: Schematic of the control volumes used in the fuel cell dynamic model

The voltage is calculated using the gas concentration at the electrolyte/electrode interface. The fuel cell consumes hydrogen along the flow channel causing a distribution in current density in the cell. In the work by Park and Min [2012] the change in concentration is simulated by spacial discretization along the gas direction. In contrast, the model used in this work assumes uniform current distribution and determines the voltage from the gas concentration based on the outlet of the cell.

HT-PEM fuel cell dynamic model assumptions

The modeling method is based on the method outlined in Park and Min [2012]. The high temperatures in the fuel cell, assumes water in vapor phase in the gas channel and electrodes, and thus, single phase flow is considered. CO degradation is not included in the model because of the relatively short time the fuel cell is operated during the experiment and the high poisoning resistance to CO as the experiments do not investigate above 2 % [Jiao et al., 2011; Andreasen et al., 2011b].

Dynamic model equations

The temperature of the solids are calculated using the following ordinary differential equation;

$$\rho V C \frac{dT}{dt} = \sum \dot{Q}_{in} + \dot{Q}_{gen} \tag{3.1}$$

where ρ is the density, V is the volume, C is the specific heat capacity, $\dot{Q}_{in}$ is the heat entering the solid and $\dot{Q}_{gen}$ is the heat generated in the solid volume. The temperature of the gas and coolant are calculated by the following energy conservation equation

$$NC_V \frac{dT}{dt} = \sum \dot{N}_{in} h_{in} - \sum \dot{N}_{out} h_{out} + \sum \dot{Q}_{in} + \dot{Q}_{gen} \tag{3.2}$$

where N is the number of moles of moles in the control volume, C_v is the specific heat of the gas/coolant, $\dot{N}_{in}$ h_{in} and $\dot{N}_{in}$ h_{out} are the enthalpy flows in and out of the control volume, $\dot{Q}_{in}$ is the heat entering and $\dot{Q}_{gen}$ is the heat generated in the volume.

The mole fraction at the exit of each volume are

$$\frac{d(N\vec{X})}{dt} = \dot{N}_{in}\vec{X}_{in} - \dot{N}_{out}\vec{X}_{out} + \sum \vec{\Phi} \tag{3.3}$$

where $\vec{X}$ is the mole fraction vector for the species, $\sum \vec{\Phi}$ is the diffusion flux from the adjacent volume. This assumes the control volume is a perfectly stirred reactor and all gases are treated as ideal. The output from this model calculates the outlet concentration of the species.

Mass transport

The mass transport in the anode and cathode diffuse through the GDL to and from the catalyst layer. At the catalyst layers (Assumed to be the interface between the GDL and the electrolyte), the gas molecules participate in electrochemical reactions at this triple-phase interface in the catalyst layer, electrolyte and gas phase. The model calculates the mass transport of hydrogen, water, oxygen and nitrogen. The mass transport coefficient from the gas channel and through the GDL is;

$$\vec{g}_m = \frac{Sh\vec{D}_m}{D_H} \tag{3.4}$$

where Sh is the Sherwood number, $\vec{D}_m$ is the diffusion coefficient and D_H is the diameter of the gas flow channel. Based on heat and mass transfer analogy the Sherwood number can be determined by

$$\frac{Nu}{Pr^n} = \frac{Sh}{Sc^n} \tag{3.5}$$

where Nu is the Nusselt number, Pr is the Pradtl number, Sh is the Sherwood number, and Sc is the Schmidt number. Rearranging eq. 3.5 to solve for the Sherwood number

$$Sh = Nu\left(\frac{Sc}{Pr}\right)^n = Nu\frac{\alpha}{D_{AB}} \tag{3.6}$$

where α and D_{AB} are the thermal and mass diffusion coefficient respectively.

The diffusion coefficient is calculated using the Bruggeman correlation with modification to account for the effect of porosity and tortuosity in the GDL

$$\vec{D}_m = \vec{D}_0\left(\frac{T}{T_0}\right)^{3/2}\left(\frac{P_0}{P}\right) \tag{3.7}$$

$$\vec{D}_m^{eff} = \epsilon^{1.5}\vec{D}_m \tag{3.8}$$

where D_0 is the diffusion coefficient at standard temperature and pressure, D_m^{eff} is the effective diffusion coefficient and ϵ is the GDL porosity.

The diffusion resistance is thereby show as

$$R_{i,diff} = A\frac{1}{\frac{1}{g_{i,m}} + \frac{t_{gdl}}{D_{i,m}^{eff}}} \tag{3.9}$$

where $R_{i,diff}$ is the diffusion resistance for each species, A is the area of diffusion, $g_{i,m}$ is the mass transport coefficient from eq. 3.4, t_{gdl} is the thickness of the GDL and $D_{i,m}^{eff}$ is the diffusion coefficient for the i^{th} species shown in eq. 3.7.

The species diffusion flux between the GDL and the gas channels is;

$$\vec{\Phi} = \vec{R}_{diff}(\vec{C}_2 - \vec{C}_1) \tag{3.10}$$

where $\vec{C}_1$ and $\vec{C}_2$ are the concentrations in GDL and the gas.

Heat transfer

The convective heat transfer between the solid volumes and gasses are calculated as;

$$\dot{Q} = hA(T_2 - T_1) \tag{3.11}$$

where h is the heat transfer coefficient, A is the area and $(T_2 - T_1)$ is the temperature difference.

Heat from conduction transfer is calculated by Fourier's law;

$$\dot{Q} = \frac{kA}{L}(T_2 - T_1) \tag{3.12}$$

where k is the conduction heat transfer coefficient, A is the conductive heat transfer area, L is the volume thickness and $(T_2 - T_1)$ is the temperature difference between the gas and solid.

HT-PEM fuel cell electrochemical reactions

Using the Nernst voltage, activation losses and the ohmic losses the model calculates the fuel cell voltage. Because the fuel cell operates at lower current

density the concentration losses are not included in the model. Thereby, the voltage is determined by the following equation

$$V_{cell} = V_{Nernst} - \eta_{act} - \eta_{ohmic} \tag{3.13}$$

where V_{Nernst} is calculated based on the temperature and concentration of H_2, O_2 and H_2O at the electrode-electrolyte interface.

$$V_{Nernst} = -\frac{\Delta G(T)}{nF} + \frac{R_u T}{nF} \ln\left(\frac{p_{\mathrm{H_2O}}}{p_{\mathrm{H_2}}\ {p_{\mathrm{O_2}}}^{1/2}}\right) \tag{3.14}$$

where $\Delta G(T)$ is the Gibbs free energy, n is the number of electrons transferred in the reaction, F is the Faraday constant, R_u is the gas constant, T(K) is the temperature, p_i is the partial pressure of the different species.

The Tafel equation is used for the activation polarization on the cathode.

$$\eta_{act} = a\ \ln\frac{j}{j_0}, \text{ and } a = \frac{RT}{2\alpha F} \tag{3.15}$$

where j is the current density, j_0 is the exchange current density, and α is the transfer coefficient. j_0 is in the model based on experimental measurements done by Hu et al. [2008].

$$j_0 = a\, exp(-bT(K)) \tag{3.16}$$

where $T(K)$ is the membrane temperature, a and b is fitting parameters.

The ohmic polarization η_{ohmic} is calculated with the contribution from the GDL on each side and the electrolyte layer.

$$\eta_{ohm} = i\left(\frac{t_{electrolyte}}{\kappa_{electrolyte}} + 2\frac{t_{GDL}}{\sigma_{GDL}}\right) \tag{3.17}$$

where $t_{electrolyte}$ and t_{GDL} is the thickness of the electrolyte and GDL, $\kappa_{electrolyte}$ is the proton conductivity, and σ_{GDL} is the electronic conductivity of the GDL.

The values shown in table 3.1 are used as input to the model. The next section will show the experimental results from polarization curves and dynamic step experiments.

2.1 Experimental results for dynamic model

The model for the HTPEM fuel cell stack is split into two sections. The first section shows the steady state performance compared to the I-V curves of the experimental data. The dynamic model is compared to a load step experiment with varying stoichiometry.

Steady state performance

The polarization curve, shown in fig. 3.4, is the fuel cell stack performance with pure hydrogen and air operated at 160 °C. The stoichiometry was set to 1.35 on the anode and 3.5 on the cathode. Error bars are shown of the cell deviation and the model is fitted to the mean cell voltage. The experiment that showed some cells in the fuel cell stack were operating at lower voltages at higher current densities. At a current density below $0.3\,\mathrm{A/cm^2}$ the model deviates slightly, however the fuel cell is not normally operated at this level. At current density $0.3\,\mathrm{A/cm^2}$, the standard deviation is below 30 mV and at $0.5\,\mathrm{A/cm^2}$ it is 80 mV. The large deviation is caused by a larger degradation of some of the cells in the stack.

The model and the experimental data agree within 10 mV of the mean cell voltage throughout the data, except at low current density. The voltage variations of the cells do not change significantly during the different experiments which is why the standard deviations are omitted in the subsequent plots to enhance readability.

The polarization plot in fig. 3.5 shows the effect of temperature on the short stack. The stack temperature is varied from 155 °C to 175 °C and both the model and experiments are shown. The higher temperatures show an increase in performance by 30 mV. The increase in performance is because of the increased kinetics and higher conductivity. The model does not include leakage current which explains the difference in the model and experiment during lower current densities, under $0.05\,\mathrm{A/cm^2}$. In the linear area of the polarization plot the dependency on current density is observed, which may be linked to the water vapor production and result in an improvement of the membrane conductivity [Cheddie and Munroe, 2006; Park and Min, 2012; Zhang et al., 2007].

Table 3.1: Model parameters used in the dynamic fuel cell model

Descriptions	**Values**	**Units**
Geometry		
Depth of gas channel (anode and cathode)	1	mm
Depth of cooling channel	2	mm
Thickness of GDL	0.4	mm
Thickness of electrolyte	0.5	mm
Thickness of separator plates	1	mm
Thermodynamic properties		
Separator plate density	2210	kg/m^3
Separator plate specific heat capacity	0.5	kJ/kg-K
Electrolyte dry density	2200	kg/m^3
Electrolyte dry equivalent weight	1000	kg/kmol
Electrolyte solid specific heat capacity	2.179	kJ/kg-K
Heat transfer properties		
Separator plate bipolar plate conduction coefficient	0.22	kW/m-K
Separator plate & bipolar plate conduction coefficient	0.22	kW/m-K
Nusselt number of anode gas & cathode gas	6	
Nusselt number of coolant liquid	15	
Mass transport properties		
GDL porosity	0.51	
GDL void fraction	0.5	
Area of diffusion	225	cm^2
Polarization constant		
GDL electronic conductivity	90	S/m
Membrane proton conductivity	20	S/m
Exchange current density		
a	$1.39x10^{-8}$	A/m^2
b	0.04	1/K

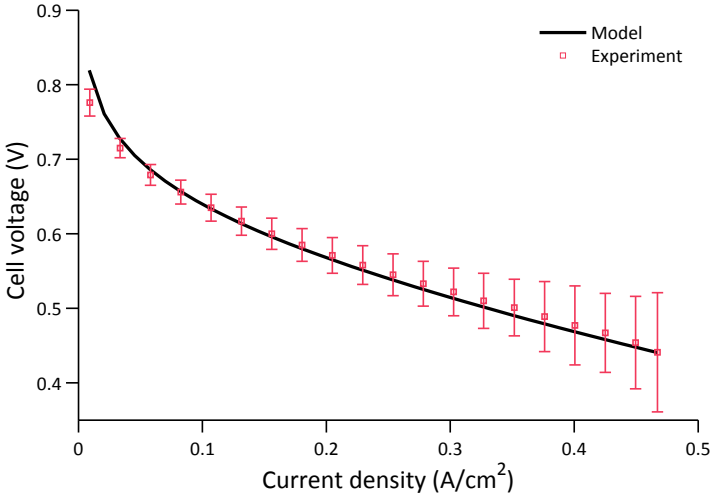

Fig. 3.4: Voltage and current of fuel cell on hydrogen and air at 160°C. Error bar shows one standard deviation

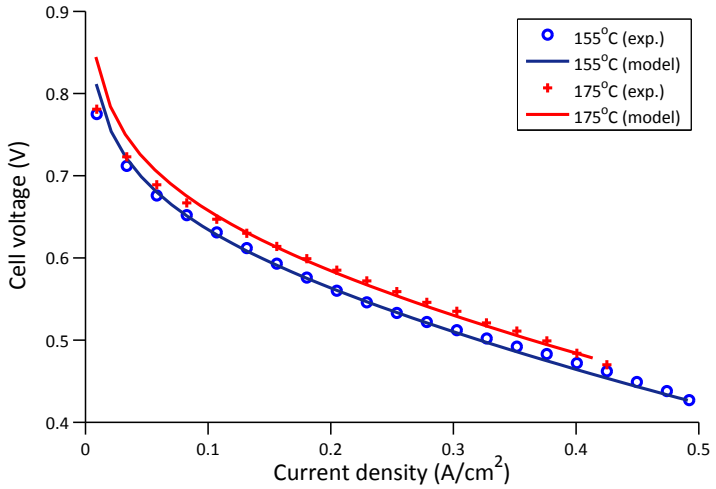

Fig. 3.5: Polarization comparing experimental and model at 155 °C and 175 °C on pure H_2 and air

A polarization curve is shown in fig. 3.6 running on pure hydrogen and reformate gas at 160 °C. The reformate gas composition is generated to replicate a steam reforming process with 60 % H_2, 24.2 % CO_2, 15 % H_2O, and 0.8 % CO. The polarization curve of 0.25 and 0.5 % CO is identical to the voltage and current when running with 0.8 % CO. The similarity shows that the CO content under 1 % is tolerable by a PBI MEA with negligible performance losses. This conclusion corresponds well with previously reported literature [Korsgaard et al., 2006].

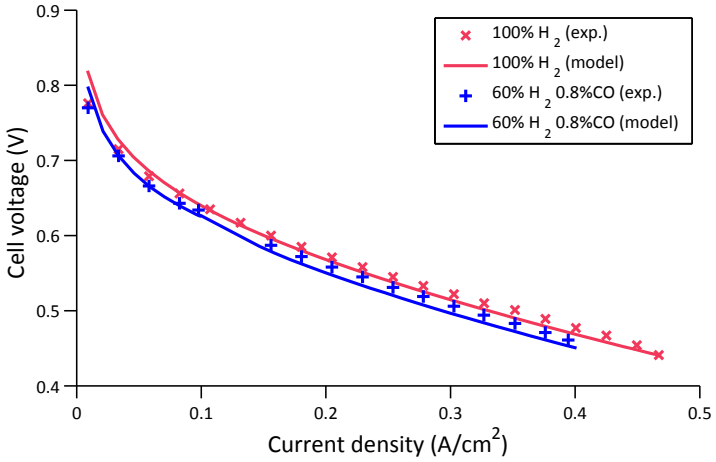

Fig. 3.6: Polarization comparing experimental and model at 160 °C with reformate gas

The fuel cell voltage is observed to be slightly higher compared to the model, especially in high current density range. An explanation for this higher experimental voltage observed in these polarization curves is that the flow rate on the anode side is higher, to maintain the same stoichiometry, which will improve the gas diffusion on the anode side and can lead to a slightly higher voltage.

Dynamic fuel cell stack performance

For each experiment a dynamic current perturbation was performed on the fuel cell stack. The current density is instantly increased from 0.09 A/cm^2 to 0.18 A/cm^2, where it stays for 30 seconds to have a stable voltage, then instantly decreases to 0.09 A/cm^2. The data is logged at 10 Hz, except the CVM system which is logged at 1 Hz. The account for the rise in current an increase in stoichiometry is performed 10 seconds before the higher current is drawn from the stack. The increase in load can be seen in fig. 3.7.

The increase and decrease in stoichiometry can also be seen in fig. 3.7, where

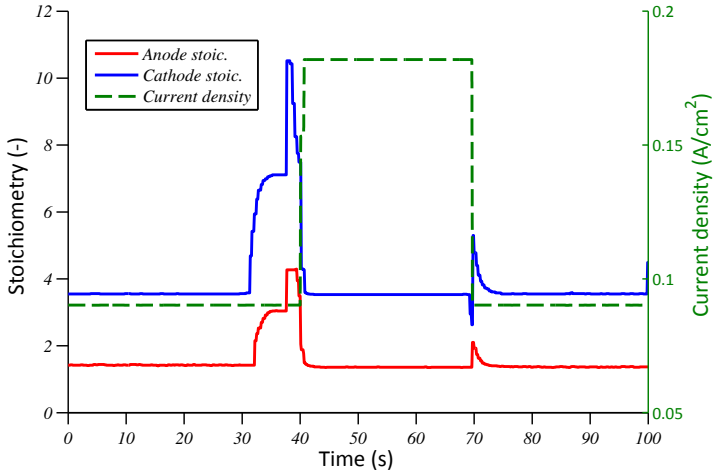

Fig. 3.7: Current step experiment from 0.09 A/cm^2 to 0.18 A/cm^2, wait 30 seconds, then back to 0.09 A/cm^2

an unexpectedly large overshoot is seen before settling to a higher flow due to internal control actions in the test station change of the mass flow controllers set point. During the decrease in current, the mass flow controllers reduce the flow with no significant undershoot. The dynamic model uses the flow rates of the fuel and air as inputs for the dynamic simulation.

The voltage of cell 5, 6, and 10 can be seen in fig. 3.8 in comparison to the dynamic model. The dynamics of the three best performing cells are presented here. The dynamics in the response of the fuel cell stack consists of three separate parts. First the fuel and air flow is increased while the current remains constant at 0.09 A/cm^2. After this the current is increased to 0.18 A/cm^2 and kept constant until the current is decreased at the same time as the flow.

The dynamic model shows a good response in the first part of the experiment(from 31 to 39 seconds) during the flow increase, the voltage increases from 0.63 V to around 0.66 V for all cells while the current is held constant. The overshoot at 39 seconds is seen in the model, however is not noticeable in the experimental data plot because of the low logging resolution. Another contribution to the lower voltage response could be the manifold volume, which can reduce the impact of the flow rate overshoot.

The second part of the dynamic response, fig. 3.8, it can be seen that the experimental data undershoots a little to about 0.52 V before settling back to 0.54 V. The undershoot most likely comes from the transient response of the flow within the cell channels which is not included in the model. After the

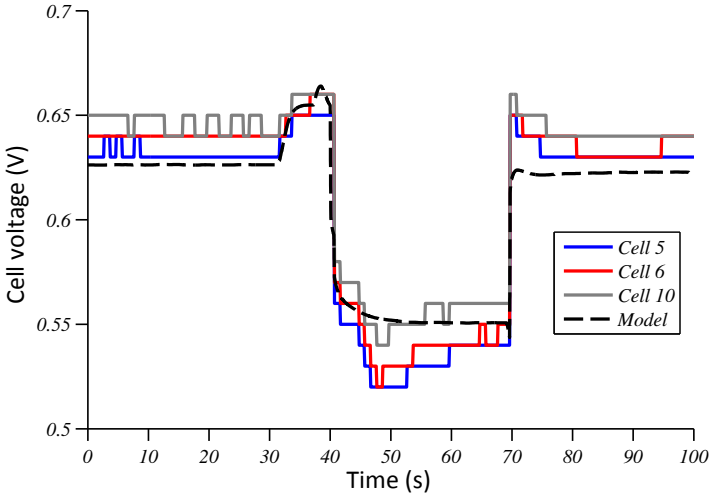

Fig. 3.8: Comparison of the voltage response for cell 5, 6 and 10 with the dynamic model

stabilization the experimental data follows the value predicted by the model. The third part of the experiment, as the current drops back to $0.09\,\mathrm{A/cm^2}$, the voltage overshoots compared to the model and stabilizes in 3 to 7 seconds. This can be explained by the hydrogen that is effectively stored in the anode flow channel volume when the current decreases.

The results indicate, for a few of the better operating cells, that the model show good dynamic similarities to the experimental data and corresponds well in steady state.

3 Methanol reformer model

To construct the system model each of main components are tested and validated. The main focus in this work has been on the reformer and the fuel cell. The reformer experiments are described below and a selection of model details are discussed.

3.1 Reformer

A 5kW electric oil heater was used instead of the fuel burner in the test of the reformer in the system. This was done based on an easier control of the tem-

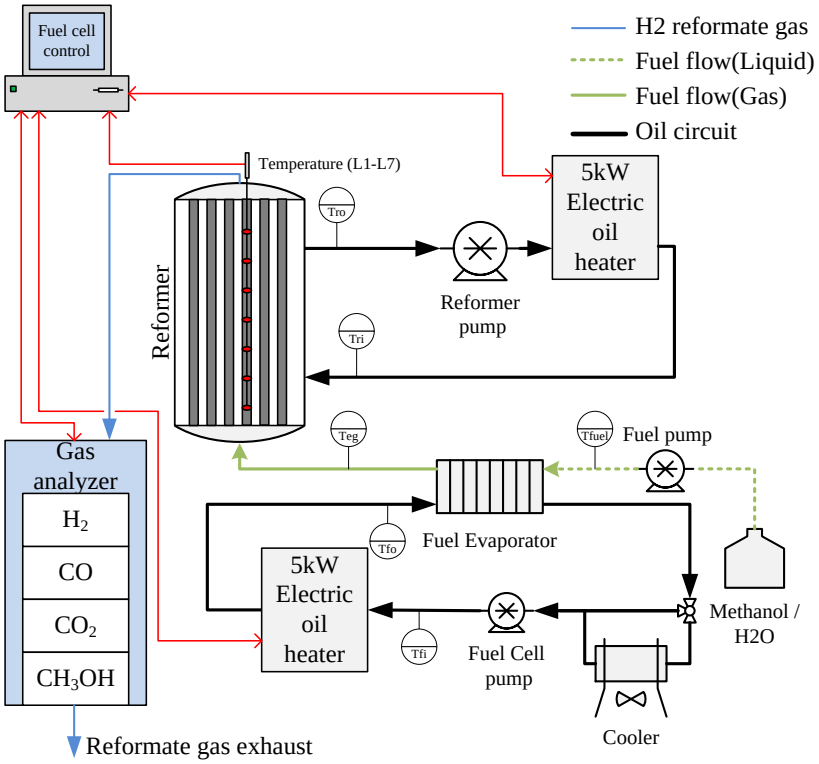

Fig. 3.9: Schematic of experimental setup for reformer with electric heaters

perature of the oil and to avoid any potential dangerous operating conditions. The two oil circuits are separated the same way as the system is described in fig. 3.1, however the fuel cell is also exchanged with an electric heater. Methanol is fed through a fuel pump and heated up in the fuel evaporator. From here the evaporated gas is led into the bottom of the reformer where the gas is split up into several 20 mm tubes. The tubes are filled with 1.5mm BASF RP/60 Cu/Zn steam reforming catalyst pellets [BASF, 2008]. The reformer used in this work is tubular with oil passing through 20 mm tubes filled with catalyst. The temperature of the reformer is measured with a multiple point type-T thermocouplers and is measured in 7 places with about 6 cm spacing between along the gas channel in one of the catalyst bed tubes. If the catalyst bed is stored it is in an oxidized state and an activation procedure is nessesary. The procedure for activating the reformer catalyst is presented below.

Catalyst activation

To prepare the reforming catalyst a series of activation procedures are needed. The activation of the catalyst can be done with a small amount of hydrogen, mixed with an inert gas, which is led into the catalyst bed and slowly increased until the catalyst is activated. The reaction is an exothermic reaction, which means that the temperature rises during activation and a careful observation of the catalyst bed temperature is required. Alternatively, another method to activate the reformer is to use the methanol/water fuel at a very low rate. During the activation of the reformer the temperature is monitored by a 7 point temperature probe, which can be seen in fig. 3.10. The temperature probes L1 to L7 are located throughout the reformer from the top to the bottom. The reformer is oriented so that the beginning of the reformer is at the bottom and the end is at the top. The temperature of the reformer is heated up to 220 °C and a feed of methanol/water is fed using 200 ml/hr during the activation process. To avoid sintering of the catalyst the temperature is kept under 300 °C at all times [BASF, 2008]. During the activation process it can be seen how the temperature rises from the start of the reformer to the end.

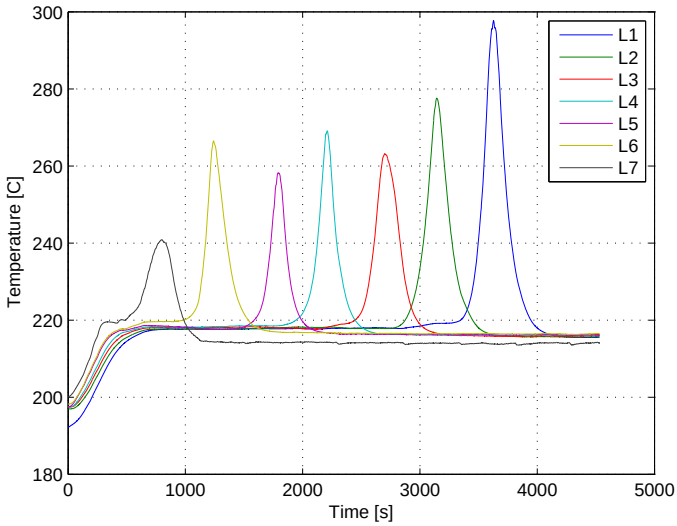

Fig. 3.10: Reformer activation sequence with 200ml/hr methanol/water activation. The temperature probe L7 is at the start and L1 is the end of the reformer

When the temperature in the reformer has reached a uniform level the activation process is complete and the reformer can be used. The catalyst is now in a reduced state and is kept in this state until oxygen is introduced.

Reformer temperature

To validate the temperature model of the reformer a series of tests were performed with the reformer. A picture of the test setup can be seen in fig. 3.11 showing the reformer, burner, evaporator and pump. Additionally two electric heaters are used to heat up the reformer and evaporator.

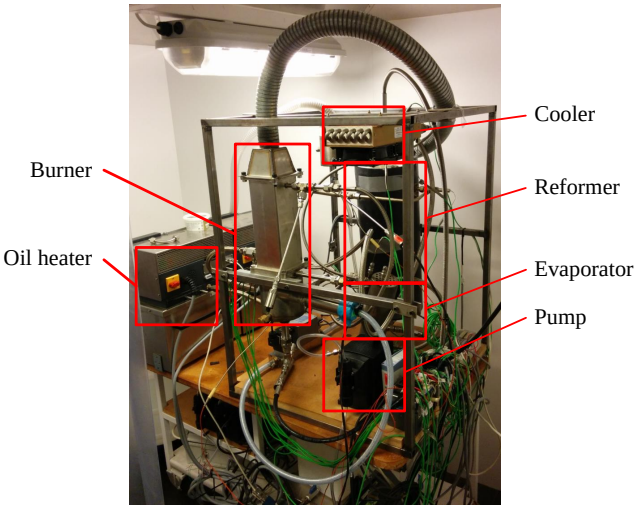

Fig. 3.11: Test system with reformer, evaporator, burner and cooler.

The reformer is about 50 cm high and isolated with a foam material with a thickness of about 50 mm. A sketch of the reformer can be seen in fig. 3.12, where the methanol input, gas output, oil input and output are shown. A section cut of the reformer is shown on the right and it can be seen how the oil is directed into the reformer. To introduce a turbulent flow in the reformer a series of plates are installed in the flow channel.

The model assumes a uniform temperature in the reformer, however the actual temperature might vary throughout the flow channel depending on the flow of methanol, oil temperature or ambient temperature. The model then assumes a mean temperature of the reformer to evaluate heat transfers from other components and the reformate gas is instead based on the input oil temperature.

The temperature of the reformer is calculated based on eq. 3.18 and eq. 3.19. The various heat contributions can be seen from eq. 3.18, where the total heat is calculated.

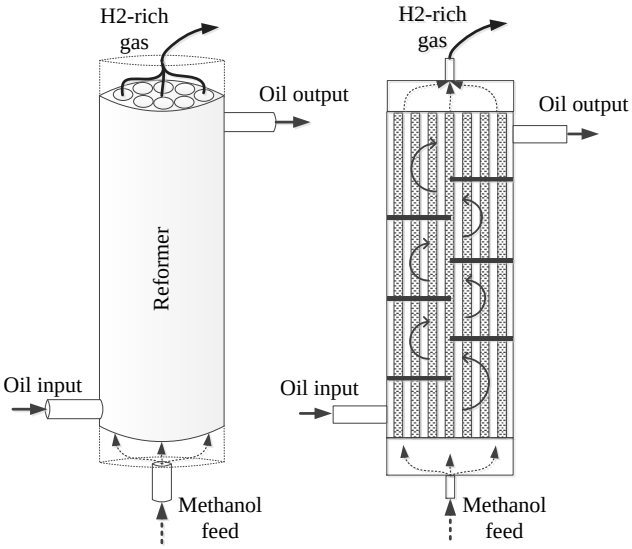

Fig. 3.12: Schematic of reformer system with oil system. Right is a drawing of the internal sections for the oil flow.

$$\dot{Q}_{reformer} = \dot{Q}_{SR} + \dot{Q}_{oil} + \dot{Q}_{convection} + \dot{Q}_{conduction} \tag{3.18}$$

$\dot{Q}_{reformer}$ is the total heat flow in the reformer, $\dot{Q}_{SR}$ is the heat required for steam reforming of methanol, $\dot{Q}_{oil}$ is the heat flow from the oil circuit, $\dot{Q}_{convection}$ is the heat convection from the gas, and $\dot{Q}_{conduction}$ is the heat radiated from the reformer via conduction.

The change in temperature can be seen in eq. 3.19 and is based on the mass of the reformer $m_{reformer}$ and the specific heat capacity $Cp_{reformer}$.

$$\Delta T_{reformer} = \frac{1}{m_{reformer} \cdot Cp_{reformer}} \cdot \int_0^t \dot{Q}_{reformer}\, dt \tag{3.19}$$

During the test of the reformer a constant oil temperature of 240 °C is used to heat the reformer during operation. The flow of methanol and water mixture is increased in steps as shown in fig. 3.13(a). The reformer is started up from ambient temperature and heated to operating temperature of 240 °C. The experimental and simulated temperature of the reformer can be seen from fig. 3.13(a). At about 25 minutes the reformer reaches 160 °C and the methanol and water mix is fed into the reformer. A gradual stepwise increase is initiated

until a maximum of 5500 ml/hr is reached at 180 minutes. A comparison of the model and reformer temperature can be seen in 3.13(b) where the temperature varies up to ±5 °C.

The exit oil temperature of the reformer is simulated to evaluate the influence on the other components. Based on the input temperature of the oil, the amount of heat loss from steam reforming, convection, and conduction the oil the output temperature is simulated which can be seen in fig. 3.14. The temperature and methanol flow are plotted and a good correlation between the model and experiment can be seen.

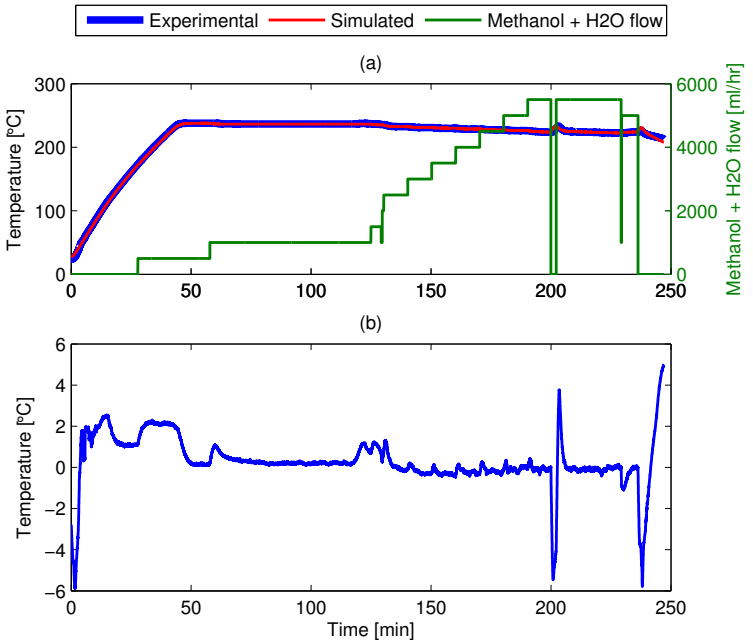

Fig. 3.13: Mean reformer temperature during startup and load step changes. (a) Comparison between experiment and simulated temperature (b) Difference between experiment and simulated temperature

The heat contributions, shown by eq. 3.18, can be seen in fig. 3.15 during the changes in methanol and water feed. It can be seen that the steam reforming process is the dominating loss in the reformer. The second largest is the convection from the methanol gas feed and last the conduction. The only heat source for the reformer is the oil circuit and under stable conditions is equal to the losses.

A verification of the conduction loss can be seen in fig. 3.16 and the heat

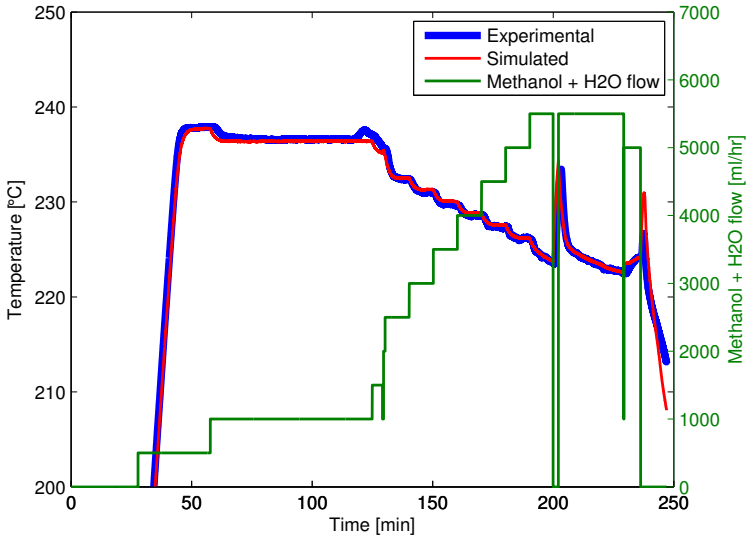

Fig. 3.14: Temperature of output oil from reformer during startup and load step changes

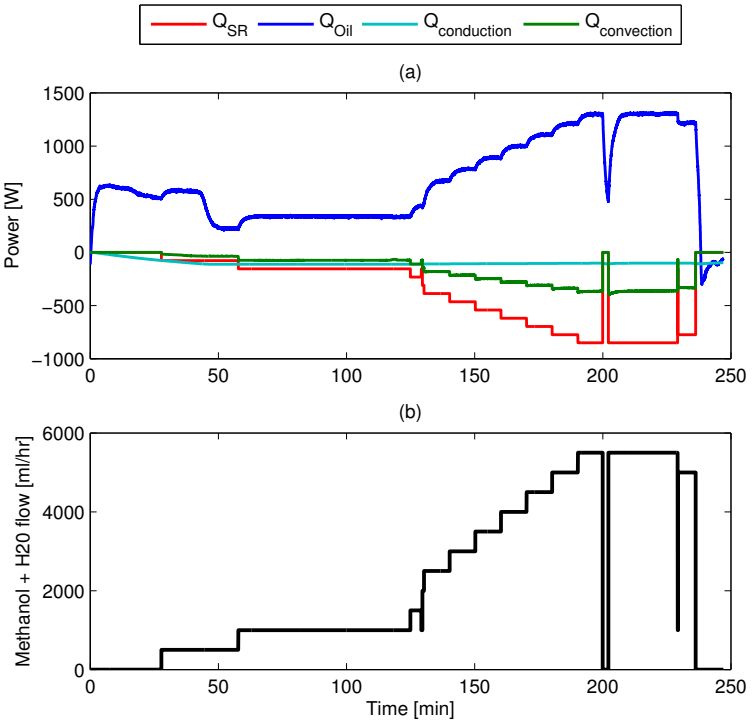

Fig. 3.15: Individual heat contributions in reformer during startup and load step changes. (a) Heat contributions (b) Methanol + water feed

loss is very small compared to steam reforming or convection. The oil flow and methanol feed was stopped and the mean temperature in the reformer was recorded. The beginning temperature is 240 °C and after about 10 hours the temperature reached 40 °C.

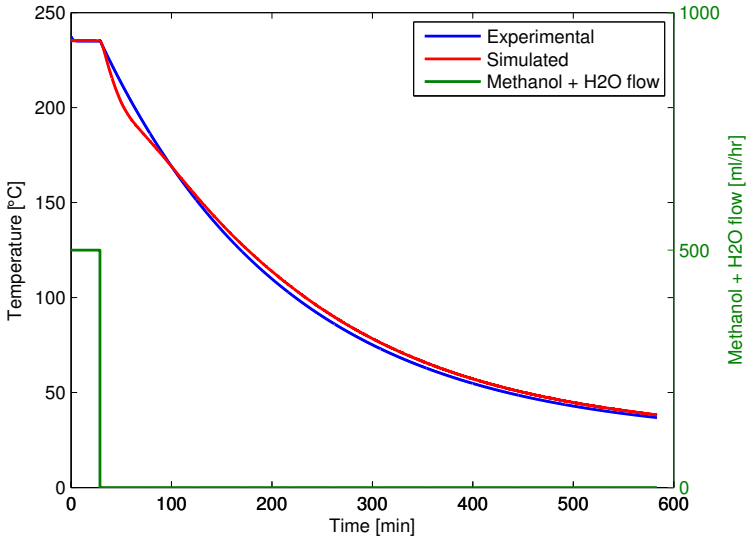

Fig. 3.16: Temperature of reformer during cooldown

The loss of heat from conduction seems insignificant when operating with a steam reformer, however the method can be used in the situation where the reformer is operated without isolation.

The next section shows the experiments measuring the gas composition at different reformer temperatures and flows.

Reformer gas composition

The reformer was tested and the gas composition was measured with focus on the methanol slip and the CO content. The gas composition was measured with a Siemens Fidamat 6, which is able to measure the Total Organic Carbon (TOC), or in this case the methanol content of the gas. The dry gas was measured with a Siemens Ultramat which measures the CO_2 and CO content and a Siemens Calomat 6 measured the H_2.

The oil inlet temperature is increased in steps of 10 °C10°C from 200 °C to 290 °C. The methanol fuel flow was increased in steps of 500 ml/hr from 0 to

9000 ml/hr and was repeated for each temperature step. To ease the use of the data in the model a fitted surface is used based on the experiment data. The methanol slip surface is shown in fig. 3.17.

The methanol slip plot, shown in fig. 3.17, shows a high amount of slip at low oil temperature and high flow. The plot shows a slip of about 80 000 ppm at 200 °C oil temperature and 9000 ml/hr. The experiments show that with an increase in fuel flow the methanol slip increases, however it is more significant at low temperatures. With an increasing temperature the methanol slip reduces, which corresponds well with an increased conversion rate.

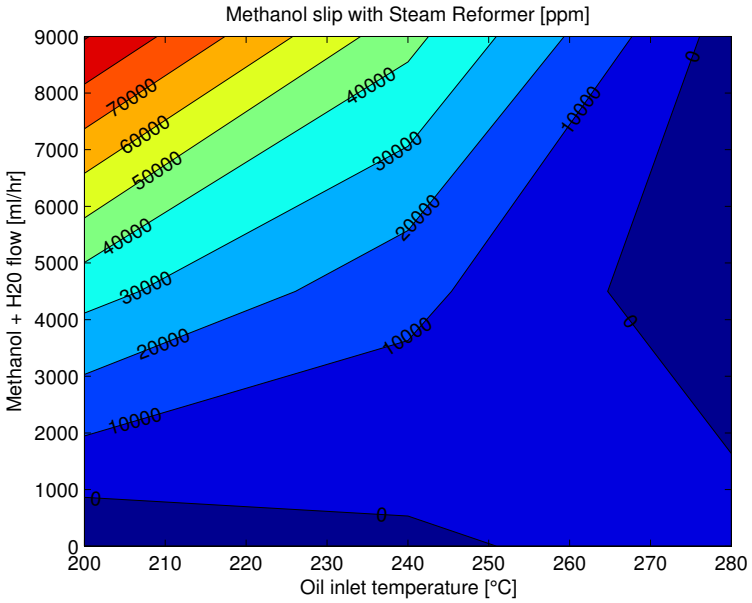

Fig. 3.17: Methanol slip from reformer compared to input oil temperature and flow

The experiments also show the reversed tendency for the CO content in the gas outlet as shown in fig. 3.18. The CO content in the gas show a higher concentration with higher temperatures and a higher flow decreases the amount.

Simon Araya et al. [2012a] studied the effects of methanol vapor mixture in the anode gas and concluded that operations with 3% or lower had negligible effect on degradation or performance. The work also showed that significantly higher concentrations of 5 % and 8 % had performance degrading properties, however the degradation was partially recovered if the methanol vapor mixture was decreased. Combining the methanol slip and CO content gives the possibility to ensure a tolerable methanol slip with a low CO content. Assuming a constant methanol slip of 2 % gives a relatively low CO content in the gas,

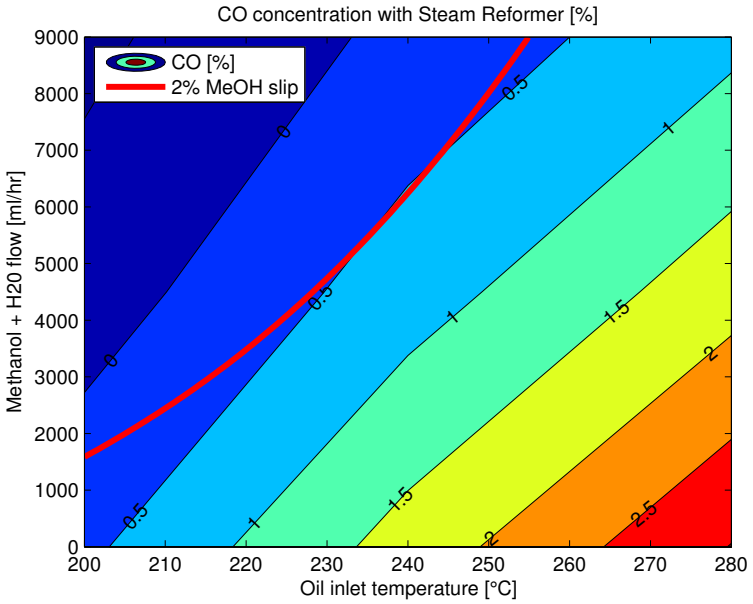

Fig. 3.18: CO gas concentration from reformer compared to input oil temperature and flow. Red line indicates a 2% methanol slip.

which is illustrated in fig. 3.18. Following the methanol slip of 2 % shows a CO content below 0.5 % with negligible effect on the performance. This is confirmed both by the tests done on a HT-PEM fuel cell stack in this work and by several independent studies [Andreasen et al., 2011b; Li et al., 2009].

The mapping of the methanol slip and CO content is used in the model for the reformate gas output and the fuel cell stack performance is evaluated. This method to evaluate the gas composition, which is based on the methanol slip, can help decrease the fuel cell stack degradation. The method is also applicable if a lower methanol slip or CO is required, for example if the type of fuel cell is different. The methanol slip and CO content can be controlled by the input oil temperature, and thereby it can be used as a parameter for controlling the reformer gas composition output. Because of the link between the oil input temperature for the reformer can determine the gas composition, it is important to know the performance of the burner.

3.2 Burner

The burner used in the system and shown in fig. 3.11 is constructed as a combination of a catalytic burner and a heat exchanger. A schematic of the burner can be seen in fig. 3.19. The burner is fed by hydrogen and air which is mixed in a chamber before the burner. The burner consists of a catalytic mesh. The hot air is directed up through a heat exchanger and the oil is heated up to the operating temperature of the reformer.

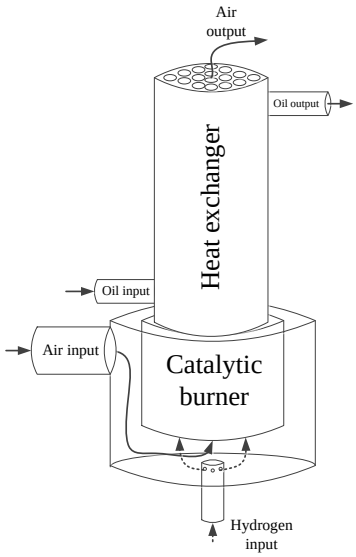

Fig. 3.19: Schematic of the catalytic burner with heat exchanger

The burner temperature is measured both in the catalyst mesh and in the air output from the heat exchanger. The oil temperature is also measured at the input and the output. During operation, the temperature of the burner air was significantly higher compared to the rest of components, which resulted in an increasing degradation of the oil in the burner heat exchanger. A redesign of the burner/reformer without the use of heat transfer oil is recommended. If the temperature increases uncontrollably in the burner, the oil can leak because of increased pressure in the system, or the oil can ignite which would cause a dangerous situation. The burner was tested and verified compared to the model, however an electric heater was used in its place for the test of the reformer. The other electric heater was used for the evaporator for pre-heating the methanol fuel before the reformer. The evaporator is shortly presented.

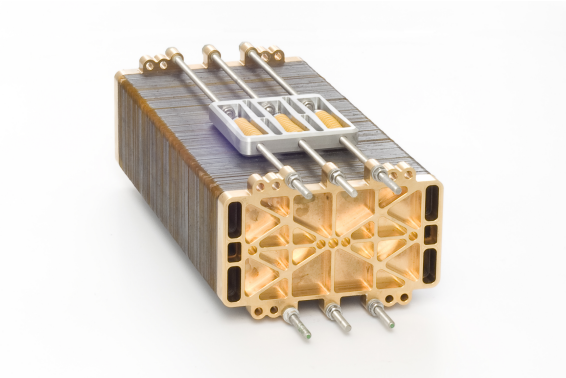

Fig. 3.20: S165L HTPEM stack from Serenergy A/S

3.3 Evaporator

The evaporator is modeled as a lumped mass with three inputs. The purpose of the evaporator is to heat up and evaporate the methanol-water mixture. The evaporator is connected to the fuel cell via the oil circuit, which also cools the fuel cell, but the heat from the air fan in the fuel cell and the exhaust air from the burner is also led through the evaporator.

3.4 Fuel Cell

The fuel cell stack modeled in this system is a 120 cell HT-PEM fuel cell stack, similar to the short stack tested Chapter 2. A picture of the stack can be seen in fig. 3.20 and the net power of the system is rated at 6 kW on dry hydrogen and 5 kW on reformate gas [Serenergy A/S, 2014].

The following section will investigate the use of lumped thermal models and the interaction between the components as shown in fig. 3.1.

4 Open loop system operation

The system simulation presented in this section is the system operating without any temperature controller on the reformer or burner. Based on an iterative training process a constant stoichiometry of 1.4 was found where reformer and fuel cell temperature is within working range. An optimal constant stoichiometry can be found if the system is only operated at a constant power, however

the efficiency and the resulting gas composition at other loads can result in several issues. First is the efficiency which is based on the gas content and the stoichiometry, but also operating at other loads can change the temperature of the reformer which can result in gas compositions that can harm the fuel cell. The simulation input is the current density and the corresponding methanol flow which can be seen in fig. 3.21.

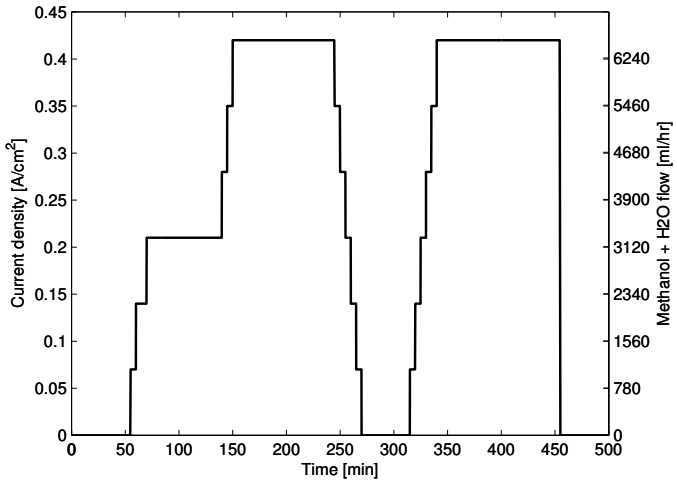

Fig. 3.21: Fuel cell current density and methanol flow used for input for the system model

The scope of model input is to investigate how rapid changes in the fuel cell current will affect the four components. Furthermore, it will show if the anode stoichiometry in the fuel cell reaches a limit where degradation can occur.

The temperatures of the four components can be seen in fig. 3.22. It can be seen that during the first step-up sequence the temperature of all the components has not reached a stable level. At 100 minutes the temperature stabilizes at about 220 °C for the reformer, 140 °C for the fuel cell and 120 °C for the evaporator. The blower in the burner is coupled directly with the estimated hydrogen fuel cell anode exhaust gas with a gain of 12. This means at a hydrogen flow of 2 l/min hydrogen calculates to a flow of 24 l/min air in the burner. The efficiency is linked to a series of parameters in the system, like gas composition and reformer temperature, however, there is a strong link between the selected stoichiometry at the fuel cell and the system efficiency. A high anode stoichiometry requires the burner fan to operate at a higher flow which results in more heat being directed into the evaporator. The increased temperature in the evaporator does not increase the electric efficiency significantly. It can be seen that during the high load($0.47\,\mathrm{A/cm^2}$) at 150 minutes the efficiency drops to about 26 % compared to the 28 % with lower load($0.24\,\mathrm{A/cm^2}$) at

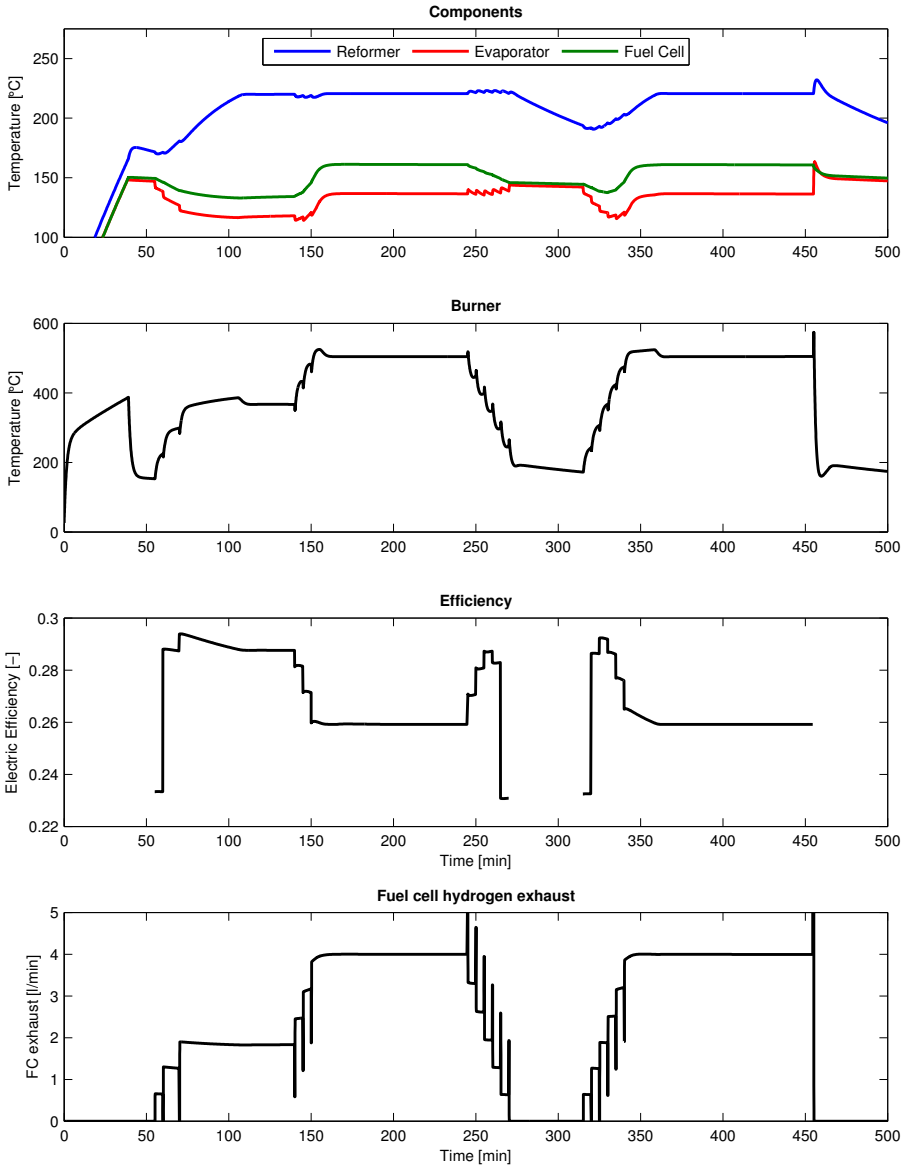

Fig. 3.22: Temperature of the four components. Reformer, Evaporator and Fuel cell and Burner. The electric efficiency of the system during and the fuel cell exhaust flow is illustrated

100 minutes. At about minute 250 the fuel cell system decreases its load until it stops at 0 load. The system is idle for about 50 minutes. As there is no fuel used in the idle mode the efficiency is 0, which explains the gap in the efficiency graph in fig. 3.22.

The reason for the lower efficiency at maximum load (5 kW or $\sim$0.47 A/cm^2) is because the heat generated in the fuel cell and burner exceeds the necessary heat for the system to run. The fuel cell is also operating at a higher load which will decrease the efficiency. The temperature of the fuel cell oil circuit is also kept at 150 °C by the use of the oil cooler, which will increase the parasitic losses. One way to increase the efficiency is to use a lower anode stoichiometry, however, it is not recommended or possible with the HT-PEM used in this work, which was a limit of 1.35.

The burner temperature is measured in the burner catalyst mesh to illustrate the quick response and the potentially high temperature. The temperature in the burner mesh is the highest temperature in the system and it is critical that this temperature is observed and controlled. fig. 3.22 also show the electric efficiency, which is based on the higher heating value of methanol and the electric output from the fuel cell.

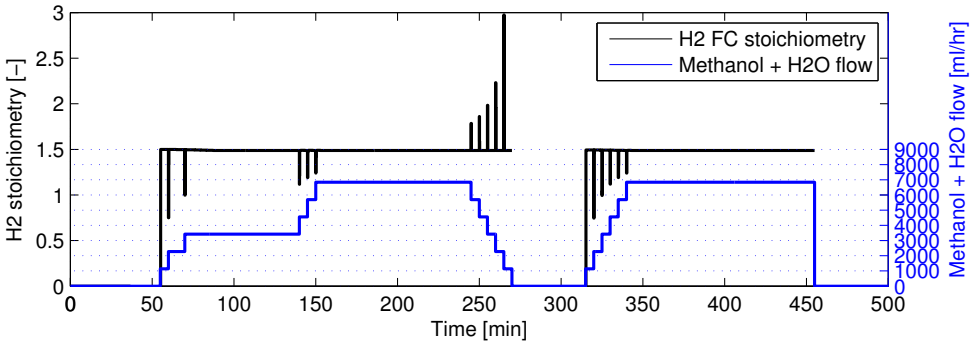

Fig. 3.23: Stoichiometry during fuel cell load steps

During the rapid step-up and step-down in the fuel cell current density a series of stoichiometry spikes can be seen in fig. 3.23. The spikes indicate the dynamics from the methanol pump, through the reformer and to the fuel cell. The model simulates a delay of 10 seconds, which can be seen as an under and over stoichiometry in fig. 3.23. Based on the discussion in Chapter 2 an under stoichiometry on the fuel cell can be a significant factor in permanent performance loss or failure.

The open loop system design shows that the system is capable at operating

without a temperature controller on the reformer, however the temperature of the components are not in any ideal range which a controller may improve.

The next section describes how a system control may be implemented on this system or similar systems. The use of a controller allows for a better control of the internal temperatures, which if not controlled in worst case can damage the system or the people operating it. Another significant gain from using a controller is the ability to ensure a constant temperature for the reformer, which results in a better gas composition and thereby a better performing fuel cell stack.

5 System control

Shown in the system schematic in fig. 3.1, the excess hydrogen from the fuel cell is used as a fuel for the burner. The rate of excess hydrogen from the fuel cell is not easily monitored so an estimation is required. This hydrogen flow estimation is based on the fuel cell load, methanol pump flow, and reformer temperature.

The fuel cell load is not used as a directly controllable parameter in this system. Using the fuel cell load to shape excess fuel amount have been studied by Justesen et al. [2013] where the load is controlled. To avoid having a variable load control in the system, a constant current request is applied. A delay and ramp are used when changing the fuel cell current to avoid starvation or overloading the burner. The delay is measured from the methanol pump to the reformate gas output of the fuel cell and is estimated to about 10 seconds. The two outputs from the main controller are the burner fan and the methanol-water pump flow.

5.1 Control design

To stabilize the system under dynamic loads and increase efficiency, a control design is presented below. The controller uses a current set-point as input and controls the burner fan, fuel cell fan, and the methanol pump. Based on previous work by the author, a combined burner and reformer heat exchanger with a cascade controller for the reformer temperature was used [Andreasen et al., 2013]. The use of a cascade controlling method is also used here and presented below.

Cascade control

Since the burner dynamics is significantly faster compared to the reformer, a cascade controller is used to control reformer temperature. As shown in figure 3.17 and 3.18 the gas composition can be estimated based on the input methanol flow and the input oil reformer temperature. The input oil reformer temperature is used as the input for the controller and is shown as $T_{r,set}$ in fig. 3.24. The burner temperature used in this controller is measured in the middle of the catalytic bed and the heat exchanger thermal dynamics is calculated separately. It is assumed that the temperature of the air in the heat exchanger is the same as the burner temperature.

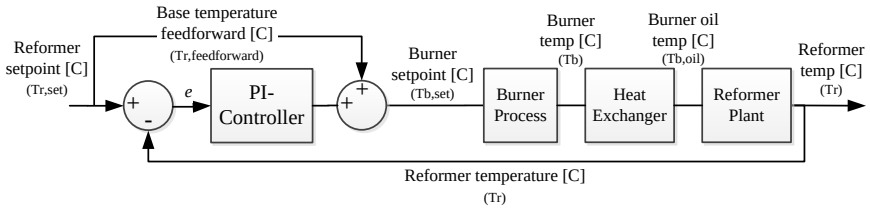

Fig. 3.24: Controller for the oil input in the reformer

A feed-forward is used to increase the set-point for the burner because the temperature of the burner would rarely be below the reformer temperature. A simple PI controller is used for the feedback loop, where the reformer temperature is the output. Reformer plant is described in chapter 3 and is based on the steam reforming reaction, heat from the oil circuit, gas convection and conduction. The feedback loop is calculated from the reformer oil temperature, which is measured at the inlet of the reformer. The error is the input for a simple PI controller.

The burner set-point temperature is calculated based on the PI controller and is the input for the burner process which can be seen as $T_{b,set}$ in figure 3.25. The measured burner process thermal time constant is 10 seconds and the reformer is about 97 seconds. The burner catalyst has a significantly lower response time compared to the thermal dynamics in the reformer system. This means that if the temperature of the burner can be stabilized it can be controlled with a much slower feedback loop as shown in fig. 3.24. The burner controller is separated into three parts "Burner control loop", the "Burner feedforward", and the "Stoichiometry controller" as shown in fig. 3.25.

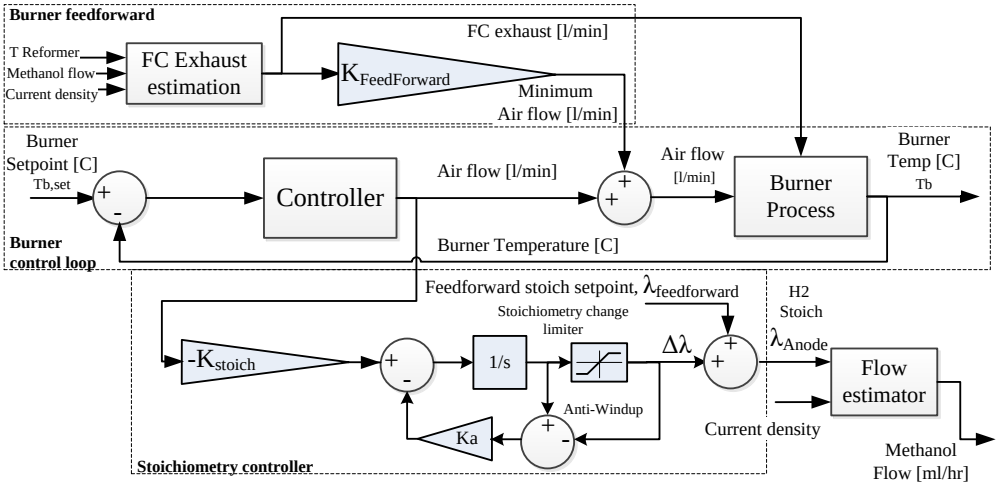

Fig. 3.25: Temperature burner controller

Burner control loop

The main loop in the burner control is the airflow controller, which is based on a feed-forward controller with a feedback control loop. The temperature of the burner is regulated with the air fan because of the fast response, however, if the air fan is increased, the stoichiometry is decreased using the stoichiometry controller.

The burner temperature is simulated and the input is both the airflow and the exhaust hydrogen flow. If the temperature is too high in the burner, the airflow is increased. The burner controller needs a lower limit to avoid the air fan from stopping if the temperature is too low. A minimum airflow is based on the estimated fuel cell exhaust flow multiplied by the gain, $K_{feedforward}$. The gain $K_{feedforward}$ depends on the type of burner used and in this work a minimum gan of 10 is used.

Burner feed-forward

The burner feed-forward part of the burner controller, as seen in figure 3.25, is used to estimate the exhaust hydrogen from the fuel cell and thereby give a minimum airflow to the burner.

The fuel cell stack exhaust is not easily measured, which is why an observer is implemented. The observer is based on the current density in the fuel cell,

the reformer temperature, and the methanol flow. The reformate gas flow is calculated based on conservation of mass and the total molar flow is estimated. The gas composition is estimated using the reformer methanol slip and CO in figure 3.17 and 3.18 and the molar flow of hydrogen is extracted. The used hydrogen in the fuel cell is calculated as shown in equation 3.20 and subtracted from the hydrogen flow.

$$H_{2,fc}[mol/s] = \frac{j \cdot n_{cell} \cdot A_{cell}}{2 \cdot F} \tag{3.20}$$

The input variable j is the current density, n_{cell} is the number of cells in the stack which is constant, like A_{cell} which is the active cell area and F is Faradays constant. A time delay of 10 seconds is added to the air flow PI controller to account for the delay between the methanol pump change and the burner.

The blower dynamics in the system is neglected, as the system is controlled with a mass flow controller with an internal feedback loop. The blower dynamics should be investigated if a normal fan is used, however, this is not covered further in this work.

Stoichiometry controller

If the temperature of the burner is a higher compared to the burner set-point, the *Burner control loop* will regulate the fan to cool the burner immediately. The *stoichiometry controller* takes the airflow input and multiplies it with the small gain $-Kp_{stoich}$. This signal is integrated, which summarizes the work done by the burner air fan, therefore, a stoichiometry change is introduced and added to the initial stoichiometry set-point. The stoichiometry is intended to be a slow reacting controller, which can make small adjustments to the system stoichiometry.

The initial purpose with this part of the controller is to decrease excessive use of the air fan for the burner. Using a slow regulating stoichiometry controller also has the benefit of increasing the total system efficiency as this is mainly linked to the stoichiometry. However, the limit of how low the stoichiometry is possible is debatable a careful study of the HT-PEM fuel cell stack is critical before implementing this controller in a system. The next section will describe the control simulation in more detail.

5.2 Control Simulation

The controller is implemented in the Matlab Simulink system model and the results can be seen in fig. 3.26. The reforming temperature is set constant to 235 °C. A constant stoichiometry set-point is set to 1.5 and the stoichiometry change limit is set to −0.2 and 0.4. The change limit ensures that the stoichiometry cannot be set to a level below 1.3, which is used as the lowest stoichiometry for a the HT-PEMFC. The higher stoichiometry is used when the system is not able to keep up the reformer temperature. A higher stoichiometry can be seen in this simulation and is used at the end of the startup sequence. If the fuel cell is degraded, a higher limit should be set, yet this will decrease the overall system efficiency. The stack tested in this work was already in a degraded state and a stoichiometry limit below 1.35 is not possible.

Table 3.2: Controller values for burner and reformer loop

Reformer	Value	Burner	Value	Stoich.	Value
K_p	20	K_p	5	K_{stoich}	2e-6
K_i	0.05	K_i	0.01	K_a	1
Top limit	800 [°C]	Top limit	800 [l/min]		
Bottom limit	200 [°C]	Bottom limit	0 [l/min]		
		$K_{feedforward}$	20		

For the control simulation the values in table 3.2 are used.

To ensure a constant power output a power set-point sequence is used as an input for the controller, thereby calculating a current density for the fuel cell stack. Based on the fuel cell voltage, a feedback loop is used to regulate the actual power output. Furthermore, included in the power controller is a rate limiter to avoid under stoichiometry in the fuel cell, as seen in the open loop simulation. The current density rate limiter is set to $0.06\,A/cm^2/min$. The first step in the power sequence is an increasing of the power set-point to 1500 W at 72 minutes and is kept for 138 minutes. Second step increases the power output to 2500 W and keeps this level for 84 minutes. The third step increases the power output to 5000 W and keeps the level for 166 minutes. The decreasing steps go to 2500 W for 84 minutes and 1500 W to the end of the simulation.

The temperature of the burner and reformer can be seen in fig. 3.26, which is based on a stepwise increase and decrease in system power output. The temperature of the burner closely follows the set-point, which shows the inner loop of the cascade controller is stable and responsive with a settling time of 5 seconds with and an overshoot of about ±10 °C. However, the reformer

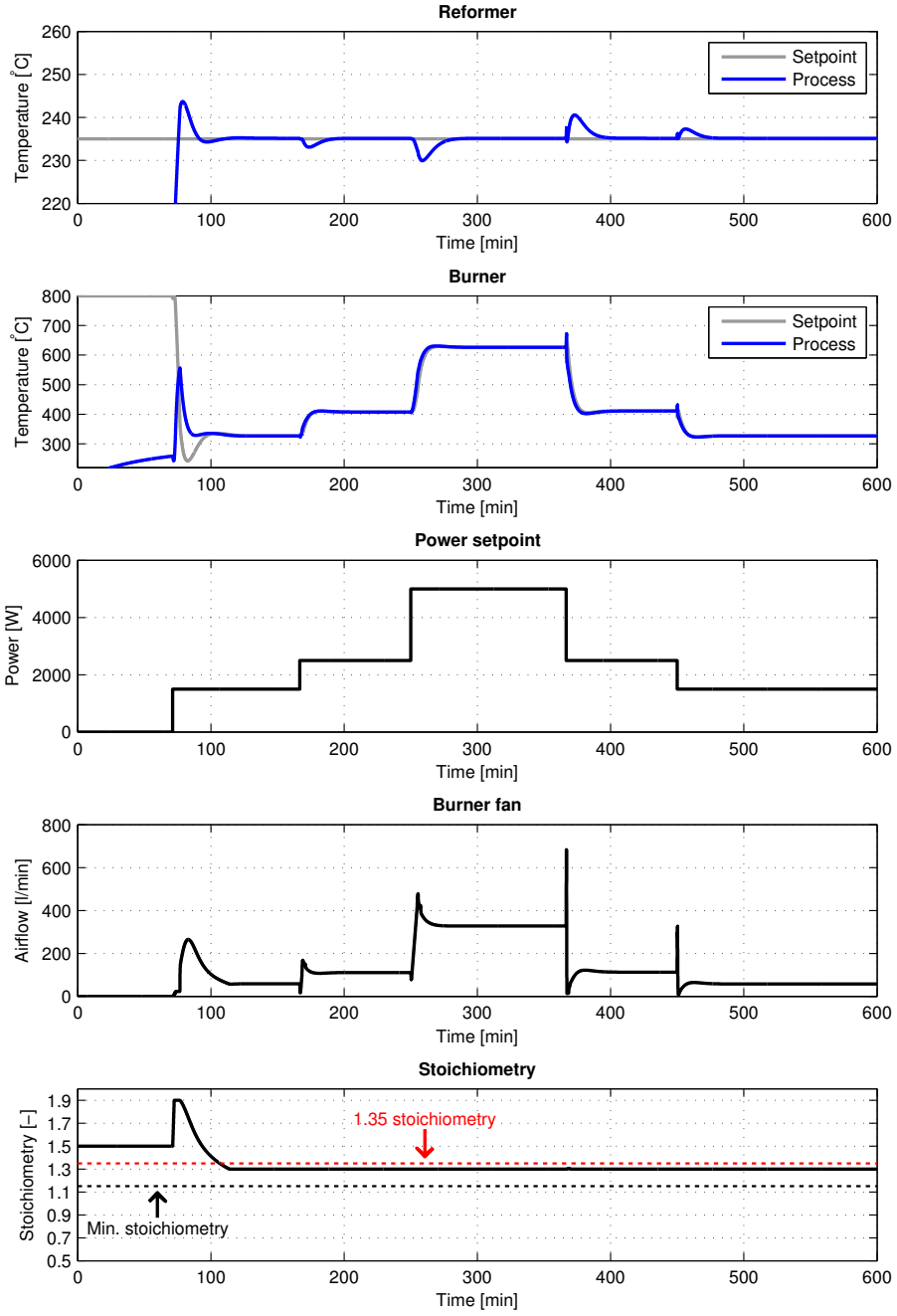

Fig. 3.26: Model results with cascade controller. Showed are the reformer and burner temperature, power set-point, burner fan output and stoichiometry set-point

temperature act significantly slower with a settling time of about 12 minutes and with an overshoot of about ±5 °C. The temperature difference between the reformer set-point and the reformer can result in a higher CO concentration and at relatively short time periods the reformer produces higher impurities, but the effects are negligible. An increase of 25 °C in the reformer temperature results in 250 °C which corresponds to a CO content of 0.5 % at 5 kW or 1.5 % at 1 kW, according to fig. 3.18.

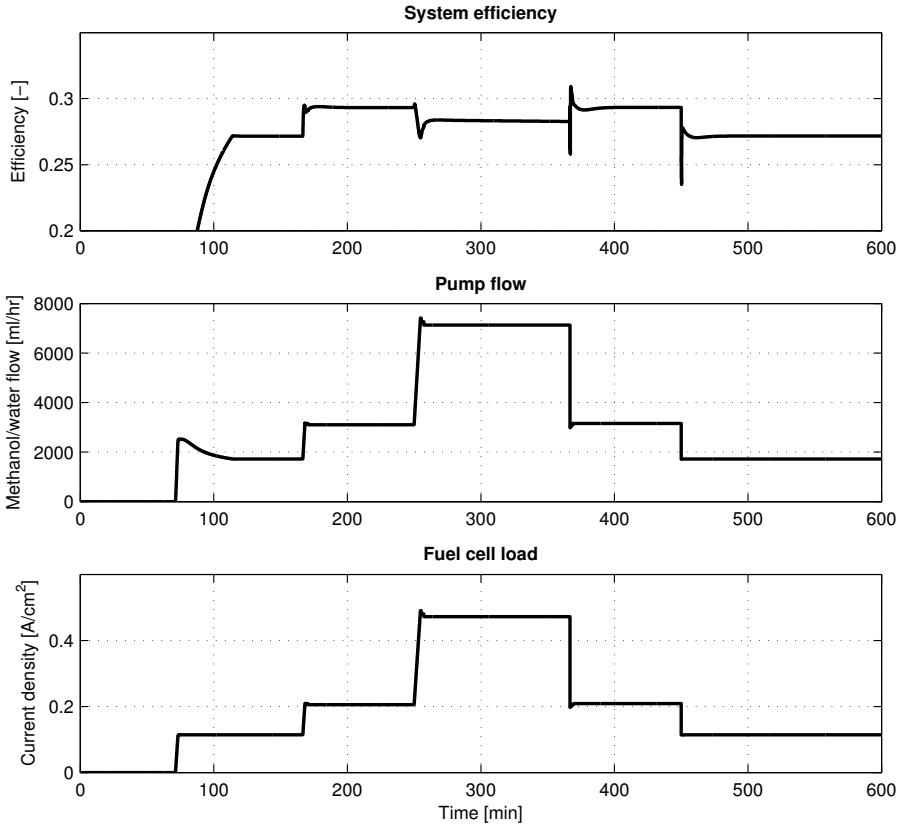

Fig. 3.27: System efficiency compared to system load and fuel cell current density

The temperature of the reformer and burner is started at 100 °C. The reformer is heated up to 180 °C, where the initial power set-point is initiated at 1500 W. Because the reformer temperature is still below the reformer set-point, a higher stoichiometry is set, which means a higher stoichiometry compared to the feed-forward stoichiometry, $\lambda_{feedforward}$. The startup sequence is complete at 120 minutes and is stable before the next step increase. During the startup, the stoichiometry change, $\Delta\lambda$, reaches the limit in how much it can deviate and

the anti-windup enables the integrator to stay within the limit and avoid an integrator windup. The anti-windup is there to avoid keeping an unnecessary high stoichiometry caused by a low reformer temperature, thereby increasing the burner temperature for a longer time.

The fuel cell anode stoichiometry can also be seen in fig. 3.26. Indicated by two lines are the minimum stoichiometry and the feed-forward stoichiometry. The minimum stoichiometry is set to 1.3, however, as shown in Chapter 2, going below limit for the fuel cell can cause it to degrade because of mass transfer, which means that this limit is not suitable for the HT-PEMFC tested in this work. A new and unused HT-PEM fuel cell might be able to work under low stoichiometry levels, but it is important to investigate the minimum possible fuel cell anode's stoichiometry. It can be seen that under 5 kW operation it can regulate the stoichiometry to 1.3, which means that other methods have to be utilized to increase the efficiency further. The efficiency of the system can be seen in fig. 3.27 and shows the system running at 27 % at 1.5 kW, 29 % at 2.5 kW, and 28 % at 5 kW. The efficiency is calculated by dividing the electric power with the higher heating value (HHV) of methanol. The parasitic power is set to a maximum of 600 W and a minimum of 200 W and is scaled according to the parasitic loads. The lower efficiency at high load is because the methanol slip is significantly higher at a higher methanol fuel flow. The use of a higher reformer temperature would increase the methanol conversion rate, however at the cost at adding more CO. To enable a better gas composition during different loads a varying reformer temperature is required and this is presented below.

5.3 Gas composition conditioning

A significant advantage of using a controlled reformer temperature is the possibility to shape the gas composition and thereby decreasing the degradation of the fuel cell or potentially prolonging the life-time of the whole system. The resulting gas composition for the controller with a constant reformer temperature can be seen in fig. 3.28. The constant reformer temperature of 235 °C shows that during high flow, corresponding to 5 kW operation, methanol slip increases to 4 %. When the temperature of the reformer stabilizes the methanol slip drops to 3.4 %, which is not desirable. Operation at 1.5 kW and 2.5 kW (minute 100 and 200) show significantly lower methanol slip at 0.24 % 0.8 %, respectively. However, the CO concentration at these temperatures are up to 1 %, which can be lowered. The reason for the spike in methanol slip and CO, during the load step, is because the reformer temperature has not stabilized yet.

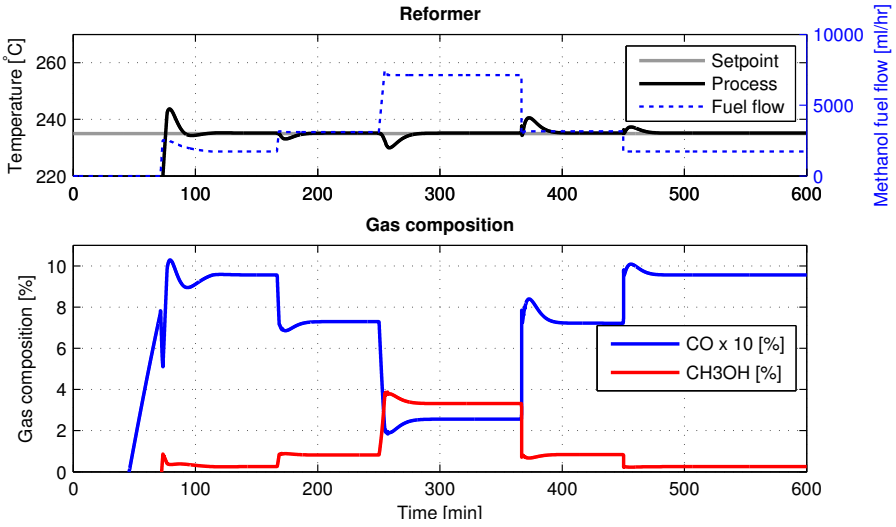

Fig. 3.28: Gas composition based on constant 235 °C reformer temperature

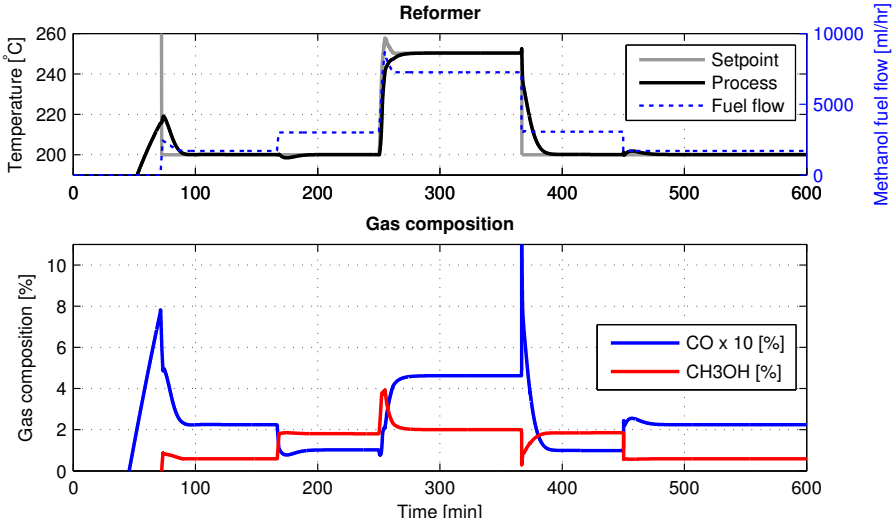

Fig. 3.29: Gas composition based on variable reformer temperature.

Using the information from fig. 3.18, with the relation between temperature and reformer at 2 % methanol slip, it is possible to condition the methanol slip by controlling the input oil for the reformer. The 2 % methanol slip curve from fig. 3.18 is used as the reformer temperature set-point, ($T_{r,set}$), as seen in the control diagram fig. 3.24. The curve is based on the methanol flow, which is used as input parameter. A temperature low limit of 200 °C is set for the reformer which corresponds to a slip of 2 % at 2.5 kW. A lower temperature of the reformer is possible, however more data on the reforming gas composition is required. Further, a minimum of 200 °C results in a maximum CO content of 0.4 % just above 0 ml/hr. The resulting gas composition and the variable reformer set-point are illustrated in fig. 3.29. The low limit of the reformer temperature of 200 °C can be seen in the beginning of the test as the reformer temperature does not change during the first load step from 1.5 kw to 2.5 kW.

During the load step to 5 kW at 250 minutes it can be seen that the temperature set-point for the burner increases to 255 °C. The increase in flow results in a high methanol slip which rises to 4 %, however, as the reformer temperature increases the methanol slip comes back to 2 %. The CO concentration can also be seen in fig. 3.29 and is not at any point above 0.5 % CO.

The two simulations shown in fig. 3.28 and fig. 3.29 show the effects of using a variable reformer temperature. The variable temperature, based on the gas composition experiment in fig. 3.17 and fig. 3.18, show that utilizing the knowledge of the reformate slip and CO can significantly improve the resulting gas composition, thereby increasing the possibility to prolong the lifetime of the HT-PEMFC, as degrading impurities can be avoided.

5.4 Efficiency and operating cost

Comparing the efficiency between the open loop and controlled operation, it can be seen that by utilizing a controller for the system can increase the efficiency in more operating conditions. The table 3.3 shows a comparison of the efficiency at two loads and compared to literature. The load of 0.24 A/cm^2 corresponds to a output power of 2.5 kW and 0.47 A/cm^2 corresponds to 5 kW.

By utilizing a controlled is possible to increase the system efficiency by 1 percentage point (*p.p.*) at 0.24 A/cm^2 and 2 *p.p.* at 0.47 A/cm^2. The increase in the efficiency confirms the usability of the controller, however, becaues the efficiency is linked directly to the stoichiometry, it depends mainly on the lowest possible stoichiometry allowed by the HT-PEMFC. Literature in the area of reformed methane or methanol fuel cell systems shows similar efficiencies. Work done by Romero-Pascual and Soler [2014] show an efficiency of 24 % on

a methanol powered combined heat and power system. A 1 kW natural gas reforming system by Desideri et al. [2012] an efficiency of 25 % to 27 % was found, and Justesen and Andreasen [2015] show an efficiency of 33 % on a 350 W reformed methanol fuel cell system. Some of the research use a lower stoichiometry than 1.35, however, they may not consider the degradation of the HT-PEM fuel cell stack.

Table 3.3: Comparison of the electric efficiency at 0.24 A/cm^2 and 0.47 A/cm^2 between the open loop controller and the cascade controller

	Efficiency		
Current Density	Open loop	Controlled	Difference
0.24 A/cm^2 (2.5 kW)	28 %	29 %	1 *p.p.*(%)
0.47 A/cm^2 (5 kW)	26 %	28 %	2 *p.p.*(%)
Litterature			
Methanol CHP system [Romero-Pascual and Soler, 2014]	24 %		
1 kW natual gas system [Desideri et al., 2012]	25 % to 27 %		
350W Methanol system [Justesen and Andreasen, 2015]	33 %		

The running cost of the system can be calculated using the price of methanol, which is set to 0.59 e/liter and €0.22 /liter. The price €0.59 /liter used is including distribution cost and taxes, which can vary depending on the amount and application [E.M.SH Ng-Tech, 2015]. The price €0.22 /liter is without the distribution cost and taxes [Methanex Corporation, 2015]. The methanol part of the fuel flow is isolated and compared to the electric power output from the fuel cell stack. The a simulation of the running cost for the system can be seen in fig. 3.30. The running cost of the system is found to be about €0.61/kWh for €0.59/liter and about €0.23/kWh for €0.22/liter. The running cost is the levelized cost of electricity (LEC) in the operating range of 1.5 to 5 kW and does not include the purchase price or disposal costs.

The efficiency and cost graph show that during high load, 5 kW, there is a small drop in efficiency which may be directly linked to the gas composition at those operating conditions. Additionally, it can be seen that the running cost and efficiency is stable in a wide operating range, which is favorable compared to gas turbines or diesel generators which are efficient in a much narrower operating range.

Work done by Oladokun and Asemota [2015] show the LEC for a diesel generator at about $0.30/kWh(€0.27kWh) and about $0.15/kWh(€0.14/kWh)

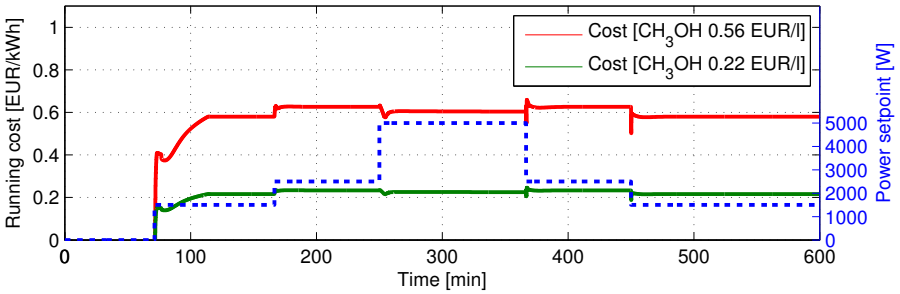

Fig. 3.30: Running cost based on the methanol price of €0.59/liter and €0.22/liter

for gas fired turbine. A price of €0.9/liter was used as the diesel price which has varied a lot the last century. Comparing the diesel generator and the reformed methanol reformer system show that the running cost is in a similar range, however, the initial purchase price of the unit is a significant factor and will probably determine the future of the RMFC technology.

Summary

A dynamic model has been presented with four main components; methanol reformer, catalytic burner, HTPEM fuel cell stack, and an evaporator. The model was made in Matlab Simulink and the purpose of the model was twofold. First the model can be used to investigate the system in operating conditions that would be damaging to the components or dangerous for bystanders. Secondly the model can be used to evaluate alternative control strategies without having to operate the system in real time. Some of the time constants for these thermal systems can be several hours before an evaluation of the controller can be made. Based on tests on a 17 cell stack a dynamic model were created. The model was based on experiments with different temperatures on dry hydrogen and reformate gas. Furthermore, tests on CO concentration and stoichiometry was performed and the anode and cathode stoichiometry was found to be minimum 1.35 and 3.5, respectively.

A load step test was performed where the anode stoichiometry, cathode stoichiometry and current density was increased and decreased rapidly. The model predicted the experimental data well, however, only for some of the non-degraded cells. During the experiments with low stoichiometry and high temperatures a few fuel cells broke and were removed.

The HT-PEM fuel cell model was included in the system model directly to

the reformer gas composition, an oil circuit and an evaporator. The reformer was tested experimentally with regards to gas composition and a temperature model estimation was made. The gas composition, with a focus on CO and methanol slip, was found to be linked to the fuel flow and the temperature of the oil inlet. A relation between the methanol slip and CO was found and a constant 2 % curve for a constant methanol slip was found.

The model was used for open loop simulation and an operational state was found with a constant stoichiometry of 1.4 and an efficiency of 26 % to 28 % was found. A cascade controller was implemented for the reformer temperature where the burner temperature set-point was controlled. Additionally, a stoichiometry controller was implemented, which was used to decrease or increase the stoichiometry based on the temperature of the burner, however, only down to an anode stoichiometry of 1.3. A variable reformer temperature, based on the 2 % methanol slip curve, was implemented and simulations confirmed the gas composition and resulting CO concentration under operation.

The efficiency of the controlled system was found to be between 29 % at 2.5 kW and 28 % at 5 kW which corresponds to an operating cost of about €0.22/kWh not including distribution and taxes.

Chapter 4

Conclusion

The topics involving HT-PEM and methanol reforming have been investigated in this work using characterization tools and dynamic models. The work can be divided into two parts. The first part investigates the influence of temperature, steam and auto-thermal reformate gas, CO content, and anode and cathode stoichiometry with the intent of characterizing the HT-PEM fuel cell stack. The second part explores the use of modeling to investigate alternative system configurations and control strategies.

The characterization of the HT-PEM fuel cell stack using polarization plots and EIS data resulted in a good insight into the degradation issues of the stack. The EIS data was analyzed using equivalent models to quantify the resistances in the stack and found the limits for stoichiometry. The limit was found using information in low frequency impedance spectrum, which is linked to mass transport losses. The data also showed how CO in small amounts did not show any significant degradation or performance loss. However, based on the condition of the used stack, it was found that some cells in the stack were degraded more than others and a minimum operating stoichiometry of 1.35 was found. The cathode stoichiometry was also tested and it was found that an air stoichiometry above 3.5 did not significantly increase performance.

A dynamic model of the HT-PEMFC was made with the help of current steps on the short stack. The fuel cell stack had an increase, both on anode and cathode stoichiometry, before the current step was conducted and the dynamic model showed how it was able to follow the changes. The same model was used to validate polarization curves, which was able to replicate the experimental data with pure hydrogen and with reformate gas. The HT-PEM stack

model was scaled to include 120 cells and was implemented in a larger system simulation together with a burner, reformer, and evaporator.

The simulation of a reformed methanol fuel cell system demonstrated how the four components are affected during various operating conditions. The resulting stoichiometry at the fuel cell stack was discovered to be in high risk of fuel starvation if the load is changed before the reformate gas feed has reached the fuel cell, which shows how critical it can be to dramatically change the load of the fuel cell stack.

A cascade controller for the reformer and burner was tested, which showed the possibility of increasing the dynamics of the system by controlling the burner temperature based on the reformer temperature. Simulations show that using the controller the reformer temperature calculated a settling time of 7 minutes with an overshoot of $\pm 5\,^{\circ}\mathrm{C}$. If the temperature varies significantly from the specified set-point, it could cause a degrading gas composition. Using the proposed controller does not completely eliminate a high methanol slip or a high CO in the transition phase, however, the amount is negligible because of the high tolerance of the HT-PEM fuel cell. The system efficiency was estimated in the range of 28 % to 29 %, which was an increase of 1 and 2 percentage points compared to the open loop operation. A levelized cost of electricity(LEC) was estimated to about €0.22/kWh, which is in range with similar scaled diesel generators.

During the experimentation with the catalytic burner there were some complications with the high temperatures and the heat transfer oil. The oil showed degrading properties when the burner was operating at high load and two electric heaters were used instead during the experiments. The author does not recommend using oil as a heat transfer liquid at these temperatures and alternative methods of heat transfer should be used. Additionally, the cost of oil pumps that can operate at these temperatures are high and the use of heat transfer oil adds to the complexity of the system.

In conclusion, despite the complexity of the system, it is possible to operate the proposed system reliably and with a high electric efficiency. This system could be a good alternative to diesel generators for applications like backup systems, battery chargers, range extenders because of the wide operating range. Furthermore, with high efficiency, silent operation, and the potentially greenhouse gas neutral operation it can open up possibilities for these kind of systems.

Future work

As with the majority of research projects done today, the research done in this study opens up more questions for investigation.

The use of HT-PEM fuel cells with reformate gas have several benefits, however, the degradation of the fuel cell stack is still under a lot of attention. Investing more attention into the EIS technique can result in a useful way to investigate the operating condition, however, only a few studies have covered the use of on-line diagnostic with EIS. Investigating the conditions and affects on the fuel cells can greatly improve the introduction of a fuel cell stack to commercialization projects. The insight in the condition of the fuel cell stack can improve troubleshooting and eventually add into finding general problems with the system in operation.

Reformed methanol fuel cell systems have in general a burner and reformer which work in cooperation in producing the reformate gas. The design and combination are something that can be improved in the area of heat distribution and cost. Additionally, using models to predict the reformer gas composition have not currently included the degrading of the catalyst performance. Predicting the reformer catalyst condition based on the operating hours can be an additional input for the reformer model. Furthermore, a methanol reforming catalysts that can operate in the range of the fuel cell temperature, $\sim$160 °C, would reduce the number of components and simplify the the system greatly.

Improvements in the startup time of the system from ambient temperatures or lower have a significant influence on the usability of the system. Many of the current commercial reformate systems still have up to an hour in startup time before operation which prohibits the use of this technology in many future applications.

References

Q Li, D Aili, H A Hjuler, and J O Jensen. *High Temperature Polymer Electrolyte Membrane Fuel Cells: Approaches, Status, and Perspectives*. Springer International Publishing, 2015. ISBN 9783319170824. URL http://www.springer.com/gb/book/9783319170817. iv

J.G.J. Olivier, G. Janssens-Maenhout, M. Muntean, and J.A.H.W. Peters. Trends in global CO2 emissions: 2015 report. Technical report, PBL Netherlands Environmental Assessment Agency, 2015. URL http://www.pbl.nl/en/publications/trends-in-global-co2-emissions-2015-report. xiii, 4

Søren Juhl Andreasen, Leanne Ashworth, Simon Sahlin, Hans-Christian Becker Jensen, and Søren Knudsen Kær. Test of hybrid power system for electrical vehicles using a lithium-ion battery pack and a reformed methanol fuel cell range extender. *Int. J. Hydrogen Energy*, 39(4):1856–1863, jan 2014. ISSN 03603199. doi: 10.1016/j.ijhydene.2013.11.068. URL http://www.sciencedirect.com/science/article/pii/S0360319913027936. xiii, 10, 11

M Prigent. On board hydrogen generation for fuel cell powered electric cars. A review of various available techniques. *Oil Gas Sci. Technol.*, 52(3):349–360, 1997. xiii, 12

IEA. World Energy Investment Outlook 2014. Technical report, 2014a. URL http://www.iea.org/publications/freepublications/publication/WEIO2014.pdf. 3

Janet L Sawin, Freyr Sverrisson, and Wilson Rickerson. Renewables 2015 Global Status Report. Technical report, REN21, 2015. URL http://www.ren21.net/wp-content/uploads/2015/07/GSR2015_KeyFindings_lowres.pdf. 3, 5

IEA. CO2 Emissions From Fuel Combustion Highlights 2014. Technical report,

2014b. URL http://www.iea.org/publications/freepublications/publication/CO2EmissionsFromFuelCombustionHighlights2014.pdf. 4

Jaeman Park, Hwanyeong Oh, Taehun Ha, Yoo Il Lee, and Kyoungdoug Min. A review of the gas diffusion layer in proton exchange membrane fuel cells: Durability and degradation. *Appl. Energy*, 155:866–880, oct 2015. ISSN 03062619. doi: 10.1016/j.apenergy.2015.06.068. URL http://www.sciencedirect.com/science/article/pii/S0306261915008260. 4, 21

Danish Ministry of Climate. Accelerating green energy towards 2020. Technical Report March, Ministry of Climate, Energy and Building, 2012. URL http://www.ens.dk/sites/ens.dk/files/dokumenter/publikationer/downloads/accelerating_green_energy_towards_2020.pdf. 5

Seyyed Mohsen Mousavi Ehteshami and S.H. Chan. The role of hydrogen and fuel cells to store renewable energy in the future energy network – potentials and challenges. *Energy Policy*, 73:103–109, oct 2014. ISSN 03014215. doi: 10.1016/j.enpol.2014.04.046. URL http://www.sciencedirect.com/science/article/pii/S0301421514002869. 5

Frano Barbir. PEM electrolysis for production of hydrogen from renewable energy sources. *Sol. Energy*, 78(5):661–669, may 2005. ISSN 0038092X. doi: 10.1016/j.solener.2004.09.003. URL http://www.sciencedirect.com/science/article/pii/S0038092X04002464. 5

Gorm B. Andresen, Rolando A. Rodriguez, Sarah Becker, and Martin Greiner. The potential for arbitrage of wind and solar surplus power in Denmark. *Energy*, 76:49–58, nov 2014. ISSN 03605442. doi: 10.1016/j.energy.2014.03.033. URL http://www.sciencedirect.com/science/article/pii/S0360544214002977. 5

F Mueller-Langer, E Tzimas, M Kaltschmitt, and S Peteves. Techno-economic assessment of hydrogen production processes for the hydrogen economy for the short and medium term. *Int. J. Hydrogen Energy*, 32(16):3797–3810, nov 2007. ISSN 03603199. doi: 10.1016/j.ijhydene.2007.05.027. URL http://www.sciencedirect.com/science/article/pii/S0360319907003011. 5, 12

Fuel Cell Today. Fuel cell history, 2015. URL http://www.fuelcelltoday.com/history. 6

J Larminie and A Dicks. *Fuel cell systems explained*. J. Wiley, 2003. ISBN 9780470848579. URL https://books.google.dk/books?id=IRAoAQAAMAAJ. 6, 7, 9

S. Martin, Q. Li, and J.O. Jensen. Lowering the platinum loading of high temperature polymer electrolyte membrane fuel cells with acid doped polybenzimidazole membranes. *J. Power Sources*, 293:51–56, oct 2015. ISSN 03787753. doi: 10.1016/j.jpowsour.2015.05.031. URL http://www.sciencedirect.com/science/article/pii/S0378775315009027. 7, 20, 21, 22

Dong Liang, Qiang Shen, Ming Hou, Zhigang Shao, and Baolian Yi. Study of the cell reversal process of large area proton exchange membrane fuel cells under fuel starvation. *J. Power Sources*, 194(2):847–853, dec 2009. ISSN 03787753. doi: 10.1016/j.jpowsour.2009.06.059. URL http://www.sciencedirect.com/science/article/pii/S0378775309010775. 10

A. Fuerte, R.X. Valenzuela, M.J. Escudero, and L. Daza. Ammonia as efficient fuel for SOFC. *J. Power Sources*, 192(1):170–174, jul 2009. ISSN 03787753. doi: 10.1016/j.jpowsour.2008.11.037. URL http://www.sciencedirect.com/science/article/pii/S0378775308021873. 12

Jin Kyung Lee, Jung Bong Ko, and Dong Hyun Kim. Methanol steam reforming over Cu/ZnO/Al2O3 catalyst: kinetics and effectiveness factor. *Appl. Catal. A Gen.*, 278(1):25–35, dec 2004. ISSN 0926860X. doi: 10.1016/j.apcata.2004.09.022. URL http://linkinghub.elsevier.com/retrieve/pii/S0926860X04007999. 12

S.T. Yong, C.W. Ooi, S.P. Chai, and X.S. Wu. Review of methanol reforming-Cu-based catalysts, surface reaction mechanisms, and reaction schemes. *Int. J. Hydrogen Energy*, 38(22):9541–9552, jul 2013. ISSN 03603199. doi: 10.1016/j.ijhydene.2013.03.023. URL http://www.sciencedirect.com/science/article/pii/S0360319913006320. 12

Kristian Kjær Justesen, Søren Juhl Andreasen, Hamid Reza Shaker, Mikkel Præstholm Ehmsen, and John Andersen. Gas composition modeling in a reformed Methanol Fuel Cell system using adaptive Neuro-Fuzzy Inference Systems. *Int. J. Hydrogen Energy*, 38(25):10577–10584, 2013. URL http://www.sciencedirect.com/science/article/pii/S0360319913014511. 12, 76

Jens Anton Christiansen. A reaction between methanol and water and some related reactions. *J. Am. Chem. Soc.*, 43:1670, 1921. 12

Jens Anton Christiansen and J. R. Huffman. The reaction between methanol and steam as an example of heterogeneous catalysis. *Z. Phys. Chem.*, A151: 269–302, 1930. 12

Jens Anton Christiansen. Use of the method of stationary velocities for the reaction CH3OH + H2O -> 3H2 + CO2. *Z. Phys. Chem.*, Bodenstein:69–77, 1931. 12

Saba Niaz, Taniya Manzoor, and Altaf Hussain Pandith. Hydrogen storage: Materials, methods and perspectives. *Renew. Sustain. Energy Rev.*, 50:457–469, 2015. ISSN 13640321. doi: 10.1016/j.rser.2015.05.011. URL http://www.sciencedirect.com/science/article/pii/S1364032115004694. 13

D.J. Durbin and C. Malardier-Jugroot. Review of hydrogen storage techniques for on board vehicle applications. *Int. J. Hydrogen Energy*, 38 (34):14595–14617, nov 2013. ISSN 03603199. doi: 10.1016/j.ijhydene.2013.07.058. URL http://linkinghub.elsevier.com/retrieve/pii/S0360319913018053. 13

Scott W. Jorgensen. Hydrogen storage tanks for vehicles: Recent progress and current status. *Curr. Opin. Solid State Mater. Sci.*, 15(2):39–43, apr 2011. ISSN 13590286. doi: 10.1016/j.cossms.2010.09.004. URL http://www.sciencedirect.com/science/article/pii/S1359028610000483. 13

P. Cotterill. The hydrogen embrittlement of metals. *Prog. Mater. Sci.*, 9(4):205–301, jan 1961. ISSN 00796425. doi: 10.1016/0079-6425(61)90005-6. URL http://www.sciencedirect.com/science/article/pii/0079642561900056. 13

S. Mekhilef, R. Saidur, and A. Safari. Comparative study of different fuel cell technologies. *Renew. Sustain. Energy Rev.*, 16(1):981–989, jan 2012. ISSN 13640321. doi: 10.1016/j.rser.2011.09.020. URL http://www.sciencedirect.com/science/article/pii/S1364032111004709. 13

Giuliana Ercolino, Muhammad A. Ashraf, Vito Specchia, and Stefania Specchia. Performance evaluation and comparison of fuel processors integrated with PEM fuel cell based on steam or autothermal reforming and on CO preferential oxidation or selective methanation. *Appl. Energy*, 143:138–153, apr 2015. ISSN 03062619. doi: 10.1016/j.apenergy.2014.12.088. URL http://www.sciencedirect.com/science/article/pii/S0306261915000057. 13

W. Wiese, B. Emonts, and R. Peters. Methanol steam reforming in a fuel cell drive system. *J. Power Sources*, 84(2):187–193, dec 1999. ISSN 03787753. doi: 10.1016/S0378-7753(99)00316-X. URL http://www.sciencedirect.com/science/article/pii/S037877539900316X. 14

Anders R. Korsgaard, Rasmus Refshauge, Mads P. Nielsen, Mads Bang, and Søren K. Kær. Experimental characterization and modeling of commercial polybenzimidazole-based MEA performance. *J. Power Sources*, 162 (1):239–245, nov 2006. ISSN 0378-7753. doi: DOI:10.1016/j.jpowsour.2006.06.099. URL http://www.sciencedirect.com/science/article/pii/S0378775306012742. 15, 59

Søren Juhl Andreasen, Jakob Rabjerg Vang, and Søren Knudsen Kær. High temperature PEM fuel cell performance characterisation with CO and CO2 using electrochemical impedance spectroscopy. *Int. J. Hydrogen Energy*, 36(16):9815–9830, aug 2011a. ISSN 03603199. doi: 10.1016/j.ijhydene.2011.04.076. URL http://www.sciencedirect.com/science/article/pii/S0360319911009414. 15

Fan Zhou, Søren Juhl Andreasen, Søren Knudsen Kær, and Donghong Yu. Analysis of accelerated degradation of a HT-PEM fuel cell caused by cell reversal in fuel starvation condition. *Int. J. Hydrogen Energy*, jan 2015a. ISSN 03603199. doi: 10.1016/j.ijhydene.2014.12.082. URL http://www.sciencedirect.com/science/article/pii/S036031991403479X. 15, 22, 26, 29

Fuel Cell Today. The fuel cell industry review 2013. Technical report, 2013. URL http://www.fuelcelltoday.com/analysis/industry-review. 17

Yun Wang, Ken S. Chen, Jeffrey Mishler, Sung Chan Cho, and Xavier Cordobes Adroher. A review of polymer electrolyte membrane fuel cells: Technology, applications, and needs on fundamental research. *Appl. Energy*, 88(4):981–1007, apr 2011. ISSN 03062619. doi: 10.1016/j.apenergy.2010.09.030. URL http://www.sciencedirect.com/science/article/pii/S0306261910003958. 17

Qingfeng Li, Jens Oluf Jensen, Robert F. Savinell, and Niels J. Bjerrum. High temperature proton exchange membranes based on polybenzimidazoles for fuel cells. *Prog. Polym. Sci.*, 34(5):449–477, may 2009. ISSN 00796700. doi: 10.1016/j.progpolymsci.2008.12.003. URL http://www.sciencedirect.com/science/article/pii/S0079670009000100. 17, 19, 20, 21, 34, 36, 70

Jianlu Zhang, Zhong Xie, Jiujun Zhang, Yanghua Tang, Chaojie Song, Titichai Navessin, Zhiqing Shi, Datong Song, Haijiang Wang, David P. Wilkinson, Zhong-Sheng Liu, and Steven Holdcroft. High temperature PEM fuel cells. *J. Power Sources*, 160(2):872–891, oct 2006. ISSN 03787753. doi: 10.1016/j.jpowsour.2006.05.034. URL http://www.sciencedirect.com/science/article/pii/S0378775306010299. 18

Søren Juhl Andreasen, Jakob Rabjerg Vang, and Søren Knudsen Kær. High temperature PEM fuel cell performance characterisation with CO and CO2 using electrochemical impedance spectroscopy. *Int. J. Hydrogen Energy*, 36(16):9815–9830, aug 2011b. ISSN 03603199. doi: 10.1016/j.ijhydene.2011.04.076. URL http://www.sciencedirect.com/science/article/pii/S0360319911009414. 18, 22, 26, 52, 70

E. Romero-Pascual and J. Soler. Modelling of an HTPEM-based micro-combined heat and power fuel cell system with methanol. *Int. J. Hydrogen Energy*, 39(8):4053–4059, mar 2014. ISSN 03603199. doi: 10.1016/j.ijhydene.2013.07.015. URL http://www.sciencedirect.com/science/article/pii/S0360319913017151. 18, 85, 86

E. Planes, L. Flandin, and N. Alberola. Polymer Composites Bipolar Plates for PEMFCs. *Energy Procedia*, 20:311–323, 2012. ISSN 18766102. doi: 10.1016/j.egypro.2012.03.031. URL http://www.sciencedirect.com/science/article/pii/S1876610212007618. 18

R F Savinell and M H Litt. Proton conducting polymers used as membranes, 1996. URL https://www.google.com/patents/US5525436. 20

R Bouchet. Proton conduction in acid doped polybenzimidazole. *Solid State Ionics*, 118(3-4):287–299, mar 1999. ISSN 01672738. doi: 10.1016/S0167-2738(98)00466-4. URL http://www.sciencedirect.com/science/article/pii/S0167273898004664. 20

Jinfeng Wu, Xiao Zi Yuan, Jonathan J. Martin, Haijiang Wang, Jiujun Zhang, Jun Shen, Shaohong Wu, and Walter Merida. A review of PEM fuel cell durability: Degradation mechanisms and mitigation strategies. *J. Power Sources*, 184(1):104–119, sep 2008. ISSN 03787753. doi: 10.1016/j.jpowsour.2008.06.006. URL http://www.sciencedirect.com/science/article/pii/S0378775308011968. 20, 21

Samuel Simon Araya, Ionela Florentina Grigoras, Fan Zhou, Søren Juhl Andreasen, and Søren Knudsen Kær. Performance and endurance of a high temperature PEM fuel cell operated on methanol reformate. *Int. J. Hydrogen Energy*, 39(32):18343–18350, oct 2014. ISSN 03603199. doi: 10.1016/j.ijhydene.2014.09.007. URL http://www.sciencedirect.com/science/article/pii/S0360319914025269. 20, 21, 22, 34

Samuel Simon Araya, Søren Juhl Andreasen, Heidi Venstrup Nielsen, and Søren Knudsen Kær. Investigating the effects of methanol-water vapor mixture on a PBI-based high temperature PEM fuel cell. *Int. J. Hydrogen Energy*, 37(23):18231–18242, dec 2012a. ISSN 03603199. doi: 10.1016/j.ijhydene.2012.09.009. URL http://www.sciencedirect.com/science/article/pii/S0360319912020125. 21, 69

Yuka Oono, Atsuo Sounai, and Michio Hori. Influence of the phosphoric acid-doping level in a polybenzimidazole membrane on the cell performance of high-temperature proton exchange membrane fuel cells. *J. Power Sources*, 189(2):943–949, apr 2009. ISSN 03787753. doi: 10.1016/j.jpowsour.2008.12.115. URL http://www.sciencedirect.com/science/article/pii/S0378775308024865. 21, 26

Søren Juhl Andreasen and Søren Knudsen Kær. Modelling and evaluation of heating strategies for high temperature polymer electrolyte membrane fuel cell stacks. *Int. J. Hydrogen Energy*, 33(17):4655–4664, sep 2008. ISSN 03603199. doi: 10.1016/j.ijhydene.2008.05.076. URL http://linkinghub.elsevier.com/retrieve/pii/S0360319908005545http://www.sciencedirect.com/science/article/pii/S0360319908005545http://www.sciencedirect.com/science/article/B6V3F-4T7D8DB-3/2/8d0c8adcdb7feb517cde3dbea8960d5c. 21, 49

S Yu, L Xiao, and B C Benicewicz. Durability Studies of PBI-based High Temperature PEMFCs. *Fuel Cells*, 8(3-4):165–174, 2008. ISSN 1615-6854. doi: 10.1002/fuce.200800024. URL http://dx.doi.org/10.1002/fuce.200800024. 21

Gang Liu, Huamin Zhang, Jingwei Hu, Yunfeng Zhai, Dongyan Xu, and Zhigang Shao. Studies of performance degradation of a high temperature PEMFC based on H3PO4-doped PBI. *J. Power Sources*, 162(1):547–552, nov 2006. ISSN 03787753. doi: 10.1016/j.jpowsour.2006.07.008. URL http://linkinghub.elsevier.com/retrieve/pii/S0378775306012468. 22

Qingfeng Li, Ronghuan He, Ji-An Gao, Jens Oluf Jensen, and Niels. J Bjerrum. The CO Poisoning Effect in PEMFCs Operational at Temperatures up to 200°C. *J. Electrochem. Soc.*, 150(12):A1599–A1605, dec 2003. doi: 10.1149/1.1619984. URL http://jes.ecsdl.org/content/150/12/A1599.abstract. 22, 43

Fan Zhou, Søren Juhl Andreasen, Søren Knudsen Kær, and Jung O. Park. Experimental investigation of carbon monoxide poisoning effect on a PBI/H3PO4 high temperature polymer electrolyte membrane fuel cell: Influence of anode humidification and carbon dioxide. *Int. J. Hydrogen Energy*, 40(43):14932–14941, nov 2015b. ISSN 03603199. doi: 10.1016/j.ijhydene.2015.09.056. URL http://www.sciencedirect.com/science/article/pii/S0360319915023460. 22

Jungtak Kang, Dong Won Jung, Soon Park, Jong-Hyun Lee, Jaejoon Ko, and Junbom Kim. Accelerated test analysis of reversal potential caused by fuel starvation during PEMFCs operation. *Int. J. Hydrogen Energy*, 35(8):3727–3735, apr 2010. ISSN 03603199. doi: 10.1016/j.ijhydene.2010.01.071. URL http://www.sciencedirect.com/science/article/pii/S0360319910001424. 22

Xiaozi Yuan, Jian Colin Sun, Haijiang Wang, and Jiujun Zhang. AC impedance diagnosis of a 500W PEM fuel cell stack. *J. Power Sources*, 161(2):929–937, oct 2006. ISSN 03787753. doi: 10.1016/j.jpowsour.2006.07.020. URL http://www.sciencedirect.com/science/article/pii/S0378775306012523. 26

Jakob Rabjerg Vang, Søren Juhl Andreasen, and Søren Knudsen Kær. A Transient Fuel Cell Model to Simulate HTPEM Fuel Cell Impedance Spectra. *J. Fuel Cell Sci. Technol.*, 9(2):021005, 2012. ISSN 1550624X. doi: 10.1115/1.4005609. URL http://dx.doi.org/10.1115/1.4005609. 26

Samuel Cruz-Manzo, Rui Chen, and Paul Greenwood. An impedance model for analysis of EIS of polymer electrolyte fuel cells under hydrogen peroxide formation in the cathode. *J. Electroanal. Chem.*, 745:28–36, may 2015. ISSN 15726657. doi: 10.1016/j.jelechem.2015.03.012. URL http://www.sciencedirect.com/science/article/pii/S157266571500123X. 26

Samuel Simon Araya, Søren Juhl Andreasen, Heidi Venstrup Nielsen, and Søren Knudsen Kær. Investigating the effects of methanol-water vapor mixture on a PBI-based high temperature PEM fuel cell. *Int. J. Hydrogen Energy*, 37(23):18231–18242, dec 2012b. ISSN 03603199. doi: 10.1016/j.ijhydene.2012.09.009. URL http://linkinghub.elsevier.com/retrieve/pii/S0360319912020125http://www.sciencedirect.com/science/article/pii/S0360319912020125. 26, 31

Jesper Lebæk Jespersen, Erik Schaltz, and Søren Knudsen Kær. Electrochemical characterization of a polybenzimidazole-based high temperature proton exchange membrane unit cell. *J. Power Sources*, 191(2):289–296, jun 2009. ISSN 03787753. doi: 10.1016/j.jpowsour.2009.02.025. URL http://www.sciencedirect.com/science/article/pii/S0378775309002742. 26, 34, 42

Po Hong, Jianqiu Li, Liangfei Xu, Minggao Ouyang, and Chuan Fang. Modeling and simulation of parallel DC/DC converters for online AC impedance estimation of PEM fuel cell stack. *Int. J. Hydrogen Energy*, dec 2015. ISSN 03603199. doi: 10.1016/j.ijhydene.2015.11.129. URL http://www.sciencedirect.com/science/article/pii/S0360319915309320. 26

M. Hinaje, I. Sadli, J.-P. Martin, P. Thounthong, S. Raël, and B. Davat. Online humidification diagnosis of a PEMFC using a static DC–DC converter. *Int. J. Hydrogen Energy*, 34(6):2718–2723, mar 2009. ISSN 03603199. doi: 10.1016/j.ijhydene.2009.01.076. URL http://www.sciencedirect.com/science/article/pii/S0360319909001323. 26

Serenergy A/S. Serenergy S165L liquic cooled HT PEM stack, 2013. URL http://serenergy.com/wp-content/uploads/2013/05/S-165L_datasheet_v1.0_0313.pdf. 26, 41

Greenlight Innovation. Greenlight Fuel Cell Test Solutions, 2014. URL http://www.greenlightinnovation.com/fuel-cell/index.php. 26

Paratherm. Data for Paratherm NF heat transfer fluid, 2014. URL http://www.paratherm.com/heat-transfer-fluids/high-temperature-heat-transfer-fluids/paratherm-nf/. 27, 48

Gamry instruments A/S. Reference 3000. URL http://www.gamry.com/products/potentiostats/. 27

Suthida Authayanun, Karittha Im-orb, and Amornchai Arpornwichanop. A review of the development of high temperature proton exchange membrane fuel cells. *Chinese J. Catal.*, 36(4):473–483, apr 2015. ISSN 18722067. doi: 10.1016/S1872-2067(14)60272-2. URL http://www.sciencedirect.com/science/article/pii/S1872206714602722. 29

Lucia Salemme, Laura Menna, and Marino Simeone. Calculation of the energy efficiency of fuel processor – PEM (proton exchange membrane) fuel cell systems from fuel elementar composition and heating value. *Energy*, 57:368–374, aug 2013. ISSN 03605442. doi: 10.1016/j.energy.2013.04.023. URL http://www.sciencedirect.com/science/article/pii/S0360544213003332. 29

Ying Zhu, Wenhua H. Zhu, and Bruce J. Tatarchuk. Performance comparison between high temperature and traditional proton exchange membrane fuel cell stacks using electrochemical impedance spectroscopy. *J. Power Sources*, 256:250–257, jun 2014. ISSN 03787753. doi: 10.1016/j.jpowsour.2014.01.049. URL http://www.sciencedirect.com/science/article/pii/S037877531400072X. 31, 32

M. Boaventura and A. Mendes. Activation procedures characterization of MEA based on phosphoric acid doped PBI membranes. *Int. J. Hydrogen Energy*, 35(20):11649–11660, oct 2010. ISSN 03603199. doi: 10.1016/j.ijhydene.2010.03.137. URL http://www.sciencedirect.com/science/article/pii/S0360319910006555. 31, 33

Jakob Rabjerg Vang, Søren Juhl Andreasen, Samuel Simon Araya, and Søren Knudsen Kær. Comparative study of the break in process of post doped and sol–gel high temperature proton exchange membrane fuel cells. *Int. J. Hydrogen Energy*, 39(27):14959–14968, sep 2014. ISSN 03603199. doi: 10.1016/j.ijhydene.2014.07.017. URL http://www.sciencedirect.com/science/article/pii/S0360319914019727. 31

Mikhail S. Kondratenko, Marat O. Gallyamov, and Alexei R. Khokhlov. Performance of high temperature fuel cells with different types of PBI membranes as analysed by impedance spectroscopy. *Int. J. Hydrogen Energy*, 37(3):2596–2602, feb 2012. ISSN 03603199. doi: 10.1016/j.ijhydene.2011.10.087. URL http://www.sciencedirect.com/science/article/pii/S036031991102461X. 31, 33

C. Siegel, I. Buder, and A. Heinzel. Sectional electrochemical impedance analysis of a high temperature polymer electrolyte membrane fuel cell with three types of flow-fields. *Electrochim. Acta*, 112:342–355, dec 2013. ISSN 00134686. doi: 10.1016/j.electacta.2013.08.142. URL http://www.sciencedirect.com/science/article/pii/S0013468613016721. 31, 39

Xiao-Zi Yuan, Chaojie Song, Haijiang Wang, and Jiujun Zhang. *Electrochemical Impedance Spectroscopy in PEM Fuel Cells*. Springer London, London, 2010. ISBN 978-1-84882-845-2. doi: 10.1007/978-1-84882-846-9. URL http://link.springer.com/10.1007/978-1-84882-846-9. 31, 32, 33, 39

X YUAN, H WANG, J COLINSUN, and J ZHANG. AC impedance technique in PEM fuel cell diagnosis—A review. *Int. J. Hydrogen Energy*, 32(17):4365–4380, dec 2007. ISSN 03603199. doi: 10.1016/j.ijhydene.2007.05.036. URL http://www.sciencedirect.com/science/article/pii/S036031990700328X. 32, 33

Constantinos G. Vayenas, editor. *Interfacial Phenomena in Electrocatalysis*, volume 51 of *Modern Aspects of Electrochemistry*. Springer New York, New York, NY, 2011. ISBN 978-1-4419-5579-1. doi: 10.1007/978-1-4419-5580-7. URL http://link.springer.com/10.1007/978-1-4419-5580-7. 33

Tatiana J.P Freire and Ernesto R Gonzalez. Effect of membrane characteristics and humidification conditions on the impedance response of polymer electrolyte fuel cells. *J. Electroanal. Chem.*, 503(1-2):57–68, apr 2001. ISSN 15726657. doi: 10.1016/S0022-0728(01)00364-3. URL http://www.sciencedirect.com/science/article/pii/S0022072801003643. 33

T. Romero-Castañón, L.G. Arriaga, and U. Cano-Castillo. Impedance spectroscopy as a tool in the evaluation of MEA's. *J. Power Sources*, 118 (1-2):179–182, may 2003. ISSN 03787753. doi: 10.1016/S0378-7753(03)00085-5. URL http://www.sciencedirect.com/science/article/pii/S0378775303000855. 33

Matthew M. Mench, Emin Caglan Kumbur, T. Nejat Veziroglu, and Shyam S. Kocha. *Polymer Electrolyte Fuel Cell Degradation*. Elsevier, 2012. ISBN 9780123869364. doi: 10.1016/B978-0-12-386936-4.10003-X. URL http://www.sciencedirect.com/science/article/pii/B978012386936410003X. 33

Ju-hyung Lee, Jong-Hak Lee, Woojin Choi, Kyung-Won Park, Hee-Young Sun, and Jae-Hyuk Oh. Development of a method to estimate the lifespan of proton exchange membrane fuel cell using electrochemical impedance spectroscopy. *J. Power Sources*, 195(18):6001–6007, sep 2010. ISSN 03787753. doi: 10.1016/j.jpowsour.2010.02.054. URL http://www.sciencedirect.com/science/article/pii/S0378775310003137. 33

J HU, H ZHANG, Y ZHAI, G LIU, and B YI. 500h Continuous aging life test on PBI/H3PO4 high-temperature PEMFC. *Int. J. Hydrogen Energy*, 31(13):1855–1862, oct 2006. ISSN 03603199. doi: 10.1016/j.ijhydene.2006.05.001. URL http://www.sciencedirect.com/science/article/pii/S0360319906001662. 33

M. Pérez-Page and V. Pérez-Herranz. Study of the electrochemical behaviour of a 300 W PEM fuel cell stack by Electrochemical Impedance Spectroscopy. *Int. J. Hydrogen Energy*, 39(8):4009–4015, mar 2014. ISSN 03603199. doi: 10.1016/j.ijhydene.2013.05.121. URL http://www.sciencedirect.com/science/article/pii/S0360319913013530. 33

A. Su, Y.M. Ferng, J. Hou, and T.L. Yu. Experimental and numerical investigations of the effects of PBI loading and operating temperature on a high-temperature PEMFC. *Int. J. Hydrogen Energy*, 37(9):7710–7718, may 2012. ISSN 03603199. doi: 10.1016/j.ijhydene.2012.02.004. URL http://www.sciencedirect.com/science/article/pii/S0360319912003011. 34, 35

Hong Liu, Peiwen Li, Alexandra Hartz, and Kai Wang. Effects of geometry/dimensions of gas flow channels and operating conditions on high-temperature PEM fuel cells. *Int. J. Energy Environ. Eng.*, 6(1):75–89, mar 2015. ISSN 2008-9163. doi: 10.1007/s40095-014-0153-x. URL http://link.springer.com/10.1007/s40095-014-0153-x. 34

David Aili, Todd Allward, Silvia Martinez Alfaro, Claire Hartmann-Thompson, Thomas Steenberg, Hans Aage Hjuler, Qingfeng Li, Jens Oluf Jensen, and Edmund J. Stark. Polybenzimidazole and sulfonated polyhedral oligosilsesquioxane composite membranes for high temperature polymer electrolyte membrane fuel cells. *Electrochim. Acta*, 140:182–190, sep 2014. ISSN 00134686. doi: 10.1016/j.electacta.2014.03.047. URL http://www.sciencedirect.com/science/article/pii/S0013468614005581. 36

Alin Orfanidi, Maria K. Daletou, Labrini Sygellou, and Stylianos G. Neophytides. The role of phosphoric acid in the anodic electrocatalytic layer in high temperature PEM fuel cells. *J. Appl. Electrochem.*, 43(11):1101–1116, nov 2013. ISSN 0021-891X. doi: 10.1007/s10800-013-0626-2. URL http://link.springer.com/10.1007/s10800-013-0626-2. 36

Samuele Galbiati, Andrea Baricci, Andrea Casalegno, Giulia Carcassola, and Renzo Marchesi. On the activation of polybenzimidazole-based membrane electrode assemblies doped with phosphoric acid. *Int. J. Hydrogen Energy*, 37(19):14475–14481, oct 2012. ISSN 03603199. doi: 10.1016/j.ijhydene.2012.07.032. URL http://www.sciencedirect.com/science/article/pii/S0360319912016096. 39, 42

Behzad Najafi, Alireza Haghighat Mamaghani, Andrea Baricci, Fabio Rinaldi, and Andrea Casalegno. Mathematical modelling and parametric study on a 30 kWel high temperature PEM fuel cell based residential micro cogeneration plant. *Int. J. Hydrogen Energy*, 40(3):1569–1583, jan 2015. ISSN 03603199. doi: 10.1016/j.ijhydene.2014.11.093. URL http://www.sciencedirect.com/science/article/pii/S0360319914032273. 39

Saswata Bose, Tapas Kuila, Thi Xuan Hien Nguyen, Nam Hoon Kim, Kintak Lau, and Joong Hee Lee. Polymer membranes for high temperature proton exchange membrane fuel cell: Recent advances and challenges. *Prog. Polym. Sci.*, 36(6):813–843, jun 2011. ISSN 00796700. doi: 10.1016/j.progpolymsci.2011.01.003. URL http://www.sciencedirect.com/science/article/pii/S0079670011000256. 43

Sebastian Kaserer, Christoph Rakousky, Julia Melke, and Christina Roth. Design of a reference electrode for high-temperature PEM fuel cells. *J. Appl. Electrochem.*, 43(11):1069–1078, nov 2013. ISSN 0021-891X. doi: 10.1007/s10800-013-0567-9. URL http://link.springer.com/10.1007/s10800-013-0567-9. 43

Tanja Vidaković. *Kinetics of Methanol Electrooxidation on PtRu Catalysts in a Membrane Electrode Assembly.* PhD thesis, 2005. 43

Johan Agrell, Henrik Birgersson, and Magali Boutonnet. Steam reforming of methanol over a Cu/ZnO/Al2O3 catalyst: a kinetic analysis and strategies for suppression of CO formation. *J. Power Sources*, 106(1-2):249–257, apr 2002. ISSN 03787753. doi: 10.1016/S0378-7753(01)01027-8. URL http://www.sciencedirect.com/science/article/pii/S0378775301010278. 48

A. Iulianelli, P. Ribeirinha, A. Mendes, and A. Basile. Methanol steam reforming for hydrogen generation via conventional and membrane reactors: A review. *Renew. Sustain. Energy Rev.*, 29:355–368, 2014. URL http://www.sciencedirect.com/science/article/pii/S1364032113005728. 48

Serenergy A/S. H3 2500/5000, 2015. URL http://serenergy.com/wp-content/uploads/2015/07/H3-2500-5000-datasheet.pdf. 49

M HARUTA and H SANO. Catalytic combustion of hydrogen I—Its role in hydrogen utilization system and screening of catalyst materials. *Int. J. Hydrogen Energy*, 6(6):601–608, 1981. ISSN 03603199. doi: 10.1016/0360-3199(81)90025-2. URL http://www.sciencedirect.com/science/article/pii/0360319981900252. 49

Ryan O'Hayre, Suk-Won Cha, Whitney Colella, and Fritz B. Prinz. *Fuel Cell Fundamentals, 2nd Edition.* John Wiley and Sons, Inc, 2005. ISBN 978-0-470-25843-9. 49

Søren Juhl Andreasen and Søren Knudsen Kær. Dynamic Model of the High Temperature Proton Exchange Membrane Fuel Cell Stack Temperature. *J. Fuel Cell Sci. Technol.*, 6(4):041006, 2009. ISSN 1550624X. doi: 10.1115/1.3081461. URL http://dx.doi.org/10.1115/1.3081461. 49

Jaeman Park and Kyoungdoug Min. A quasi-three-dimensional non-isothermal dynamic model of a high-temperature proton exchange membrane fuel cell. *J. Power Sources*, 216:152–161, oct 2012. ISSN 03787753. doi: 10.1016/j.jpowsour.2012.05.054. URL http://www.sciencedirect.com/science/article/pii/S0378775312009238. 51, 52, 56

Kui Jiao, Ibrahim E. Alaefour, and Xianguo Li. Three-dimensional non-isothermal modeling of carbon monoxide poisoning in high temperature proton exchange membrane fuel cells with phosphoric acid doped polybenzimidazole membranes. *Fuel*, 90(2):568–582, 2011. URL http://www.sciencedirect.com/science/article/pii/S0016236110005582. 52

Jingwei Hu, Huamin Zhang, and Liu Gang. Diffusion–convection/electrochemical model studies on polybenzimidazole (PBI) fuel cell based on AC impedance technique. *Energy Convers. Manag.*, 49(5):1019–1027, may 2008. ISSN 01968904. doi: 10.1016/j.enconman.2007.10.002. URL http://www.sciencedirect.com/science/article/pii/S0196890407003470. 55

Denver Cheddie and Norman Munroe. Mathematical model of a PEMFC using a PBI membrane. *Energy Convers. Manag.*, 47(11-12):1490–1504, jul 2006. ISSN 01968904. doi: 10.1016/j.enconman.2005.08.002. URL http://www.sciencedirect.com/science/article/pii/S0196890405001937. 56

Jianlu Zhang, Yanghua Tang, Chaojie Song, and Jiujun Zhang. Polybenzimidazole-membrane-based PEM fuel cell in the temperature range of 120–200°C. *J. Power Sources*, 172(1):163–171, oct 2007. ISSN 03787753. doi: 10.1016/j.jpowsour.2007.07.047. URL http://www.sciencedirect.com/science/article/pii/S0378775307015261. 56

BASF. BASF Catalyst Selectra RP-60, 2008. 62, 63

Serenergy A/S. Datasheet S165L Liquid cooled HTPEM stack, 2014. URL http://serenergy.com/. 72

Søren Juhl Andreasen, Søren Knudsen Kær, and Simon Sahlin. Control and experimental characterization of a methanol reformer for a 350 W high temperature polymer electrolyte membrane fuel cell system. *Int. J. Hydrogen Energy*, 38(3):1676–1684, feb 2013. ISSN 03603199. doi: 10.1016/j.ijhydene.2012.09.032. URL http://www.sciencedirect.com/science/article/pii/S0360319912020678. 76

Umberto Desideri, Jinyue Yan, Nicola Zuliani, and Rodolfo Taccani. Microcogeneration system based on HTPEM fuel cell fueled with natural gas: Performance analysis. *Appl. Energy*, 97:802–808, 2012. URL http://www.sciencedirect.com/science/article/pii/S0306261911008956. 86

Kristian Kjær Justesen and Søren Juhl Andreasen. Determination of optimal reformer temperature in a reformed methanol fuel cell system using ANFIS models and numerical optimization methods. *Int. J. Hydrogen Energy*, 40(30):9505–9514, aug 2015. ISSN 03603199. doi: 10.1016/j.ijhydene.2015.05.085. URL http://www.sciencedirect.com/science/article/pii/S0360319915012719. 86

E.M.SH Ng-Tech. Methanol Pricing, 2015. URL http://emsh-ngtech.com/methanol/methanol-pricing/. 86

Methanex Corporation. Methanex posts regional contract methanol prices for North America, Europe and Asia, 2015. URL https://www.methanex.com/our-business/pricing. 86

V.O. Oladokun and O.C. Asemota. Unit cost of electricity in Nigeria: A cost model for captive diesel powered generating system. *Renew. Sustain. Energy Rev.*, 52:35–40, dec 2015. ISSN 13640321. doi: 10.1016/j.rser.2015.07.028. URL http://www.sciencedirect.com/science/article/pii/S1364032115006759. 86

Part II

List of papers

* list of papers

Paper A

System Model Development for a Methanol Reformed 5kW High Temperature PEM Fuel Cell System

Paper B

Parametric Characterization of Reformate-operated and PBI-based High Temperature PEM Fuel Cell Stack

Paper C

Dynamic modeling and experimental investigation of a high temperature PEM fuel cell stack

Paper D

Test of hybrid power system for electrical vehicles using a lithium-ion battery pack and a reformed methanol fuel cell range extender

SUMMARY

Many fuel cells systems today are operated with compressed hydrogen which has great benefits because of the purity of the hydrogen and the relatively simple storage of the fuel. However, compressed hydrogen is stored in the range of 800 bar, which can be expensive to compress.One of the interesting topologies is the Reformed Methanol Fuel Cell (RMFC) system that operates on a mix of methanol and water. The fuel is reformed with a steam reforming to a hydrogen rich gas, however with additional formation of Carbon Monoxide and Carbon Dioxide. High Temperature Polymer Electrolyte Membrane Fuel Cell (HT-PEMFC) has the benefit of being resistant to CO poisoning. The HT-PEM fuel cell operates at elevated temperatures (above 100 oC) and therefore uses phosphoric acid as a proton conductor.

Using a HT-PEMFC in a RMFC system enables the use of exhaust gas from the fuel cell in a catalytic burner which is able to heat up the steam reforming process. However, utilizing the excess hydrogen in the system complicates the RMFC system as the amount of hydrogen can vary depending on the fuel methanol supply, fuel cell load and the reformer gas composition. This PhD study has therefore been involved in investigating the gas composition of the reformer and the affects to the HT-PEM fuel cell. Additional,a focus on the dynamics and system control of the RMFC have been studied, which have also been a big part of the motivation for this work.

ISSN (online): 2246-1248
ISBN (online): 978-87-7112-466-8

AALBORG **UNIVERSITETSFORLAG**